

1 **LOUISIANA COASTAL PROTECTION AND RESTORATION**
2 **TECHNICAL REPORT**

3
4
5
6
7 ***DRAFT***

8
9
10
11 **HYDRAULICS AND HYDROLOGY**
12 **APPENDIX**

13
14
15
16
17
18
19
20
21
22 February 2008



25 **U. S. Army Corps of Engineers**
26 **New Orleans District**
27 **Mississippi Valley Division**
28



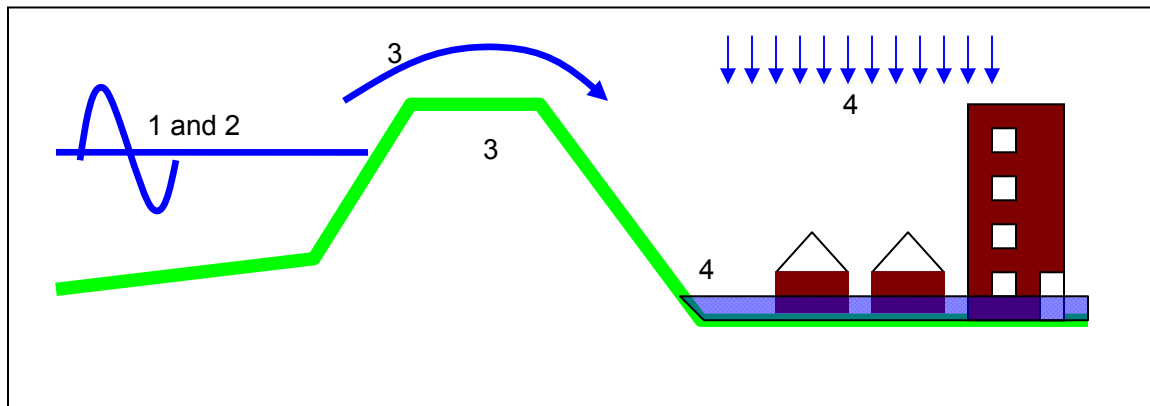
Volume I - Background and Methodology

29
30

31 **SUMMARY**

32 In the framework of LACPR the hydraulic analysis plays a key role in the cost-benefit analysis of
33 the alternatives in the various planning units. Each levee alternative affects the surge and the
34 waves during a storm in a different way. The differences in storm surge and wave characteristics
35 result in varying overtopping volumes and stage frequency curves. The stage frequency curves are
36 an important input for the economic analysis to estimate the damage in the economic sub basins,
37 and the levee heights need to be known for the cost estimates. This report describes the
38 methodology of the hydraulic analysis that has been followed to determine the exterior and interior
39 stages, and the levee heights. The results of this hydraulic analysis for the various planning units
40 are described in Volume 2 of this appendix. The use of this data within the economic analysis and
41 the cost estimates are described in separate appendices.

42
43
44



45
46

47 **Figure 1 - Schematic overview of the step-wise approach in the hydraulic analysis in the**
48 **framework of LACPR**

49

50 The hydraulic analysis of each alternative in LACPR consisted of the following consecutive steps
51 (see also Figure 1):

52
53
54
55
56
57

- 52 1. Numerical computations of surge levels and wave characteristics using ADCIRC, WAM and
53 STWAVE;
- 54 2. Frequency analysis using the JPM-OS method and the determination of exterior stage
55 frequency;
- 56 3. Determination of the levee heights and overtopping volumes;
- 57 4. Determination of the interior stages including rainfall;

58

59 To provide a range of alternatives for evaluation and to enable the economic evaluation it was
60 decided to evaluate each levee alignment alternative for different protection levels and event
61 frequencies. A levee design was made for three different levels of protection (100-year, 400-year,
62 1000-design year). Given the level of protection, the overtopping volumes were computed for four
63 return periods of the outside surge level and wave characteristics (100-year, 400-year, 1000-year
64 and 2000-year event). For all alternatives, the 10-year rainfall was added to the overtopping
65 volume to establish the interior stage frequency curve and pumping was taken into account.

66

67 The four steps in the hydraulic analysis are discussed in detail below.

68

69 **Step 1: Surge levels and wave characteristics**

70

71 The numerical computations for the surge levels and the wave characteristics were carried out with
72 the numerical models ADCIRC, for surge levels, and WAM/STWAVE, for the wave characteristics.
73 These models are state-of-the art models and have already been applied extensively during the
74 IPET and 100-year design study for the hurricane protection system around New Orleans. Two
75 basic ADCIRC modeling grids were developed to cover the southern coast of Louisiana. Several
76 wave grids were developed for STWAVE to compute the wave characteristics.

77

78 A base set of 56 hurricane conditions have been evaluated with the modeling suite
79 ADCIRC/STWAVE for the 2010 Base condition. The modeled storms are different in terms of the
80 hurricane tracks, minimum pressure, and radius amongst other parameters. The 2010 Base
81 condition consists of the existing condition with a levee system with a 100-year protection level
82 including the barrier at MRGO. The different levee alignments for the various alternatives (e.g.
83 barrier plan or West Bank alignment along GIWW) have been implemented in the model grids to
84 evaluate the behavior of the surge levels and waves. In addition, computations have been carried
85 out to evaluate the future effects of sea level rise and marsh improvement/degradation. For all of
86 the alternatives, the number of storms that were evaluated was reduced because of time
87 constraints.

88

89 **Step 2: Frequency analysis**

90

91 Based on the results from ADCIRC and STWAVE in step 1 a frequency analysis has been carried
92 out to determine the surge levels and wave characteristics for different return periods. The method
93 adopted was is the Joint Probability Method with Optimal Sampling (JPM-OS) that takes into
94 account the joint probability of forward speed, size, minimum pressure, angle of approach and
95 geographic distribution of the hurricanes. It needs to have a set of 152 storms to establish the
96 frequency curves for surge and waves, whereas the various alternatives were only run for 56 or
97 less storms. Results for the remaining storms were established using correlation techniques in
98 order to carry out the frequency analysis with the JPM-OS method.

99

100 The frequency analysis has resulted in stage frequencies for the exterior areas, i.e. the areas that
101 are not protected by the levees. Furthermore, this analysis has provided the surge levels and the
102 wave characteristics for different return periods along the levee system as needed for the levee
103 design and overtopping volumes in step 3.

104

105 **Step 3: Levee design and overtopping volumes**

106

107 For the levee designs the step-wise procedure that was used for the 100-year design elevations
108 has been followed in a slightly adapted way. In short, this procedure has been applied as follows in
109 LACPR:

110

- 111 • Use the surge level and wave characteristics at the levees for a given level of protection
112 (e.g. 100-year) and assume a simplified levee design for this planning effort, i.e. a levee

- 113 with a wave berm at the still water level and a constant slope near the crest of the levee of
114 1:4.
- 115 • Determine the overtopping rate using empirical formulations. A Monte Carlo Simulation
116 was adopted to compute the uncertainty in the overtopping rate given the uncertainties in
117 the hydraulic boundary conditions and the empirical coefficients in the overtopping
118 formulations.
 - 119
 - 120 • Establish the levee height in such a way that the overtopping rate is less than 0.1 cft/s per
121 ft with 90% confidence. The levee heights for the various alternatives have been used as
122 an input for the interior drainage analysis and costs estimates.

123
124 The overtopping volumes were computed using the information on the surge level hydrographs
125 from ADCIRC. Based on a statistical analysis, a correlation was established between the duration
126 of the surge and the maximum surge level. This correlation has been applied to compute the
127 overtopping rate during the storm assuming that the wave characteristics are constant around the
128 peak of the storm.

129 130 **Step 4: Interior stage frequency**

131
132 The final step was to determine the interior stage frequency for each economic sub basin. Each
133 sub basin has been schematized as a box model for which a stage-storage curve has been
134 established. This information has been extracted from existing rainfall-runoff models or from
135 LIDAR data for these areas. The interior stage frequency has been based on the sum of the
136 overtopping volume from step 3 together with the 10-year rainfall in the sub basin. The effect of
137 pumping has been taken into account if applicable. Where economic sub basins join, flow of water
138 has been allowed to occur above define thresholds.

139
140

141	CONTENTS		
142			Page
143	SUMMARY		I
144	CONTENTS		IV
145	LIST OF FIGURES		VI
146	LIST OF TABLES		VII
147	1	INTRODUCTION	1
148	1.1	Background	1
149	1.2	Purpose of LACPR	1
150	1.3	Planning area	1
151	1.4	Hydraulic evaluation	2
152	1.5	Report outline	4
153	2	SURGE AND WAVE MODELING	6
154	2.1	Description of the modeled hurricanes	7
155	2.2	Atmospheric-Hydrodynamic Modeling System	9
156	2.3	Modeling validation	14
157	2.4	Description of alternatives	17
158	2.5	Storm selection	26
159	2.6	Point sets	30
160	3	FREQUENCY ANALYSIS WITH JPM-OS METHOD	33
161	3.1	JPM-OS method	34
162	3.2	Fit procedure for surge levels	36
163	3.3	Fit procedure for wave characteristics	40
164	3.4	Validity of fit procedure	43
165	4	DETERMINATION OF LEVEE HEIGHTS	45
166	4.1	Step-wise design approach	46
167	4.2	Design assumptions	47
168	4.3	Uncertainty analysis	50
169	5	OVERTOPPING RATES	52
170	5.1	Parametrical description of hydrographs	52
171	5.2	Overtopping volumes	56
172	6	INTERIOR DRAINAGE	60
173	6.1	Storage areas	60
174	6.2	Methodology	64
175	6.3	Rainfall	65

176	6.4	Overtopping	66
177	6.5	Pumping	67
178	6.6	Flood Volumes and Stage Frequencies	68
179	7	REFERENCES	69
180	ANNEXES		70
181			

182 **LIST OF FIGURES**

183

184 Figure 1.1 - LACPR planning area 2

185 Figure 1.2 - Schematic overview of the step-wise approach in the hydraulic analysis in the framework of

186 LACPR 3

187 Figure 1.3 - Flow diagram of hydraulic analysis in LACPR framework (in blue) 4

188 Figure 2.1 - Flow diagram of hydraulic analysis in LACPR framework 6

189 Figure 2.2 - Storm tracks for Eastern Louisiana. 8

190 Figure 2.3 - Modelling system with the four modelling components and their interaction..... 10

191 Figure 2.4 - Example of the wind field of one storm at landfall from the entire suite of 152 storms. This

192 specific storm has a minimum pressure of 900 mbar and a maximum radius of 17 nautical

193 miles..... 11

194 Figure 2.5 - STWAVE Grid coverage 12

195 Figure 2.6 - ADCIRC Grid coverage..... 13

196 Figure 2.7 - Comparison between High water marks and ADCIRC results for Katrina..... 15

197 Figure 2.8 - Alignment alternatives LA East-A and LA East-B..... 20

198 Figure 2.9 - Alignment alternatives LA East-C and LA East-D. 21

199 Figure 2.10 - Alignment alternatives LA West-A and West-B. 25

200 Figure 2.11 - Alignment alternatives LA West-C (upper panel) and Plaquemines-1 (lower panel)..... 26

201 Figure 2.12 - Relative Water Level Increases by Reach. 26

202 Figure 2.13 - Examples of storm tracks (storms 56 and 87)..... 28

203 Figure 2.14 - Point sets (East Grid)..... 31

204 Figure 2.15 - Point sets (West Grid)..... 32

205 Figure 3.1 - Flow diagram of hydraulic analysis in LACPR framework 33

206 Figure 3.2 - Numerical results at Lake Pontchartrain (upper panel) and MRGO (lower panel) from

207 ADCIRC and STWAVE (Base condition 2007). The marks (o, x, +) represent 152 storm

208 results..... 35

209 Figure 3.3 - Correlation between maximum surge levels at Lake Pontchartrain for Base condition 2010

210 and Base condition 2007..... 37

211 Figure 3.4 - Correlation between maximum surge levels at Lake Pontchartrain for Base condition 2010

212 and Base condition 2007..... 38

213 Figure 3.5 - Effect of maximum surge level at Lake Pontchartrain (grid 2010 East A) with fit for all storms 39

214 Figure 3.6 - Effect of maximum surge level at Lake Pontchartrain (grid 2010 East A) with fit for different

215 storm tracks..... 40

216 Figure 3.7 - Wave characteristics at Lake Pontchartrain for 56 storms 42

217 Figure 3.8 - Wave characteristics at MRGO for 56 storms 43

218 Figure 3.9 Comparison between the 1% still water levels based on the full storm set of 152 storms and

219 based on the 42 storms using the fit procedure..... 44

220 Figure 4.1 - Flow diagram of hydraulic analysis in LACPR framework 45

221 Figure 4.2 - Simplified levee cross section in LACPR evaluation 47

222 Figure 4.3 - Result for 100-year design height along MRGO levee (Base condition 2010). 51

223 Figure 5.1 - Flow diagram of hydraulic analysis in LACPR framework 52

224 Figure 5.2 - Example of hydrograph from ADCIRC results..... 53

225 Figure 5.3 - Real hydrograph from ADCIRC (in red) and parameterized hydrograph (in red) 55

226 Figure 5.4 - Normalized surge from ADCIRC plotted against the normalized parameterized surge 55

227 Figure 5.5 - Width of the hydrograph plotted against the maximum surge level. Crosses indicate the
228 different storms, the lines are the fit through the data points 56
229 Figure 5.6 - Overtopping rates for different return periods (100-year, 400-year, 1000-year and 2000-
230 year) at a level with a 1% design elevation 58
231 Figure 6.1 - Flow diagram of hydraulic analysis in LACPR framework 60
232 Figure 6.2 - Subunits Planning Unit 1 61
233 Figure 6.3 - Subunits Planning Unit 2 62
234 Figure 6.4 - Planning Subunits and Drainage Areas for Planning Unit 3a 62
235 Figure 6.5 - Planning Subunits and Drainage Areas for Planning Unit 3b 63
236 Figure 6.6 - Planning Subunits and Drainage Areas for Planning Unit 4 63
237 Figure 6.7 - Principle water system 64
238 Figure 6.8 - Internal planning subunit and stage storage relationship 65
239 Figure 6.9 - Standardized rainfall hydrograph 66
240 Figure 6.10 - Rainfall Hydrograph of NEO (design standard 100 year en return period 100 year (left) and
241 return period 400 year (right))..... 67
242 Figure 6.11 - Water volumes flowing between adjacent sub-units..... 68
243
244
245

LIST OF TABLES

247
248 Table 2.1 - Saffir-Simpson Classification (source: en.wikipedia.org)..... 7
249 Table 2.2 - Description of the alternatives and the number of storms modelled in LACPR framework..... 16
250 Table 2.3 - Detailed overview of measures in LA East grid models for Planning Unit 1 and 2. 19
251 Table 2.4 - Detailed overview of measures in LA West grid models for Planning Unit 3a/b and 4. 23
252 Table 2.5 - Selected storms for West alternatives. 29
253 Table 2.6 - Selected storms for the East alternatives 30
254 Table 2.7 - Overview of point sets used 30
255 Table 4.1 - Stepwise approach..... 46
256
257
258
259
260

261 **1 INTRODUCTION**

262 **1.1 Background**

263 Hurricanes have caused extensive damage to coastal parishes in Louisiana since the time of
264 earliest settlement. Over 40 hurricanes have impacted the coast of Louisiana within the last
265 century. From 1900 to 1950, ten major storms (27 total) struck Louisiana’s coastline killing 671
266 people. After 1950 the National Weather Service started naming storms and since then thirteen
267 hurricanes (Flossy, Audrey, Betsy, Camille, Carmen, Juan, Andrew, Georges, Isidore, Lili, Cindy,
268 Katrina, and Rita) have caused extensive destruction and loss of life in Louisiana. In 2005 alone,
269 Hurricanes Katrina and Rita, which both grew to powerful Category 5 strength as they approached
270 the Louisiana coast, claimed over 1,500 lives and could finally result in a total economic impact in
271 the hundreds of billions of dollars within the State.

272
273 In response to the devastating destruction caused by Hurricanes Katrina and Rita, both the
274 Louisiana legislature and the United States Congress provided legislative directives to investigate
275 and integrate flood control, hurricane risk reduction and coastal restoration for South Louisiana.
276 Development of plans to meet these directives is being undertaken as a joint effort of the multiple
277 parts of the Federal government and in partnership with the State of Louisiana. Although the State
278 and Federal legislative directives are not identical, they do share the common fundamental
279 objectives of considering the complete spectrum of landscape level uses and needs, and of
280 incorporating a full range of potential risk reduction measures into an integrated plan. This plan will
281 be evaluated based on its benefits in reducing storm damage to coastal communities and
282 infrastructure, as well as for its ecosystem impacts and benefits.

283
284 Authorization and direction for such a plan, the Louisiana Coastal Protection and Restoration
285 (LACPR) project, was granted in November 2005. The U.S. Congress has directed the Secretary
286 of the Army, through the Chief of the U.S. Army Corps of Engineers to “conduct a comprehensive
287 hurricane protection analysis and design to develop and present a full range of flood control,
288 coastal restoration, and hurricane protection measures and the Secretary shall consider providing
289 protection for a storm surge equivalent to a Category 5 hurricane and the analysis shall be
290 conducted in close coordination with the State of Louisiana.”

291
292 **1.2 Purpose of LACPR**

293 The purpose of the LACPR effort is to identify risk reduction measures that can be integrated to
294 form a system that will provide enhanced protection of coastal communities and infrastructure, as
295 well as for restoration of coastal ecosystems. The scope of the LACPR technical report is to
296 address the full range of flood control, coastal restoration, and hurricane protection measures
297 available, including those needed to provide comprehensive “Category 5” protection.

298
299 **1.3 Planning area**

300 The LACPR planning area stretches across Louisiana’s coast from the Pearl River, on the
301 Mississippi border, to the Sabine River, on the Texas border. The planning area is comprised of
302 two wetland-dominated ecosystems, the Deltaic Plain of the Mississippi River and the closely
303 linked Chenier Plain, both of which are influenced by the Mississippi River. The Deltaic Plain

304 contains ecologically important estuaries fronted by numerous barrier islands and headlands,
305 including the Chandeleur Islands, Barataria Basin Barrier Islands, and Terrebonne Basin Barrier
306 Islands. The Chenier Plain contains important diverse wildlife and fisheries habitats that extend
307 from the Teche/Vermilion Bays to Louisiana’s western border with Texas, and is characterized by
308 several large inland lakes, marshes, Cheniers (oak ridges), and coastal beaches.
309

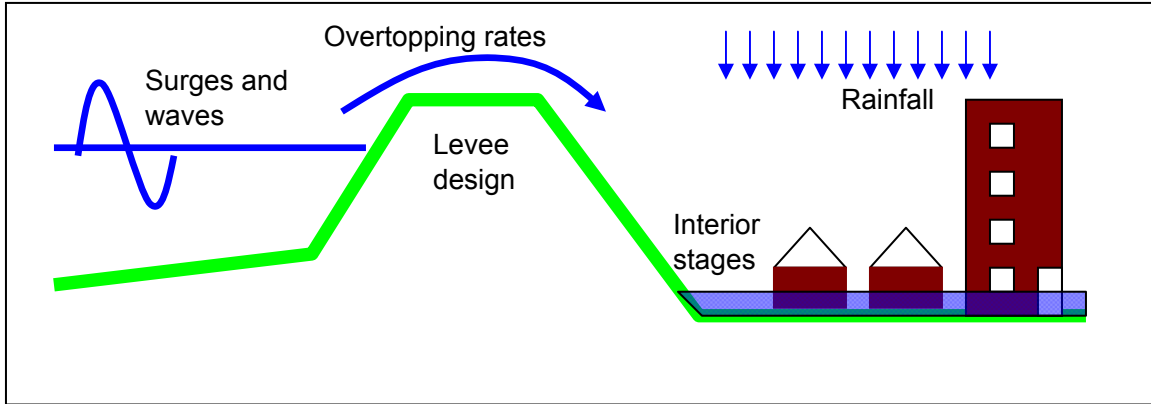


310
311 **Figure 1.1 - LACPR planning area**

312
313 **1.4 Hydraulic evaluation**

314 This report describes the methodology for the hydraulic evaluation of the alternatives within the
315 framework of the LACPR project. This hydraulic analysis has been visualized in **Figure 1.2**. Each
316 levee alternative affects the propagation of the surge and the waves during a storm in a different
317 way. The differences in storm surge and wave characteristics result in varying levee designs,
318 overtopping volumes and stage frequency curves. The stage frequency curves are an important
319 input for the economic analysis to estimate the damage in the economic sub basins, and the levee
320 heights need to be known for the cost estimates. Hence, the hydraulic analysis plays a key role in
321 the cost-benefit analysis.

322
323
324
325



326
327
328
329
330
331
332
333
334
335

Figure 1.2 - Schematic overview of the step-wise approach in the hydraulic analysis in the framework of LACPR

336
337
338
339
340
341
342
343

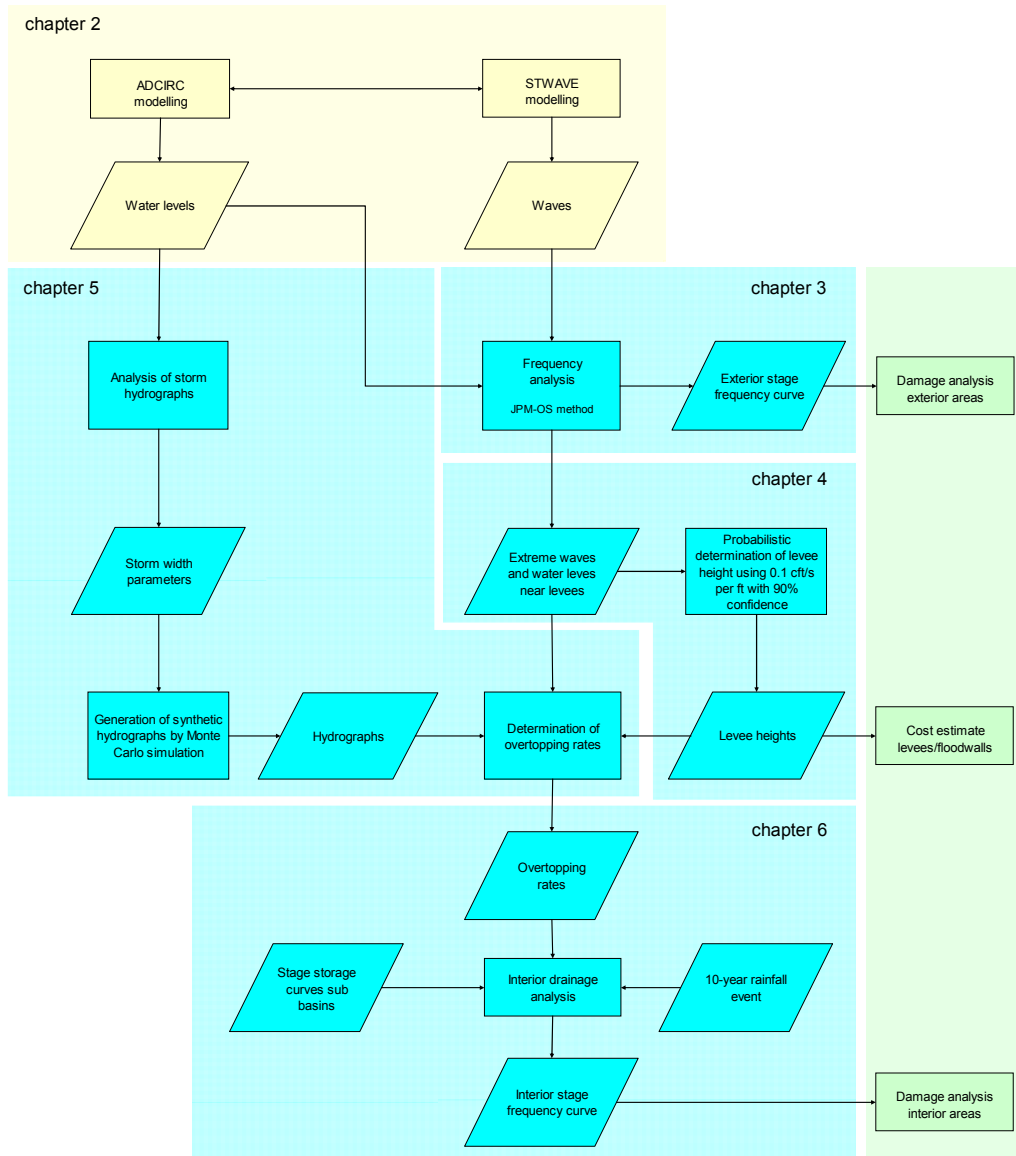
The flow chart below (see Figure 1.3) visualizes in detail the various steps to facilitate the hydraulic evaluation of the various alternatives. To evaluate various alternatives numerical modeling with ADCIRC and STWAVE was carried out to simulate the water levels and wave heights (in yellow). The water levels and the waves are used in the hydraulic analysis to determine the levee heights, the exterior stage frequency curves and the interior stage frequency curves (in blue). Additionally, economic damage assessments, levee construction cost estimate as well as risk and reliability tasks can be performed with the resulting datasets (in green).

344
345
346
347
348
349
350
351
352
353

To provide a range of alternatives for evaluation and to enable a robust economic evaluation, it was decided to evaluate each levee alignment alternative for different protection levels and event frequencies. A levee design was made for three different levels of protection (100-year, 400-year, 1000-year). For each level of protection, the overtopping volumes were computed for four return periods of the outside surge level and wave characteristics (100-year, 400-year, 1000-year and 2000-year). For all alternatives, the 10-year rainfall was added to the overtopping volume and used to establish the interior stage frequency curve.

The work as presented in Chapter 3 – 6 of this report has been done from June to September 2007 as cooperation between the United States Army Corps of Engineers, New Orleans District and Haskoning Inc¹. The methods and results as described within this report are limited to the technical aspects only and no economic evaluation is provided. The main deliverables of this study are the stage frequency curves and the design heights of the levees. The stage frequency curves will be used for the economic evaluations and the damage studies. Note that the methodologies described within this report are developed to enable the relative comparison of various design alternatives. More detailed study will be needed for doing actual design.

¹ Chapter 2 is added to this report to present the complete picture of the hydraulic analysis in the framework of LACPR. The work as presented in Chapter 2 summarizes the result of a combined effort of FEMA and USACE, universities and various consultancy firms.



354
355
356
357
358
359

Figure 1.3 - Flow diagram of hydraulic analysis in LACPR framework (in blue)

1.5 Report outline

360 The outline of this report follows the structure of the hydraulic analysis in Figure 1.3. Chapter 2
361 briefly describes the numerical modeling with ADCIRC and STWAVE. The background to the
362 processes, the modeled alternatives and summaries of the model output are presented. The focus
363 of Chapter 3 is to describe the frequency analysis undertaken to come up with the surge levels
364 and wave characteristics for different return period events. Chapter 4 deals with the levee design
365 procedure that has been applied within the LACPR framework and chapter 5 discusses the

366 determination of the overtopping volumes. The development of the interior stage frequency curves
367 is described in Chapter 6. This report closes with conclusions and recommendations in Chapter 7.

368 **2 SURGE AND WAVE MODELING²**

369 The surge level and wave computations with an atmospheric-hydrodynamic modeling system form
 370 the basis of the hydraulic analysis within the framework of LACPR (Figure 2.1). The main
 371 components and the validation of this modeling process are briefly summarized in Section 2.1 and
 372 Section 2.2. For more detailed information, the reader is referred to various earlier studies in which
 373 this modeling suite was applied (IPET, 2007; FEMA, 2007). The LACPR effort evaluates several
 374 alternative storm surge protection systems using many levee alignments. For each of these
 375 alternatives, a model grid has been created to model the system and provide results from which
 376 levee heights can be determined. These model grids are discussed in Section 2.3. Section 2.4
 377 describes the selection of hurricanes that have been evaluated for the alternatives because it was
 378 impossible to run all hurricanes for all alternatives. Finally, the output locations and results of the
 379 modeling system at these points that have been used for LACPR are summarized in Section 2.5.
 380 These results are input into the frequency analysis (Chapter 3) and the determination of the
 381 overtopping volumes (Chapter 5).

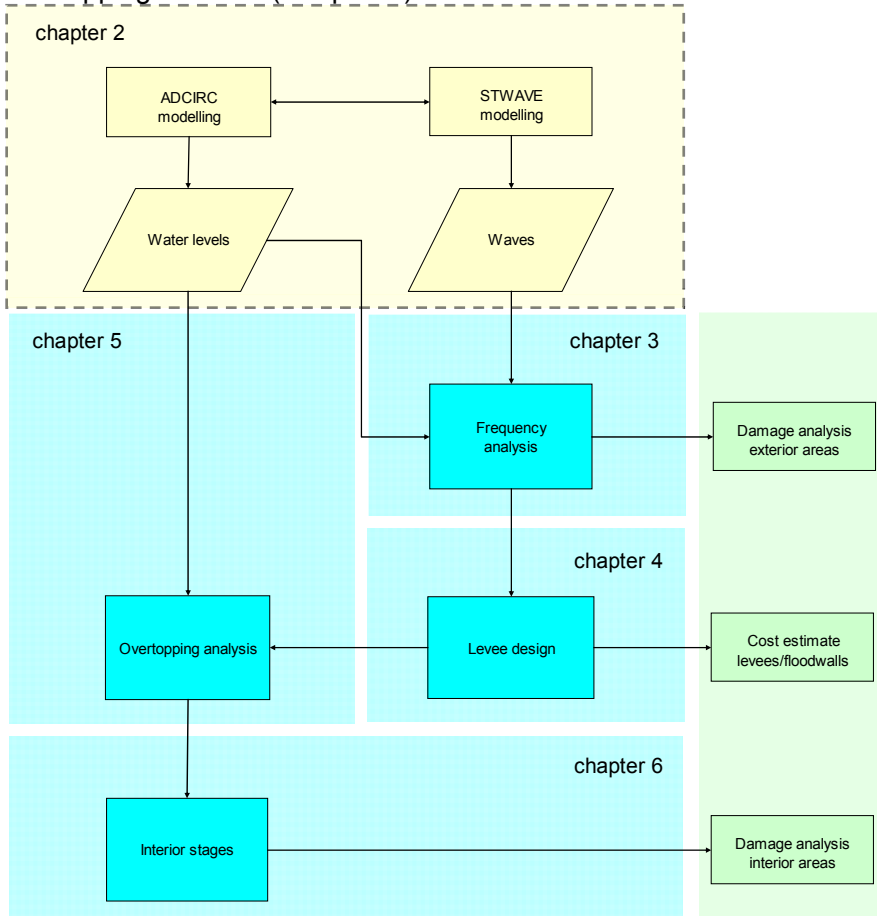


Figure 2.1 - Flow diagram of hydraulic analysis in LACPR framework

² The work as presented in Chapter 2 summarizes the result of a combined effort of FEMA and USACE, universities and various consultancy firms. Section 2.1 – 2.5 of this Chapter were written by the ADCIRC/STWAVE team (Joannes Westerink, Mary Cialone, Allison Sleith, John Atkinson, Jay Ratcliff).

382 **2.1 Description of the modeled hurricanes**

383 The authorization of the LACPR project states that “.....*the Secretary shall consider providing*
384 *protection for a storm surge equivalent to a Category 5 hurricane within the project area and may*
385 *submit reports on component areas of the larger protection program for authorization as soon as*
386 *practicable.....*”. Previously, it was believed that a single parameter, the Saffir-Simpson intensity
387 scale (see Table 2.1), dictated the potential surge levels that a storm could generate. Based on
388 this concept, previous design-storm concepts used terms such as a “Category 5 Storm” to denote
389 a particular class of storm.

390
391 **Table 2.1 - Saffir-Simpson Classification (source: en.wikipedia.org).**

Saffir-Simpson Category	Wind speeds (m/s)	Pressure (mbar)	Historical examples at the Atlantic Ocean
1	33-42	980	Jerry (1989), Danny (1997)
2	43-49	965-979	Diana (1990), Erin (1995)
3	50-58	945-964	Roxanne (1995), Isidore (2002)
4	59-69	920-944	Galveston (1900), Betsy (1965), Iris (2001), Charley (2004)
5	> 70 m/s	< 920	Camille (1969), Katrina (2005), Rita (2005)

392
393 Recent analyses have clearly demonstrated that coastal surge levels are significantly affected by
394 storm size as well as storm intensity (Saffir-Simpson category). It is now recognized that a small
395 “Category 5 Storm” will generate a smaller surge than a large “Category 3 Storm” in coastal areas
396 where the offshore slope is very small, such as along much of the Louisiana-Mississippi coastline.
397 Thus, it is important to consider a range of storm sizes in conjunction with a fixed “Category 5”
398 intensity, in order to represent the actual range of conditions that a “Category 5 Storm” can
399 generate. This insight changes the manner in which a storm must be specified for planning and
400 design purposes.

401
402 A USACE and FEMA consensus procedure was developed in order to define the relevant storms
403 that affect Southern Louisiana (FEMA, 2007). It was agreed that the Joint Probability Method
404 (JPM) allows for the richest storm set but that many of the storms are either irrelevant or have a
405 very low probability of occurrence due to dependencies in the parameter space. A set of 152
406 storms were developed for eastern Louisiana by combining the “probable” combinations of central
407 pressure, radius to maximum winds, forward speed, angle of track relative to coastline, and track.
408 Tracks were defined by 5 primary tracks and 4 secondary tracks (see Figure 2.2). Central pressure
409 and radius to maximum relationships were also developed that modify the storms as the coastline
410 is approached. A storm matrix was developed based on these parameters and proposed to FEMA
411 and USACE for concurrence. A concurrent set of 152 storms was developed for western
412 Louisiana.
413

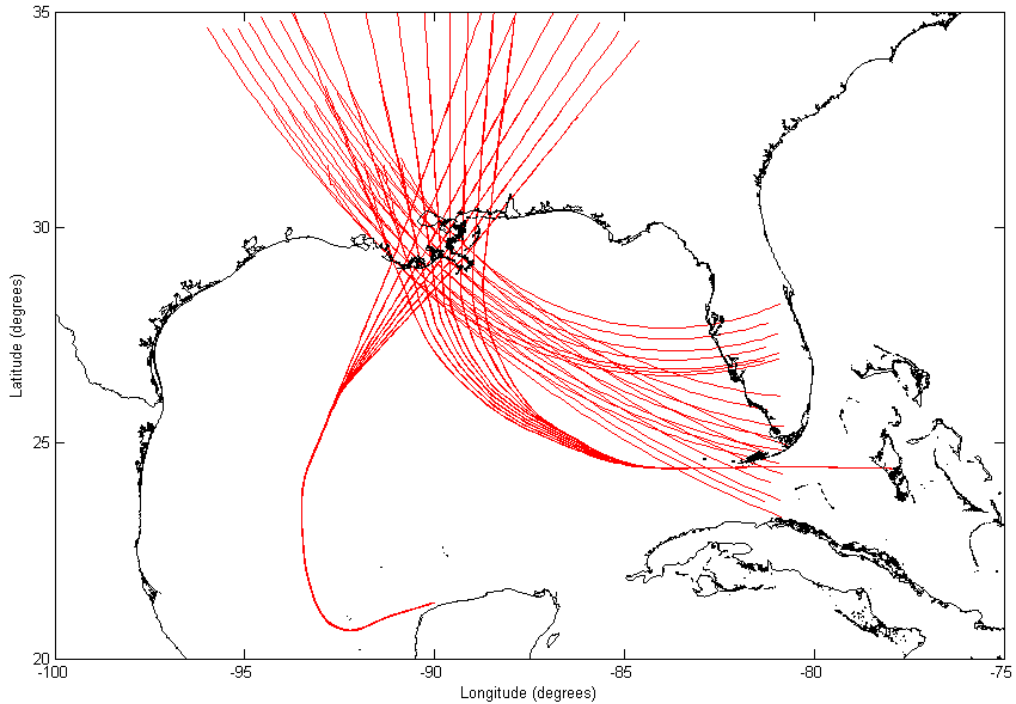


Figure 2.2 - Storm tracks for Eastern Louisiana.

414

415

416

417

418

419

420

421

422

423

424

425

426

427

428

429

430

431

432

433

434

435

The storm set of 152 storms contains 50 “Category 3 storms”, 52 “Category 4” storms and 50 “Category 5” storms. As discussed above, these subsets of storms are classes of storms that can result in different hydrodynamic behavior depending on the storm size and other factors. The following ranges of storm sizes are considered in the set with 152 storms:

- Category 3: 11 – 35 nautical miles
- Category 4: 8 – 25 nautical miles
- Category 5: 6 – 21 nautical miles

The probability of occurrence of the 152 storms covers a frequency range between approximately 1/50 yr and 1/5,000 yr.

In the framework of LACPR, hydraulic events with different return periods have been chosen as a basis for evaluation (and not the Saffir-Simpson Scale). These events are: 100-year event, 400-year event, 1,000-year event and 2,000-year event. The 100-year event has been chosen because that return period serves as a basis for the current design effort the Hurricane Protection System. The 400-year event is a proxy for Katrina, because this is the estimated return period for this hurricane (see Resio et al., 2007). The 1,000-year and 2,000-year event are chosen based on practical considerations. The maximum frequency of the storm set is approximately 5,000 year. The 1,000 year and 2,000 year events were considered appropriate choices to have enough coverage in the storm set. Note that all these events cover different “Cat 5 hurricanes” with increasing storm size. Apart from this, an additional analysis was done regarding the so-called

436 Maximum Possible Hurricane (MPI). Appendix B describes the background and characteristics of
437 the MPI, and some preliminary results with the MPI for the Louisiana Coastal area.
438

439 The storm set of 152 storms has been used as a starting point to analyze the surge levels and the
440 waves at the Louisiana coastline. The setup and interaction between the various atmospheric and
441 hydrodynamic models to compute the actual surge levels and waves is the topic of the next
442 section.
443

444

445 **2.2 Atmospheric-Hydrodynamic Modeling System**

446 In pursue of a common technical framework of al Federal Agencies involved in assessing hurricane
447 related threats to coastal communities, an atmospheric-hydrodynamic modeling system has been
448 implemented. The goal of this hydrodynamic model development has been to implement a
449 simulation capability that represents the basic physics of the system as it is observed and that
450 does not require ad hoc tuning. Therefore the hydrodynamic models should define the physical
451 system as it exists and should consider wind, atmospheric pressure, short period wind waves,
452 tides, and riverine flows in a comprehensive way. In order to achieve the required accuracy, a
453 sequence of state of the art, well verified and validated wind, short period wind wave and coastal
454 circulation models were coupled together as an atmospheric-hydrodynamic modeling system and
455 applied to Southern Louisiana and Mississippi.
456

457 The modeling suite consists of four major components:

- 458 • Wind and pressure model (PBL)
- 459 • Surge model (ADCIRC)
- 460 • Deep water wave model (WAM)
- 461 • Shallow water wave model (STWAVE)

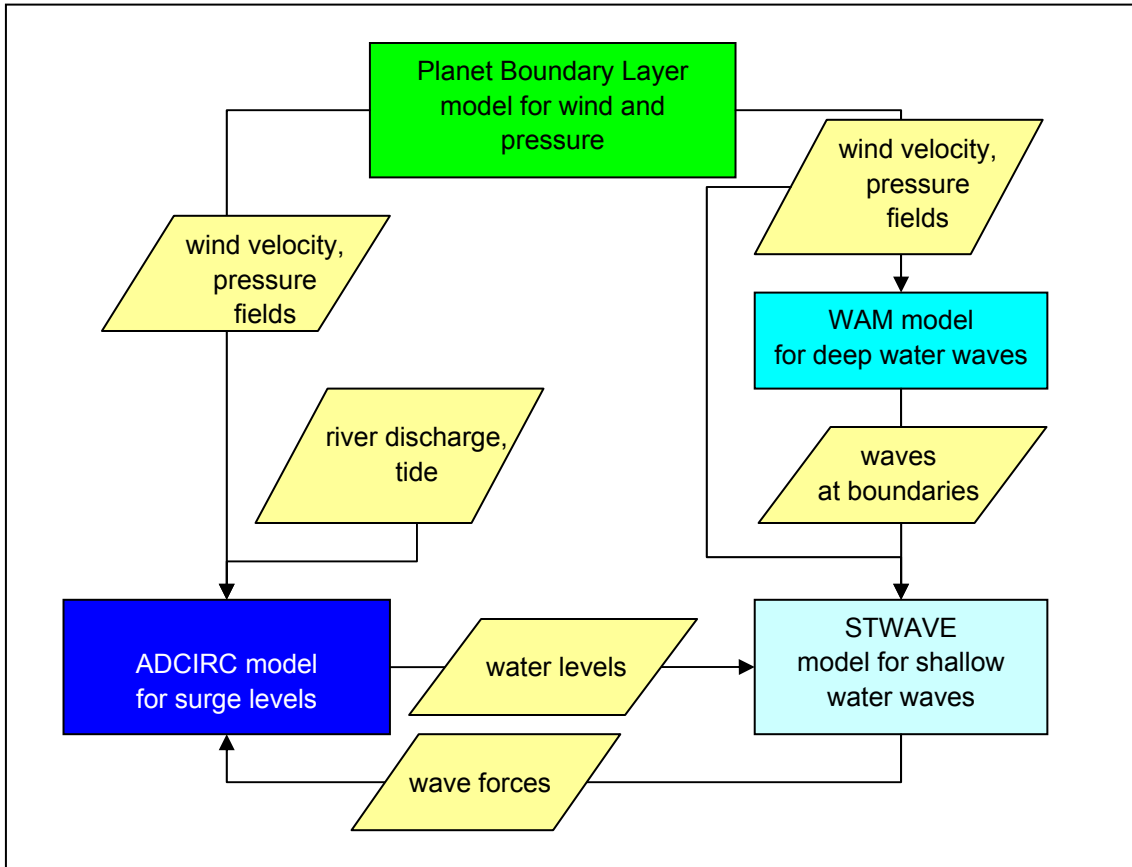
462

463 The coherence and interaction between these models is visualized in Figure 2.3.
464

465 The first component in the modeling sequence is the wind and atmospheric pressure field model.
466 For hindcasting historical storms, kinematic H*WIND and IOKA models that use data assimilation
467 methods in order to define wind fields and pressure decay relationships in conjunction with
468 observational data were employed. For synthetic hurricanes in the statistical storm set, a dynamic
469 wind model, the Planetary Boundary Layer (PBL) model was applied. A comparative analysis was
470 done between the PBL and Hurricane Boundary Layer (HBL). Models were run to determine the
471 best fit for this analysis and the PBL was selected. An example of one storm track and its wind
472 speed distribution is given in Figure 2.4.
473

474 It should be recognized that the wind forcing is not based on the ADCIRC grid geometry. Thus the
475 surge responses that maintain similar topography in different alternative grids (see section 2.4) will
476 then be almost exactly the same from the same storm. The final maximum peak surge levels are
477 the direct results of the wind forcing which is exactly the same in the base as well as the
478 alternative geometry simulations. An introduction of levee barriers can and does produce non-
479 similar results near and far from the geometry change. These changes are clearly seen in the
480 analysis point locations, especially where surges are greatly reduced with an alternative barrier in

481 place. The surge results at point locations within and outside of alternative levee configurations
482 are analyzed and used to quantify the economic benefits and also compute levee heights.
483



484
485 **Figure 2.3 - Modelling system with the four modelling components and their interaction.**
486
487

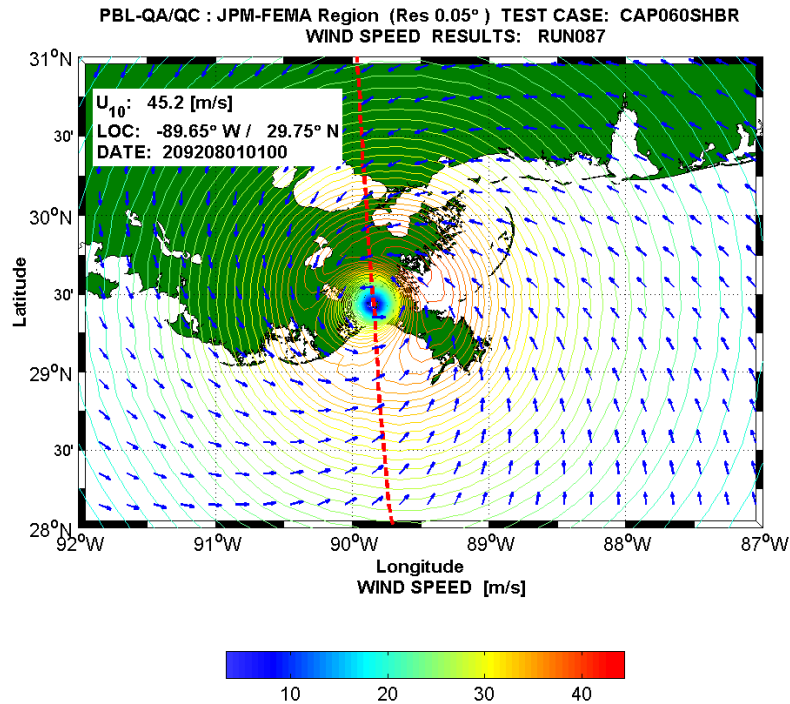


Figure 2.4 - Example of the wind field of one storm at landfall from the entire suite of 152 storms. This specific storm has a minimum pressure of 900 mbar and a maximum radius of 17 nautical miles.

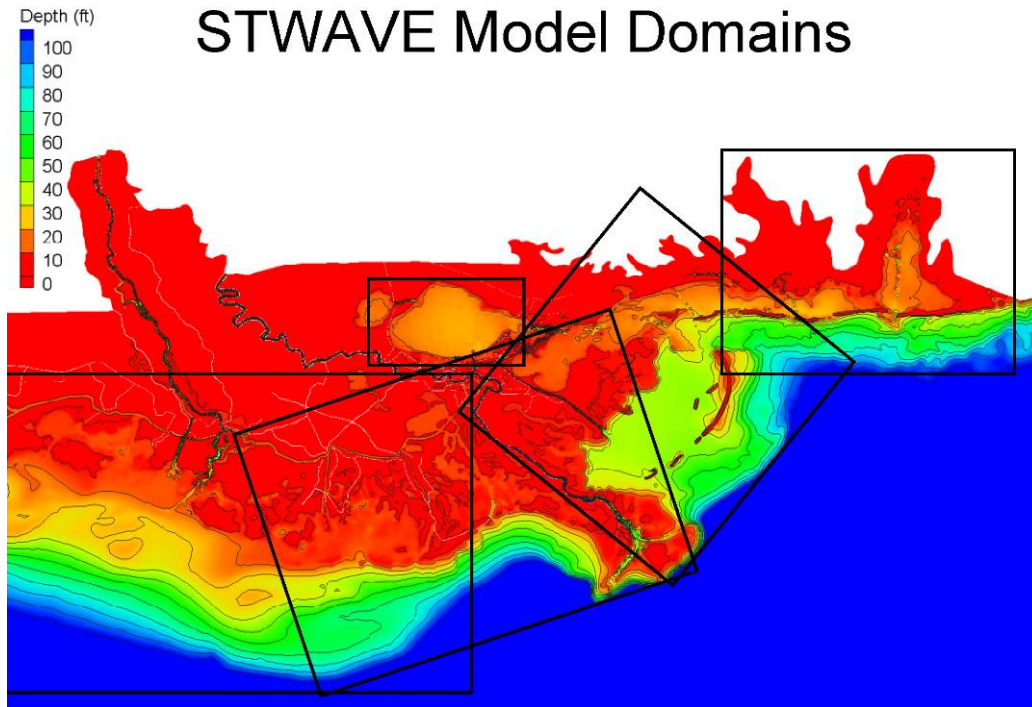
488

489 Once the winds are generated, the basin scale WAVE prediction Model (WAM) is run in order to
490 generate deep water waves in a Gulf of Mexico domain. These results are then applied as
491 boundary conditions in a finer scale regional WAM model that covers the continental shelf in
492 Southern Louisiana and Mississippi. The regional scale WAM results were then applied as
493 boundary conditions in four to five regional finer scale STWAVE models that provide
494 comprehensive coverage in Southern Louisiana. The STWAVE computations also included water
495 levels obtained from ADCIRC. The last component to be applied was the ADCIRC hydrodynamic
496 model, which is forced with wind and atmospheric pressure, wind wave radiation stresses from
497 STWAVE, riverine flows and tides for hindcast cases.

498

499 There is significant interaction between the various component models. The wind models produce
500 marine winds that are reduced for overland areas depending on the upwind roughness length
501 scales and the existence of canopies. However, once an area is inundated, the physical
502 roughness elements are subject to immersion, and the nominal roughness length scales are
503 subsequently reduced. Upon full immersion of the physical roughness elements, marine winds are
504 again applied.

505
506



507
508 **Figure 2.5 - STWAVE Grid coverage**

509

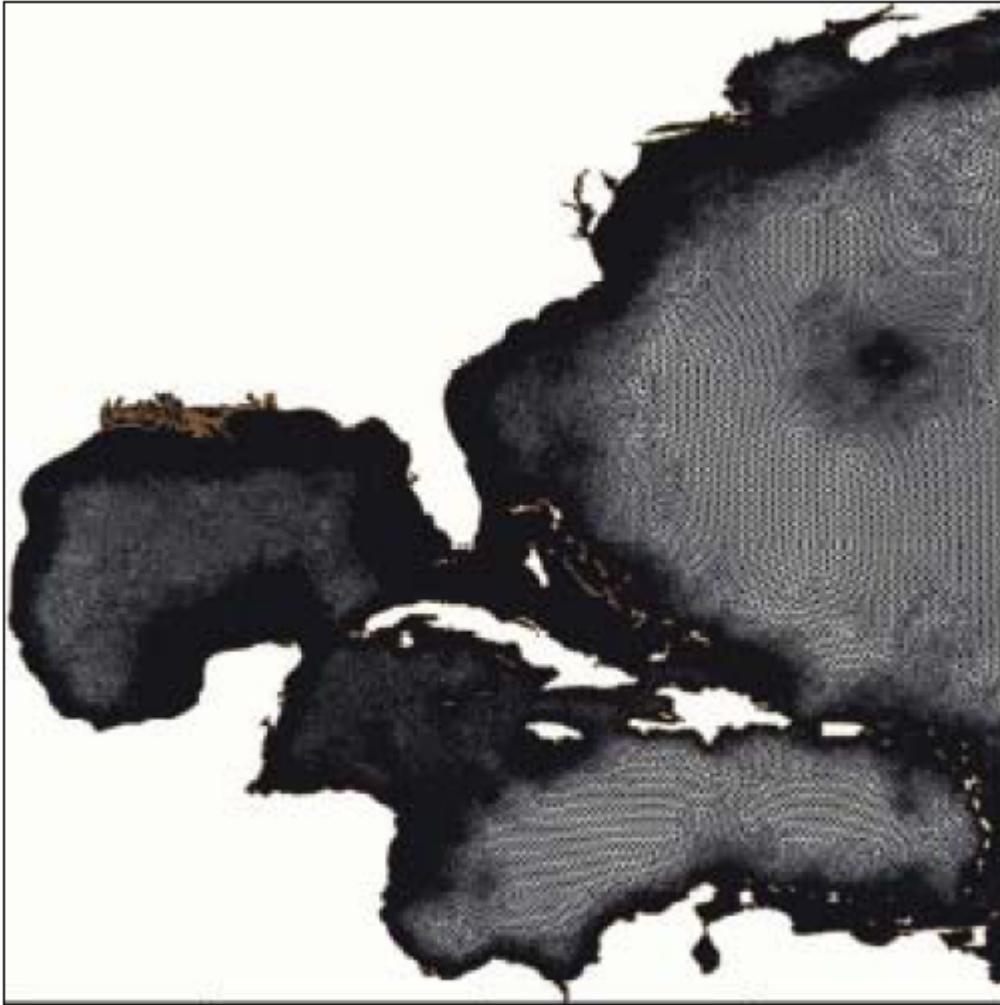
510 In addition to quantifying the wind waves themselves, wind-waves influence surge height with
511 wind-wave radiation stress forcing, modify bottom friction as well as influence the sea surface
512 roughness. Wind-waves reach shore prior to the peak surge driven by the strongest hurricane
513 winds, so combined wind and wind-wave surge builds up earlier than solely wind driven surge.
514 Furthermore, draw-down caused by winds coming from shore tends to be reduced by waves that
515 are still coming into shore. In this modeling system, the interaction between the wind-waves and
516 the surge is considered by applying wave radiation stress forcing. The effect on bottom friction or
517 the influence of waves on surface roughness as they affect air-sea interaction, are not included
518 since these effects are currently not well understood for hurricane conditions.

519

520 ADCIRC computations are forced with wave radiation stresses from the four to five localized
521 STWAVE grid domains for western Louisiana, west of the Mississippi river, east of the Mississippi
522 river, south of the Mississippi-Alabama coasts and within Lake Pontchartrain. The STWAVE
523 computations themselves were made with boundary forcing information from the regional WAM
524 model (which is forced with the Gulf wide WAM solution) as well as preliminary water level and
525 current information from ADCIRC. The preliminary ADCIRC simulations included all forcing
526 functions with the exception of the wave radiation stresses.

527

528



529
530 **Figure 2.6 - ADCIRC Grid coverage**

531
532 In addition to the effects of waves, there can be significant effects on surge due to coastal tides
533 and riverine currents. Because the tide range in Southern Louisiana is limited (about a 1.5 ft
534 range), the nonlinear impact on the high water is limited. Therefore when looking at the statistical
535 high water studies, tides can be linearly added in most areas without incurring significant error.
536 However previous studies indicate that the shape of the tides themselves is significantly affected
537 by the surge and therefore for purposes of model validation it is of significant interest to include
538 them.

539
540 Finally it is noted that significant currents flow through the Mississippi and Atchafalaya Rivers and
541 that these river currents strongly interact with tides and surge. For example, tides are substantially
542 attenuated as they propagate up the Mississippi River for high flow/stages compared to low
543 flow/stage. The level of interaction for storm surge wave propagating up the river is unknown but it
544 may be important given the depth of the river and the magnitude of the currents. ADCIRC
545 computations were therefore made simultaneously including wind, atmospheric pressure, riverine

546 flows, wave radiation stresses and for hindcast studies tides so that all significant coastal and
547 riverine currents could fully interact nonlinearly in the computation.

548
549 **2.3 Modeling validation**

550 The atmospheric-hydrodynamic modeling system was extensively validated. A brief summary of
551 the validation is given here. For complete documentation on system validation, the reader is
552 referred to earlier studies in which the modeling suite was applied (IPET 2006, FEMA 2007). The
553 surge model was validated for Hurricanes Katrina and Rita. These storms were selected due to the
554 unprecedented quality of the system definition, storm data, resulting high water marks (HWM) and
555 the vertical leveling information. In addition the extent of inland inundation was unprecedented
556 allowing for a unique opportunity to validate the effectiveness of modeling the effects of
557 topography, overland resistance, and decreases in overland wind speeds. The offshore wave
558 model was validated with data from Hurricanes Rita, Ivan, Camille, Katrina, and Andrew and the
559 wind model was validated with data from these storms plus Hurricane Betsy. The nearshore wave
560 model was compared to available data in Lake Pontchartrain acquired during Hurricane Katrina.

561
562 For the surge model, maximum surge levels were compared to between 80 and 204 open water
563 and inland HWM's. Estimated model errors are based on these comparisons and the estimated
564 accuracy of the HWM's themselves. As an example, Figure 2.7 presents a comparison between
565 the HWM's and the ADCIRC results for Katrina. The resulting modeling system error standard
566 deviations, which include inaccuracies in the kinematic wind models, air-sea momentum transfer,
567 wave radiation forcing, system definition and the hydrodynamic model itself, are estimated to be
568 1.47 ft (IPET HWM for Katrina), 1.36 ft (FEMA HWM for Katrina), and 1.21 ft (FEMA HWM for
569 Rita). This indicates that about 68% of the predictions can be expected to be within 1.3 ft and 95%
570 of the predictions can be expected to be within 2.6 ft of accuracy.
571

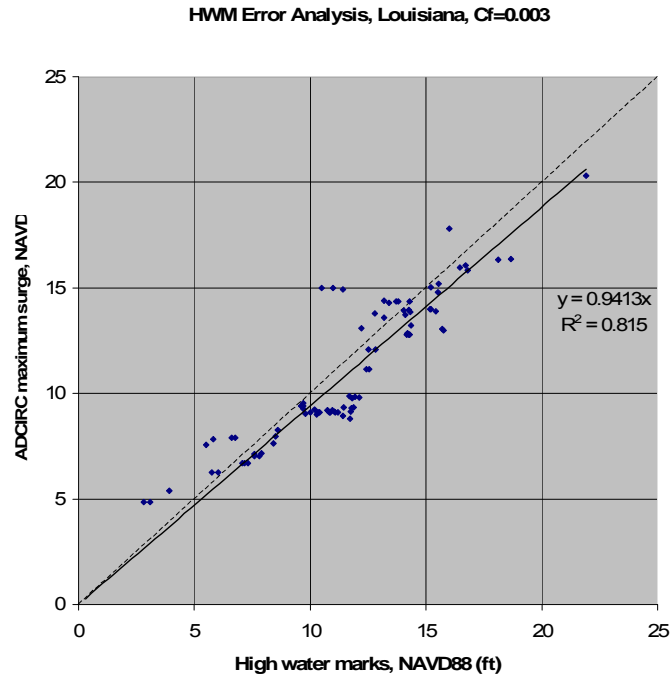


Figure 2.7 - Comparison between High water marks and ADCIRC results for Katrina.

572
573
574
575
576
577
578
579
580
581
582
583
584
585
586
587
588
589
590
591
592
593

Winds were verified to point source measurements. The WAM model was validated to data from NOAA NDBC buoys for Hurricanes Rita, Katrina, Ivan, and Andrew and data from the Ocean Data Gathering Project for Hurricane Camille. The waves were validated against peak wave conditions and time variations during a storms passage. Few data are available to validate the nearshore wave model for hurricanes in Louisiana. However, two small wave buoys were deployed in Lake Pontchartrain during Katrina and results compared favorably to these data.

After completion of the surge and wave modeling, an independent analysis examined results from several nearshore wave models and a variety of conditions with a focus on wave energy dissipation effects. Careful review of simulated wave heights at some locations inshore of coastal marsh areas indicates that the with-friction STWAVE results may underestimate the wave height. In the interest of conservatism and in the absence of field-verified values for friction coefficients due to bottom and vegetation interaction, the design process applied STWAVE simulations without frictional dissipation. Uncertainty in future location and density of coastal marshes, in part due to local subsidence and lack of appropriated funding for marsh restoration, provides additional rationale for excluding the effects of friction in the nearshore wave simulations. Future planned efforts to obtain the necessary field data along with more accurate estimates of future wetland conditions should provide improved quantitative estimates of friction coefficients suitable for design purposes.

594
595
596
597

Table 2.2 - Description of the alternatives and the number of storms modelled in LACPR framework.

Situation	Short description	Number of storms
2007 Base Case	Present levee system with upgrades and fixes after Katrina	152
2010 Base Case East	Levee system in 2011 with anticipated changes : barrier at MRGO and 1% levee heights around the entire system	56
East A	See 2010 Base case and full closure of Lake Pontchartrain along US90, full closure of IHNC/GIWW along west shore of Lake Borgne, full closure West Bank from between Bell Chasse to Larose along GIWW	48
East B	See 2010 Base case and weir closure of Lake Pontchartrain along US90 with structures in Chef and Rigolet tidal passes, full closure of IHNC/GIWW along west shore of Lake Borgne, weir closure West Bank from Bell Chasse to Larose along GIWW	42 / 152
East C	See 2010 Base case and weir closure of Lake Pontchartrain along US90 without structures in Chef and Rigolet tidal passes, full closure of IHNC/GIWW along west shore of Lake Borgne, weir closure West Bank from Bell Chasse to Larose along GIWW	48
East D	See 2010 Base case and isolating Lakes Pontchartrain and Borgne from each other by building a levee across Lake Borgne from Verret to Slidell, full closure West Bank from Bell Chasse to Larose along GIWW	40
Plaquemines	Option 1: Two spill ways in the levee system along Plaquemines	17
	Option 2: Full removal of levee system along Plaquemines to river embankment level	17
Barrier Islands	1) No barrier island	15
	2) Restored island	15
	3) Post-Katrina with forest	15
	4) Restored island with forest	15
Marsh Alternatives	1) Degraded marshes 50 years from now without increased action	174
	2) Restored marshes 50 years from now based on the New Orleans District's improved action plan	46
Sea level Rise (2007 Base case)	1) +1 ft sea level rise	9
	2) +2 ft sea level rise	9
	3) +3ft sea level rise	9
2010 Base Case West	Levee system in 2011 with anticipated changes : barrier at MRGO and 1% levee heights around the entire system	152
West-A	2007 Base Case and non-overtopping levee alignment from Larose to Golden Meadow and along GIWW	28
West-B	2007 Base Case with 100-year level alignment from Larose to Golden Meadow, a non-overtopping levee along the ridge and a ring levee alignment in the western part	28
West-C	2007 Base Case and non-overtopping levee alignment from Larose to Golden Meadow and along the ridge, and an overtopping levee along GIWW with a ring levee around Lake Charles	28

598
599

600 **2.4 Description of alternatives**

601 Various alternatives were evaluated with the modeling system and these results were applied
602 within the LACPR framework. The evaluated alternatives that were used in the LACPR framework
603 are summarized in Table 2.2. These alternatives are discussed more in detail in this paragraph.
604 The number of storms per alternative is also listed in Table 2.2. The storm selection for these
605 alternatives is discussed in the next paragraph.
606

607 *The 2007 Base Case* In order to update the 2005 hindcast grid to the system that exists in the
608 summer of 2007, levee definitions were updated to reflect the upgrades and system fixes that were
609 implemented as part of the USACE Task Force Guardian and by the USACE HPO and MVN. This
610 system was then run with the 152 storms for eastern Louisiana and 152 storms for western
611 Louisiana in order to define 100 and 500 year water levels and corresponding wave conditions.
612 This information serves as a base condition to which alternative levee systems, degraded or
613 improved barrier islands and marshes can be compared.
614

615 *The 2010 Base Case* In addition to evaluating the 2007 system, the proposed system
616 improvements anticipated for 2010 were investigated. This included raising levees across the
617 system as well as a closure of the combined MRGO/GIWW east of Paris Road. Note that the area
618 west of Larose to Golden Meadow is equal in both the 2007 and 2010 Base Case.
619

620 *Proposed LACPR East Levee System Alternatives in Planning Unit 1 and 2* In order to
621 understand the performance and implications of a variety of levee system improvements as
622 developed by the USACE and the State of Louisiana's CPRA, four east levee configurations were
623 studied for Planning Unit 1 and 2. The modeled levee configurations are the so-called East A, B, C
624 and D grid. The east configurations considered included a variety of alignments and elements that
625 are summarized in the Table 2-2. Figure 2.8 and Figure 2.9 present the levee alignments for East
626 A, B, C, D.
627

628 *Proposed LACPR West Levee System Alternatives Planning Unit 3 and 4* Similarly to the LA
629 East alignments, three different west alignments were examined with various configurations
630 including a solid line of protection that runs north of the bays and lakes of western Louisiana as
631 well as more localized ring levees that locally protect the population centers. The west
632 configurations considered included a variety of alignments and elements that are summarized in
633 the Table 2-3. Figure 2.10 and Figure 2.11 present the levee alignments for West A, B and C.
634

635 *Plaquemines Parish River and Back Levees (Plaquemines-1 and Plaquemines-2)* In order to
636 understand the influence of the Mississippi River levees and adjacent back levees in lower
637 Plaquemines Parish, spillways were incorporated into these levees (option 1) and the levees were
638 entirely eliminated (option 2). This study component was designed to understand how surge builds
639 up along these levees from Breton Sound and propagates towards New Orleans and Baton Rouge
640 in the Mississippi River. In addition, the effectiveness of building localized ring levees to provide a
641 higher level of protection in Lower Plaquemines Parish can be ascertained.
642

643 *Influence of Barrier Islands* A sensitivity analysis was performed to assess the impact of
644 bathymetric and frictional resistance changes for the barrier islands on ADCIRC-simulated peak

645 surge elevations and STWAVE-simulated waves. The sensitivity storm suite consisted of fifteen
646 storms of varying intensities and five barrier island configurations. The barrier island
647 configurations modeled were:

648

649 1) no barrier islands with open water Manning's n value = 0.02;

650 2) a restored barrier island configuration of 12 ft (NAVD88 2004.65) for Cat Island, Ship Island,
651 Horn Island, Petit Bois Island, and Dauphin Island and 6 ft (NAVD88 2004.65) for the Chandeleur
652 Islands;

653 3) the existing Post-Katrina degraded condition with a forest Manning's n = 0.15;

654 4) a restored barrier island configuration with a forest Manning's n = 0.15.

655

656 In general, raising the barrier islands caused a decrease in peak water level and wave energy
657 landward of the barrier islands when compared to the peak water level and wave energy for the
658 baseline Post-Katrina configuration and an increase in peak water level and wave energy seaward
659 of the barrier islands.

660

661 *Marsh Alternatives* The marsh alternatives included a predicted wetland definition 50 years
662 into the future with no increased action (NIA) taken and a restored/improved marsh condition. The
663 NIA condition was developed as part of the Coastal Louisiana Ecosystem Assessment and
664 Restoration (CLEAR) Program. The forecasting model developed by CLEAR predicts physical
665 processes, geomorphic features, water quality, and ecological succession.

666 Geomorphic/bathymetric changes are based on the likelihood of discretized regions changing from
667 open water to marsh or marsh to open water. The future condition of Coastal Louisiana predicted
668 by CLEAR, referred to as the degraded condition, in fact does predict degradation in Southern
669 Louisiana, but also predicts growth in the Atchafalaya basin and Plaquemines Parish. The CLEAR
670 future condition bathymetry was applied to the model grids and mesh and a series of storm
671 simulations was made.

672

673 The restored condition was developed by ERDC-CHL under the direction of the New Orleans
674 District's improved action plan. The District provided CHL with marsh creation locations and type,
675 freshwater diversion locations, and the volume of sediment diverted. CHL implemented these
676 restoration features into a marsh creation program and modifications were made to the
677 bathymetry, Manning's n values, and directional roughness lengths. These changes were applied
678 to the model grids, mesh, and frictional files and a series of storm simulations was made.

679

680 *Sea Level Rise Effects* Appendix A describes an analysis of the relative sea level rise in
681 detail for the Chenier Plain, the Delta Plain and the Pontchartrain Basin. The relative sea level rise
682 is estimated at 1 – 3 ft based on two future scenarios. Based on this analysis, it was decided to
683 evaluate the effect of sea level rise by applying a 1, 2, and 3-ft change in the vertical datum to the
684 2007 bathymetric configuration.

685

686 A subset of storms were selected from the 2007 simulations to target the 100-yr water level in
687 various areas and each storm was run with the 1 ft, 2 ft, and 3 ft datum changes (Figure 2.12).
688 Surge results indicate that the relative increase in water level for a given storm and location
689 decreases as the sea level rise increases. For instance, the response at Canaevon for storm 24
690 clearly shows this effect. A sea level rise of 1ft results in a 4.5ft rise, whereas a sea level rise of 3ft

691 results in a 2.5ft rise. The reason is that the amount of surge for a given fetch and wind speed is
692 inversely proportional to the depth. The West Bank and Canaervon areas showed the largest
693 variability in response due to the geometric complexity in these regions. Wave results indicate that
694 wave heights generally increase by less than 1 ft. Some areas, however, had 2-3 ft increases in
695 wave height. As with the surge, the rate of wave height increase is less for the larger values of
696 sea level rise.

697
698
699
700

Table 2.3 - Detailed overview of measures in LA East grid models for Planning Unit 1 and 2.

Unit	Planning Unit 1 (Lake Pontchartrain Basin)	Planning Unit 2 (Barataria Basin)
Model grid		
Base condition	Current levee system to 100-year level of protection/authorized grade (whichever is greater) in combination with barrier at MRGO	Current levee system to 100-year level of protection/authorized grade (whichever is greater)
East A	Modeling a non-overtopping levee adjacent to or on US 90 to close Lake Pontchartrain Modeling a non-overtopping levee along the west shore of Lake Borgne	Modeling non-overtopping levees along the GIWW as well a closures further north Modeling a non-overtopping levee following a southern alignment from Larose to Morgan City
East B	Modeling a weir at 12.5ft adjacent to or on US 90 and closure gates in the Rigolets and Chef Menteur Passes Modeling a non-overtopping levee along the west shore of Lake Borgne	Modeling an overtopping levee at 12.5ft along the GIWW as well a closures further north Modeling an overtopping levee at 100-year level following a southern alignment from Larose to Morgan City and a non-overtopping back levee along GIWW
East C	Modeling a non-overtopping levee adjacent to or on US 90 and openings in the Rigolets and Chef Menteur Passes Modeling a non-overtopping levee along the west shore of Lake Borgne	Modeling a non-overtopping levee following the US90 alignment with a central overtopping weir Modeling an overtopping levee at 100-year level following a southern alignment from Larose to Morgan City and a non-overtopping back levee along GIWW
East D	Modeling a non-overtopping levee across Lake Borgne from Verret to Slidell	Modeling non-overtopping levees along the GIWW as well a closures further north Modeling a non-overtopping levee following a southern alignment from Larose to Morgan City

701
702

703

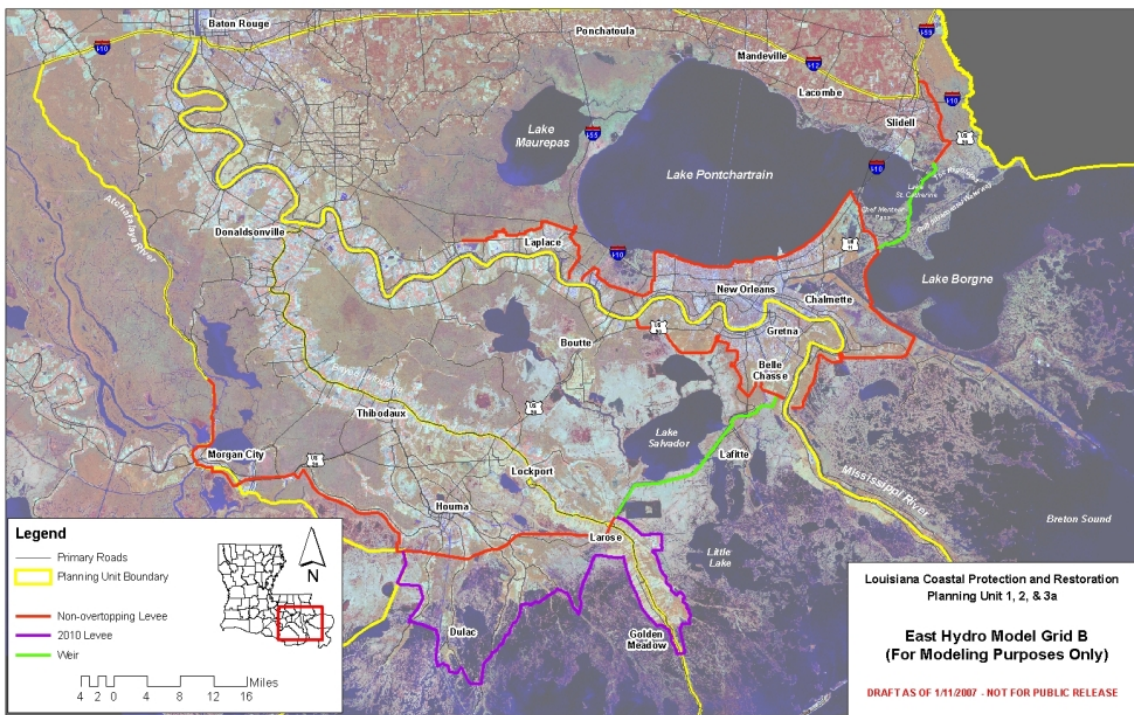
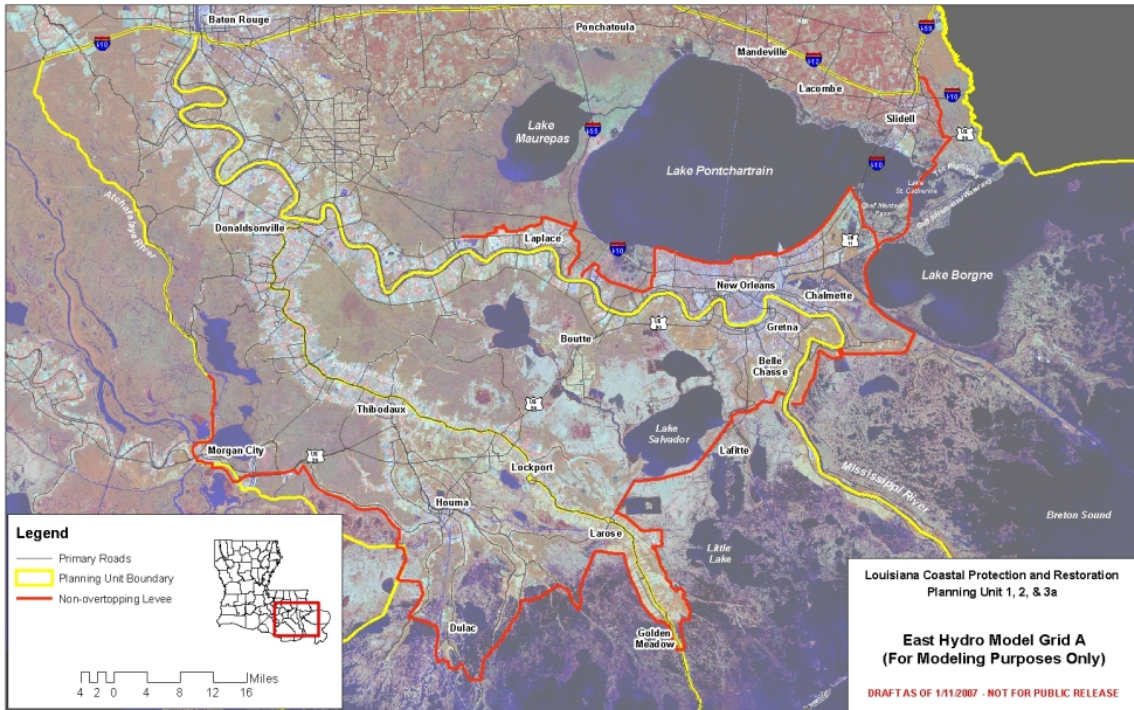


Figure 2.8 - Alignment alternatives LA East-A and LA East-B.

704

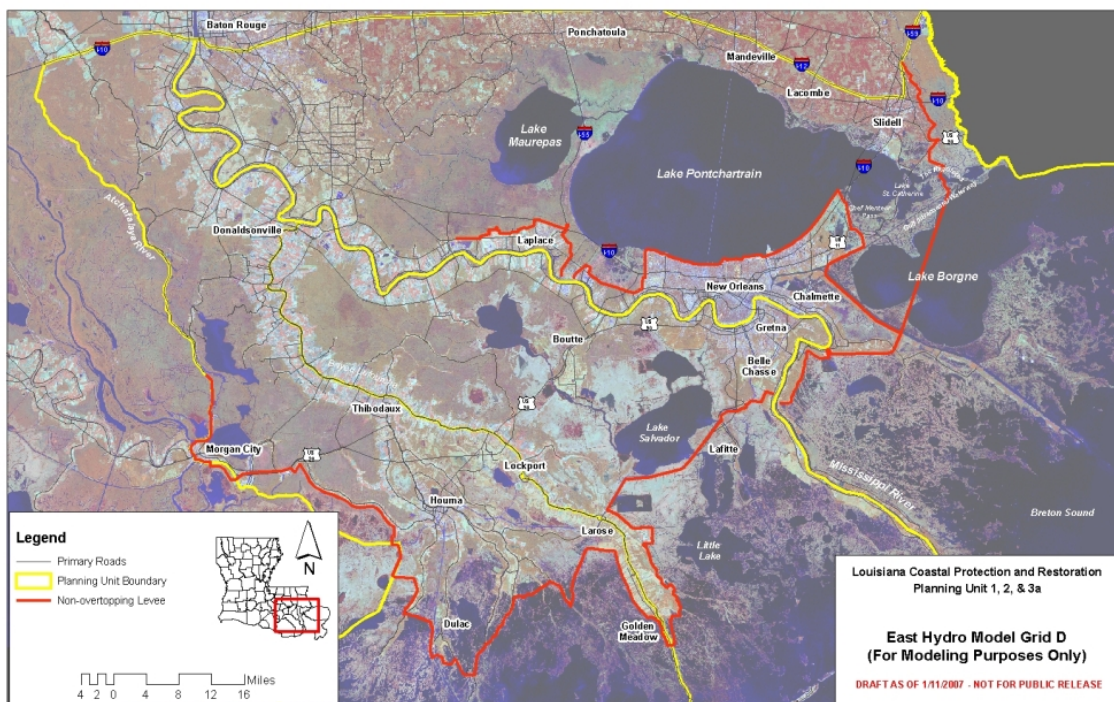
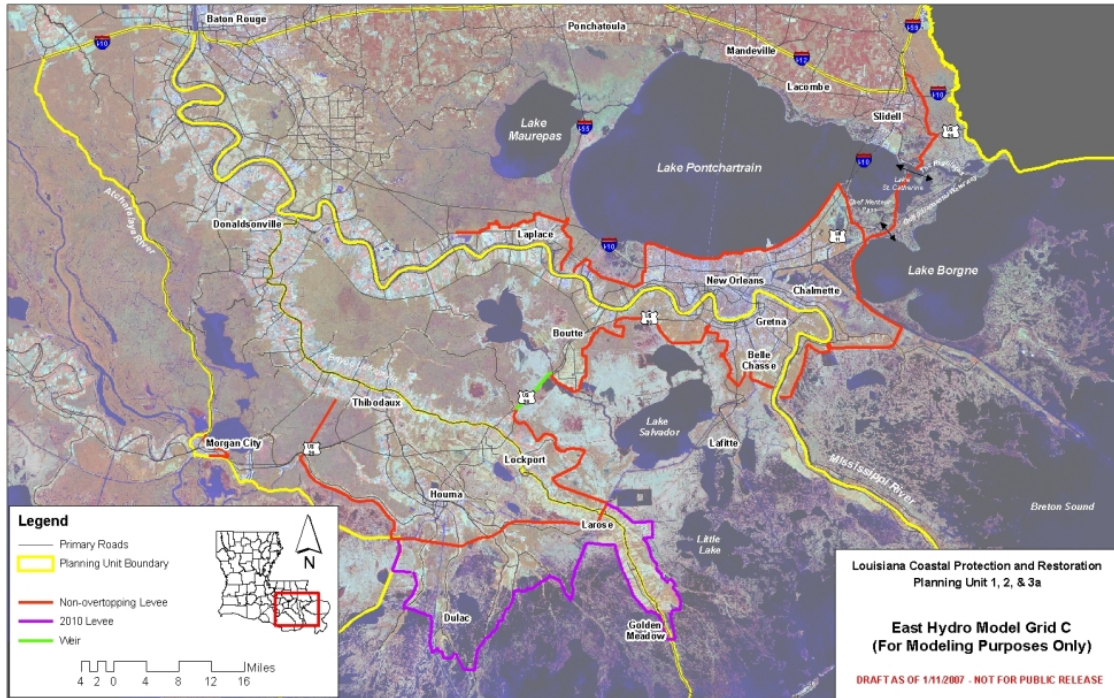


Figure 2.9 - Alignment alternatives LA East-C and LA East-D.

705

706

Unit	Planning Unit 3a	Planning Unit 3b	Planning Unit 4
Model grid			
Base condition	2007 situation	2007 situation	2007 situation
West A	Non-overtopping levee (10 m) along Larose to Golden Meadow alignment	Non-overtopping levee (10 m) along GIWW	Non-overtopping levee (10 m) along GIWW
West B	Levee at 100-year elevation along Larose to Golden Meadow alignment with non-overtopping back levee along GIWW	Non-overtopping levee along ridge north of GIWW	Non-overtopping (10 m) ring levee alignment Lake Charles, Vinton, Kaplan, and Gueydan
West C	Non-overtopping levee (10 m) along Larose to Golden Meadow alignment (similar to West A)	Non-overtopping levee along ridge north of GIWW (similar to West B)	Non-overtopping (10 m) ring levee alignment Lake Charles in combination with overtopping levee along GIWW alignment

707
708
709

Table 2.4 - Detailed overview of measures in LA West grid models for Planning Unit 3a/b and 4.

710

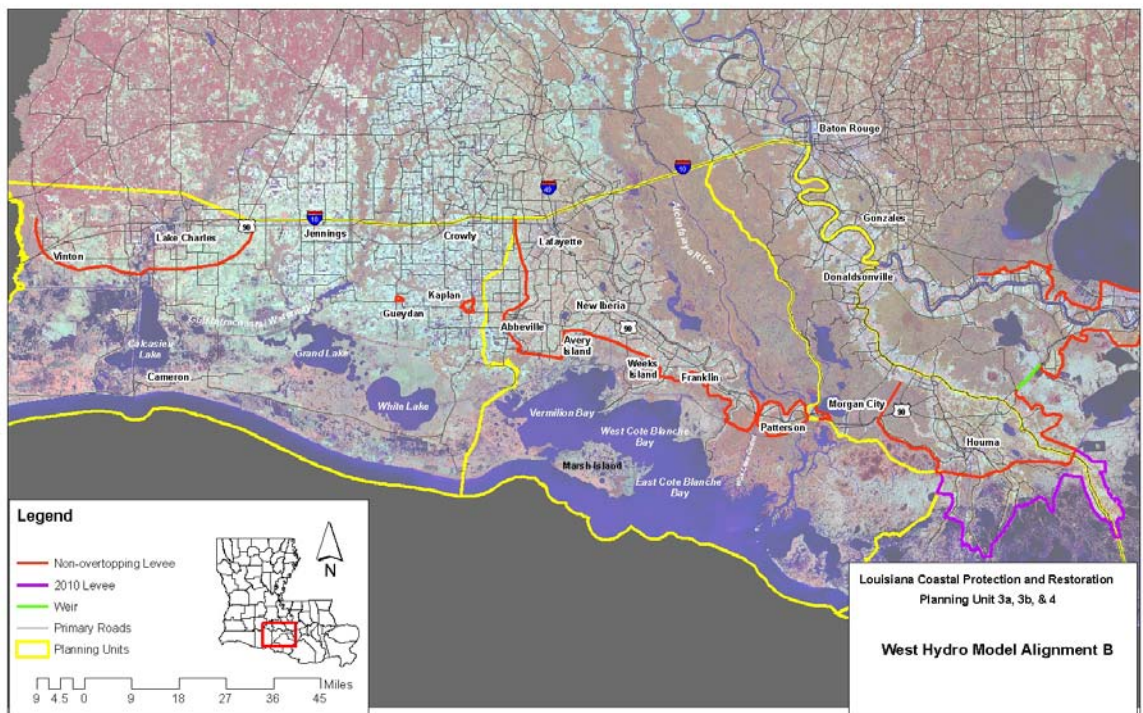
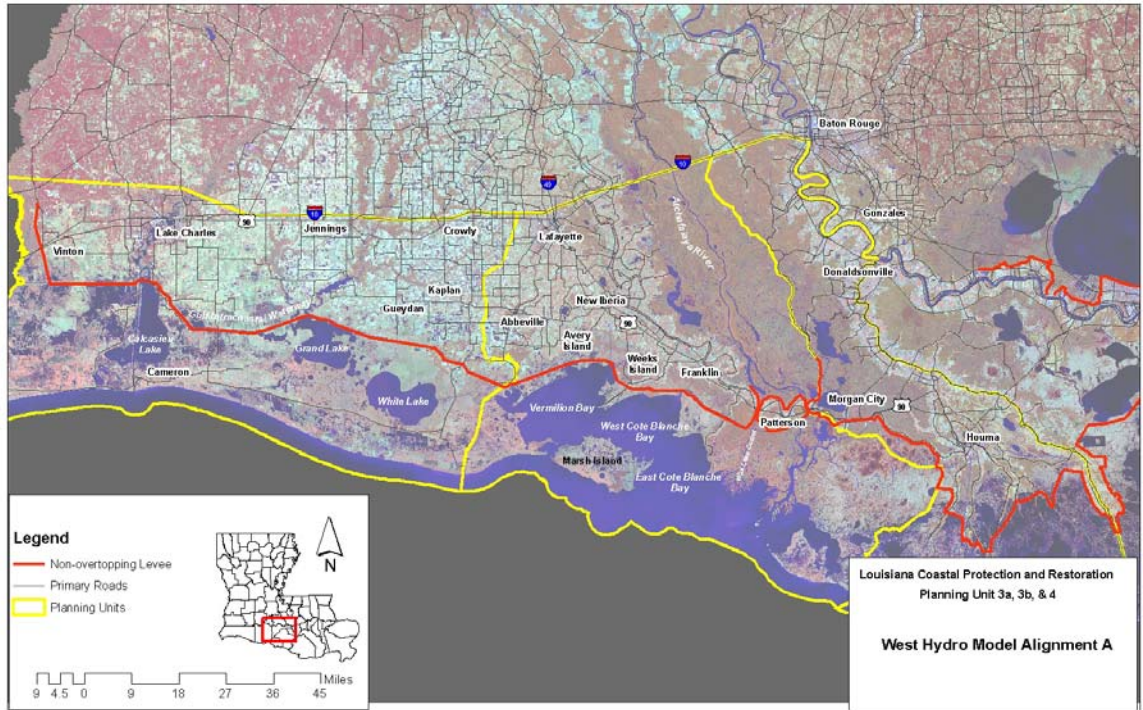


Figure 2.10 - Alignment alternatives LA West-A and West-B.

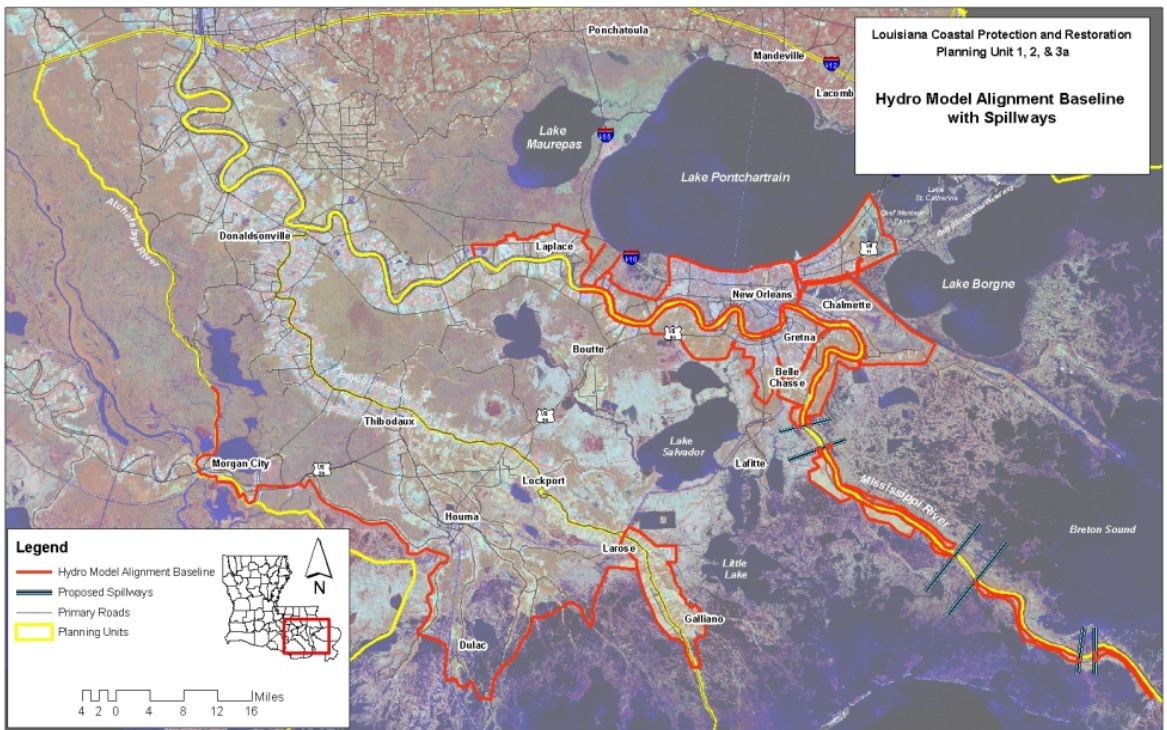
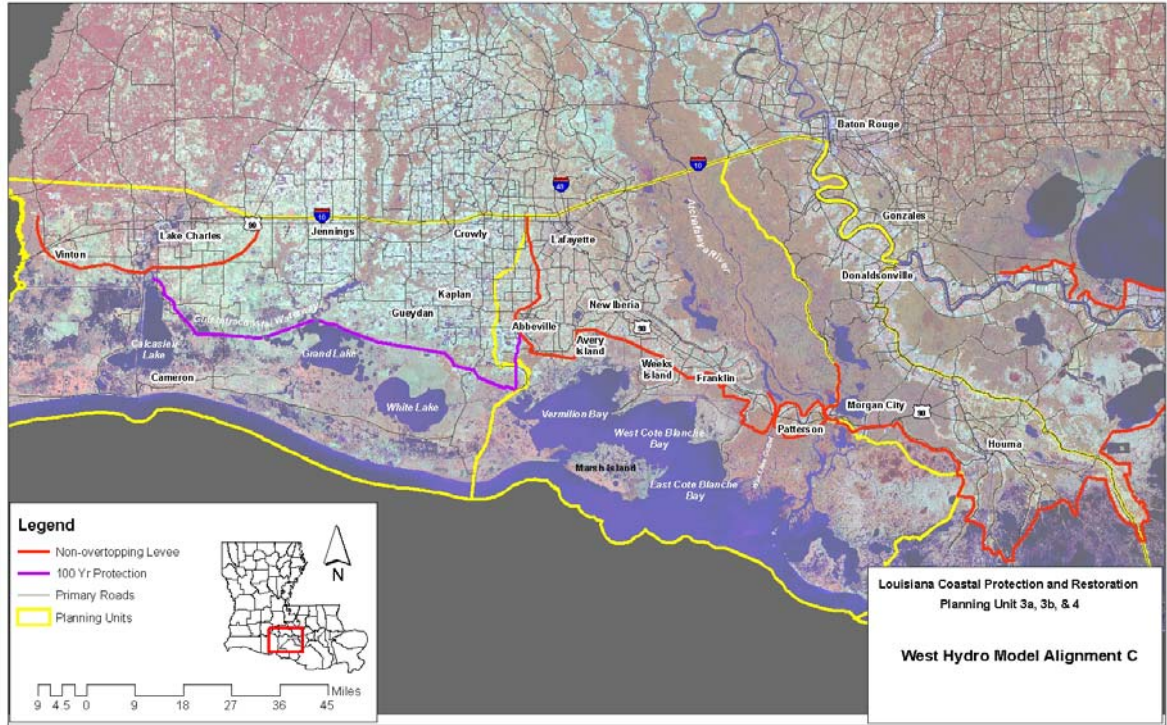


Figure 2.11 - Alignment alternatives LA West-C (upper panel) and Plaquemines-1 (lower panel).

711

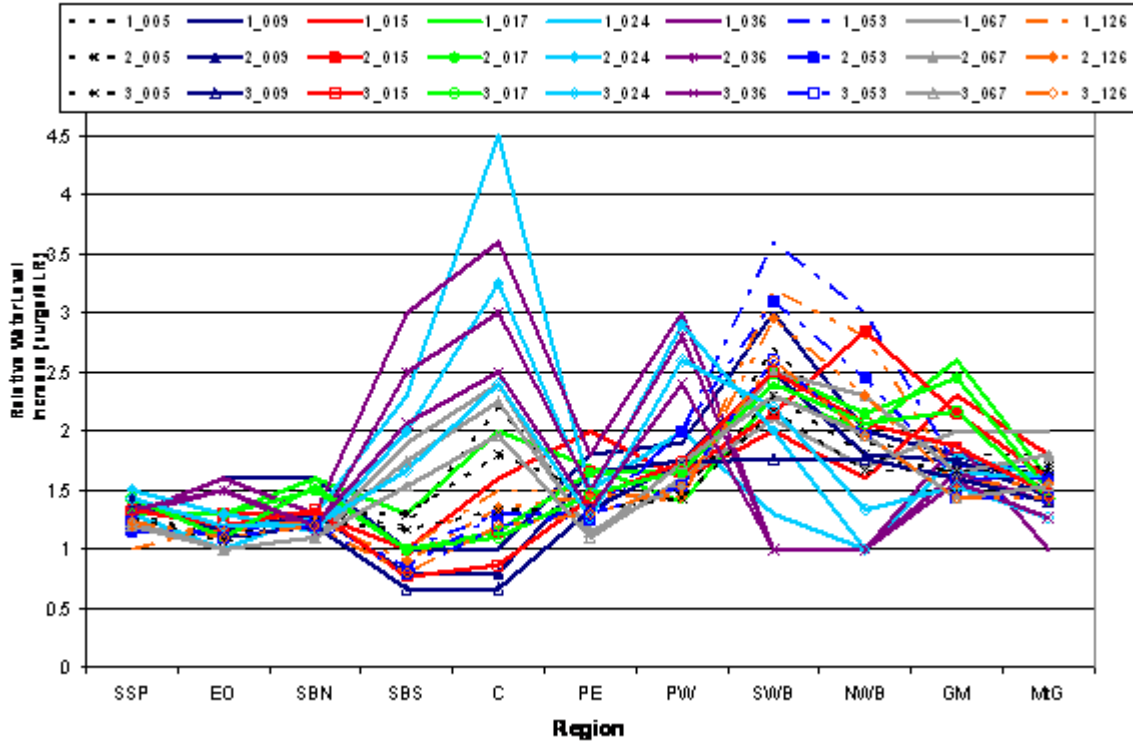


Figure 2.12 - Relative Water Level Increases by Reach.

The legend provides the sea level rise (1, 2, and 3 ft) and storm number (5, 9, 17, 24, 36, 53, 67, 126). The regions are: SSP = South shore Lake Pontchartrain, EO = East Orleans, SBN = St Bernard, C = Canaervon, PE = Plaquemines East, PW = Plaquemines West, SWB = West Bank South, NWB = West Bank North, GM = Golden Meadow, MtG = Morganza to Gulf.

712
 713
 714

2.5 Storm selection

715 Due to mandated project time constraints as well as to reduce the significant computation
 716 requirements not all 152 storms could be simulated for the numerous project alternatives. Thus,
 717 only a subset of the 152 storms was simulated for each project alternative. The selected subset
 718 was created by selecting storms whose tracks and characteristics spanned the range of parameter
 719 space defined in the JPM-OS methodology. Additionally, the subset of storms was based on the
 720 degree and location of the changed geometry for each alternative.

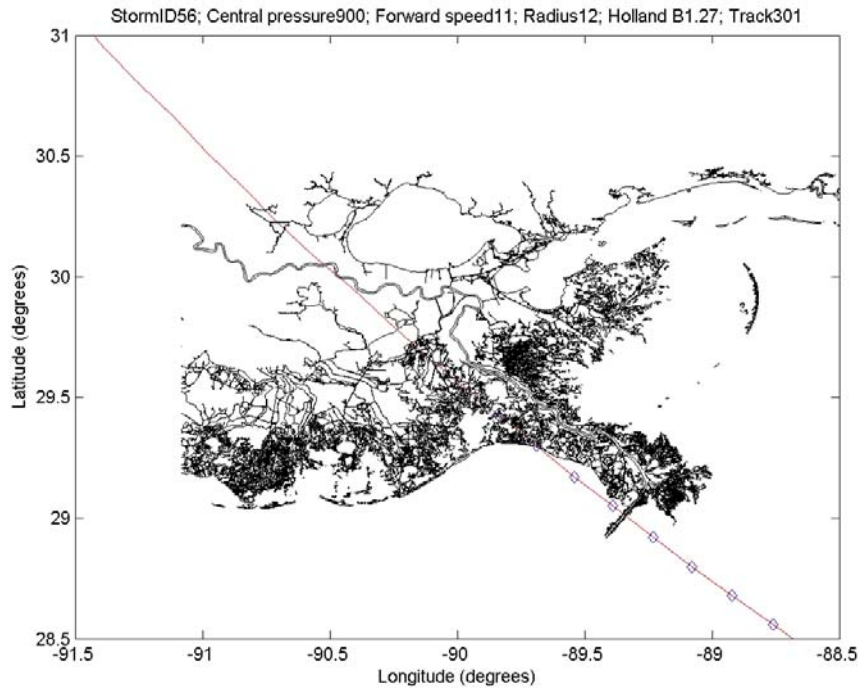
721

722 For example, 56 storms were selected for the 2010 baseline conditions based storm
 723 characteristics as well as geographic areas they affected and the 2010 geometry that was different
 724 than the 2007 geometry.

725

726 Table 2.6 lists the storms simulated for the East alternatives. The storms are ordered in groups as
 727 defined in the JPM-OS White Paper (see Resio et al, 2007). These storms characteristics cover

728 most of the important range of parameter space and thus provide a confident response surface
729 generated from the JPM-OS code. As an example, two storm tracks of this set are shown in Figure
730 2.13. Similarly, the storms for the West Alternatives are listed in Table 2.5.
731



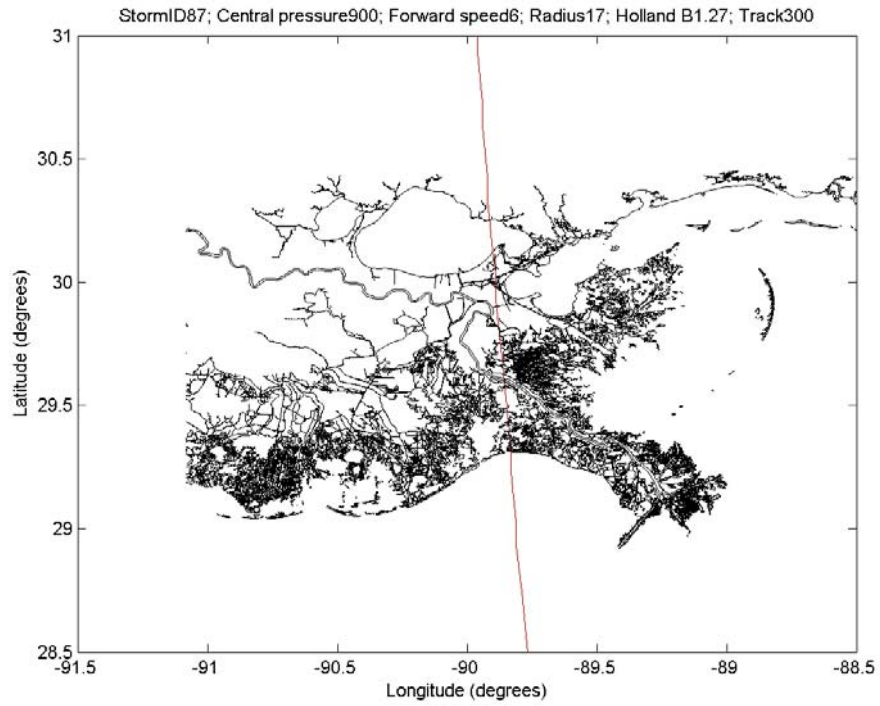


Figure 2.13 - Examples of storm tracks (storms 56 and 87).

732

West A	West B	West C	Marsh degraded	Marsh restored
203	203	203	202	202
205	205	205	205	205
208	208	208	211	211
209	209	209	214	214
212	212	212	217	217
214	214	214	220	220
217	217	217	223	223
218	218	218	226	226
221	221	221	229	229
223	223	223	232	232
226	226	226	235	235
227	227	227	238	238
230	230	230	241	241
232	232	232	244	244
235	235	235	267	267
236	236	236	269	269
239	239	239	271	271
241	241	241	273	273
244	244	244	275	275
245	245	245	277	277
315	315	315	279	279
316	316	316	281	281
317	317	317		
318	318	318		
319	319	319		
320	320	320		
321	321	321		
322	322	322		

733
734
735
736

Table 2.5 - Selected storms for West alternatives.

East A (48)	East B* (42)	East C (48)	East D (40)	Plaq Spill 1 (17)	Plaq Spill 2 (17)	Barrier islands (15)	Marsh degraded (24)	Marsh restored (24)				
5	69	5	75	5	69	5	75	14	14	29	2	2
6	71	6	77	6	71	6	77	15	15	32	3	3
8	73	8	83	8	73	8	83	17	17	35	5	5
9	75	9	85	9	75	9	85	18	18	36	6	6
14	77	14	86	14	77	14	86	23	23	38	8	8
15	82	15	87	15	82	15	87	24	24	41	9	9
17	83	17	88	17	83	17	88	26	26	44	11	11
18	84	18	89	18	84	18	89	27	27	45	12	12
23	85	23	92	23	85	23	92	52	52	59	14	14
24	86	24	93	24	86	24	93	53	53	61	15	15
26	87	26	94	26	87	26	94	56	56	67	17	17
27	88	27	95	27	88	27	95	57	57	68	18	18
32	89	33	97	32	89	33	98	69	69	79	20	20
33	90	35	98	33	90	35	99	73	73	80	21	21
35	91	36	99	35	91	36	100	77	77	81	23	23
36	92	49	100	36	92	49		32	32		24	24
48	93	52		48	93	52		35	35		26	26
49	94	53		49	94	53					27	27
52	95	56		52	95	56					29	29
53	97	57		53	97	57					30	30
56	98	60		56	98	60					32	32
57	99	61		57	99	61					33	33
60	100	69		60	100	69					35	35
61		71		61		71					36	36
67		73		67		73						

737
738
739
740
741

Table 2.6 - Selected storms for the East alternatives

2.6 Point sets

742 A number of different model output point sets have been developed to present the results from the
743 ADCIRC and STWAVE modeling. Three different point sets have been used within the LACPR
744 project. These are:

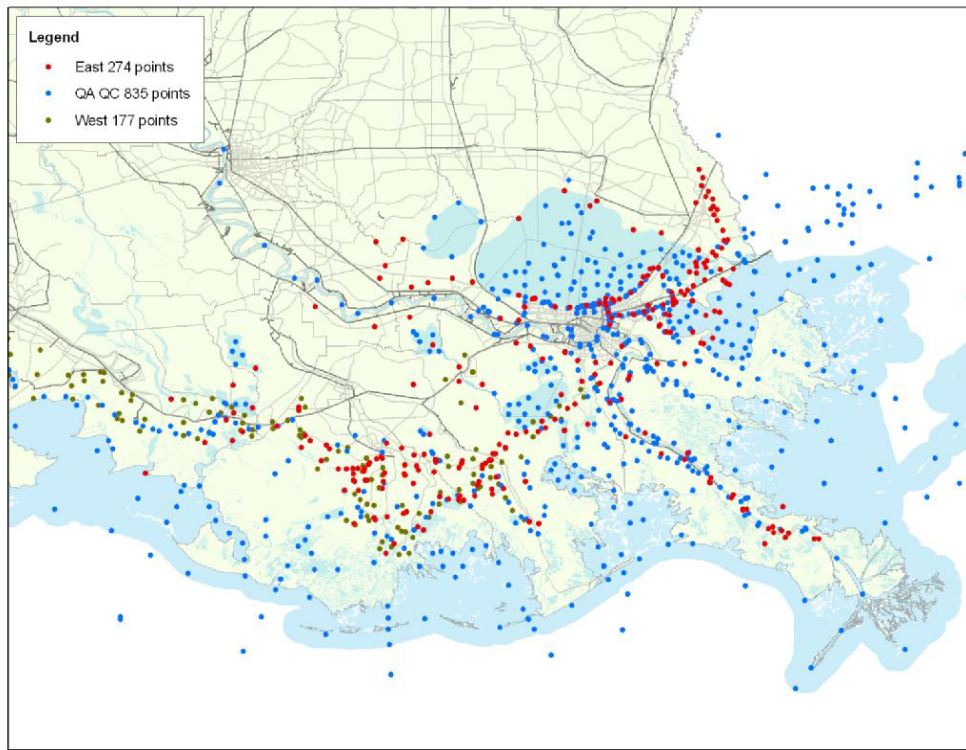
745
746

Table 2.7 - Overview of point sets used

Point set	Purpose
L 274	To select data for levee height design and overtopping rates for the east grid
W 177	To select data for levee height design and overtopping rates for the west grid
Q 835	To evaluate potential impacts of alternatives on the Mississippi coastline

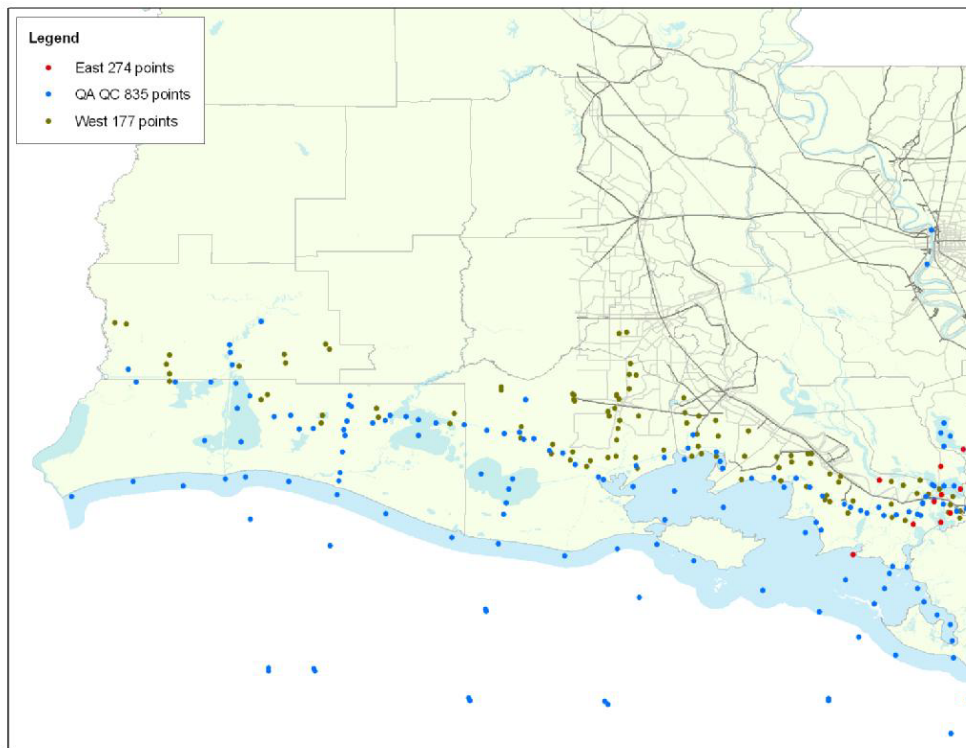
747
748
749

These point sets are visualized below.



750
751

Figure 2.14 - Point sets (East Grid)



752

753 **Figure 2.15 - Point sets (West Grid)**

754 **3 FREQUENCY ANALYSIS WITH JPM-OS METHOD**

755 This chapter describes the development of the frequency statistics for the surge level and wave
756 characteristics. Inputs for this analysis are the results from the ADCIRC and STWAVE
757 computations (Figure 3.1). The key element in this frequency analysis is the Joint Probability
758 Method with Optimal Sampling (JPM-OS method). The background of this method is briefly
759 summarized in Section 3.1. The JPM-OS method requires a full set of 152 storms to compute the
760 frequency statistics for surge and wave characteristics. However, for all levee alignments in the
761 LACPR project less storms were simulated due to time constraints. To use the method for these
762 levee alignments a fitting procedure was developed for surge levels (Section 3.2) and wave
763 characteristics (Section 3.3) so as to create values for all 152 storms. To check the validity of this
764 procedure, a check has been carried out for one specific alternative, see Section 3.4. The
765 frequency statistics are used as input into the determination of the levee heights (Chapter 4) and
766 the overtopping volumes (Chapter 5), and they are also used to provide stage frequency results for
767 areas outside of a levee system.
768

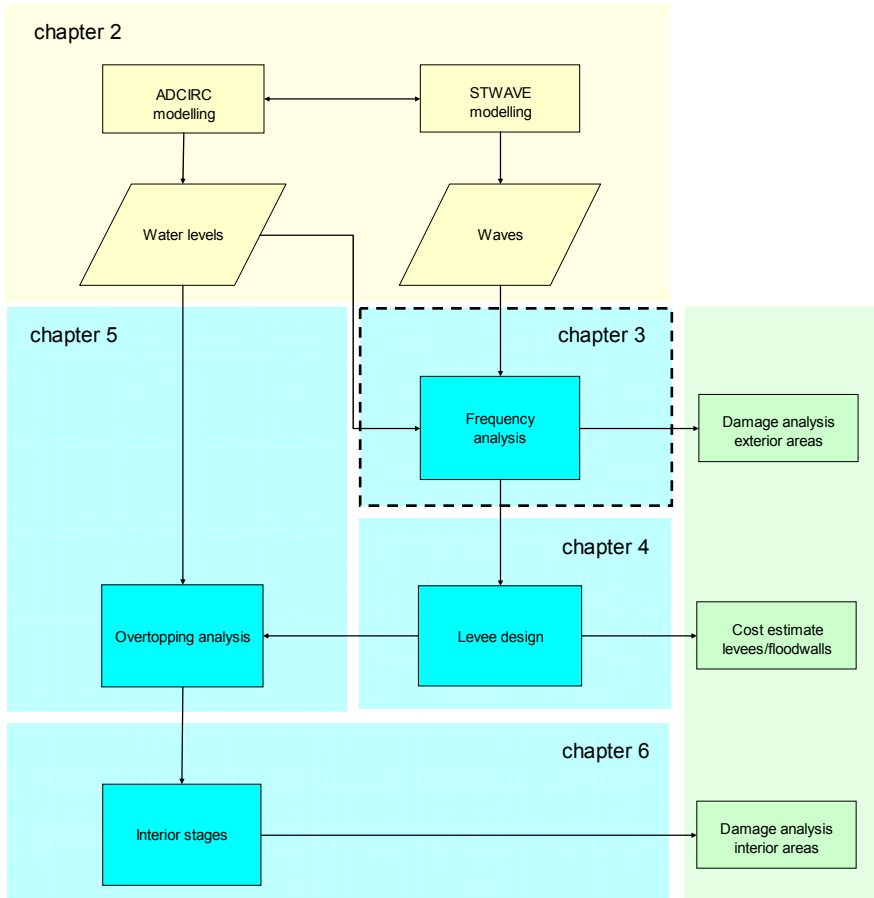


Figure 3.1 - Flow diagram of hydraulic analysis in LACPR framework

769

770

771 **3.1 JPM-OS method**

772 In 2006 and 2007, a team from the Corps of Engineers, FEMA, NOAA, private sector, and
773 academia developed a new process for estimating hurricane inundation probabilities, the Joint
774 Probability Method with Optimal Sampling process (JPM-OS). This work was initially begun for the
775 Louisiana Coastal Protection and Restoration study (LACPR), but now is being applied to Corps
776 work under the 4th supplemental appropriation, the Interagency Performance Evaluation Team
777 (IPET) risk analysis, and FEMA Base Flood Elevations for production of DFIRMs for coastal
778 Mississippi, Louisiana, and Texas.

779

780 For most Joint Probability Methods, several thousand events are evaluated. With the JPM-OS
781 method, optimal sampling allows for a smaller number of events to be used. The JPM-OS method
782 computes the frequency of occurrence of surges at specific geographic points or stations. For
783 each of these points a surge response from each of 152 specific storms is required. The JPM-OS
784 method has been used to derive the still water elevation, wave height, and wave period frequency
785 curves at specific points using output from ADCIRC and STWAVE. JPM-OS takes into account the
786 joint probability of forward speed, size, minimum pressure, angle of approach and geographic
787 distribution of the hurricanes. For more details, the reader is referred to Resio et al. (2007), see
788 Appendix B.

789

790 The output from the ADCIRC and STWAVE models used in the JPM-OS analysis are the
791 maximum still water elevation and maximum wave characteristics (significant wave height, peak
792 period, and wave direction) at specified points. An example of the model output at two locations is
793 shown in Figure 3.2. The wave characteristics along Lake Pontchartrain are typically wind-
794 generated and depth-limited waves. There is a high correlation between the wave height and the
795 wave period and between the surge level and wave height for this area. In contrast, the results at
796 the MRGO are much more scattered. The relationship between the surge level and the wave
797 height is less evident, and the wave period strongly varies as a function of the wave height. Long
798 wave periods are observed for a few storm conditions. The long wave periods are related to swell
799 waves from the ocean.

800

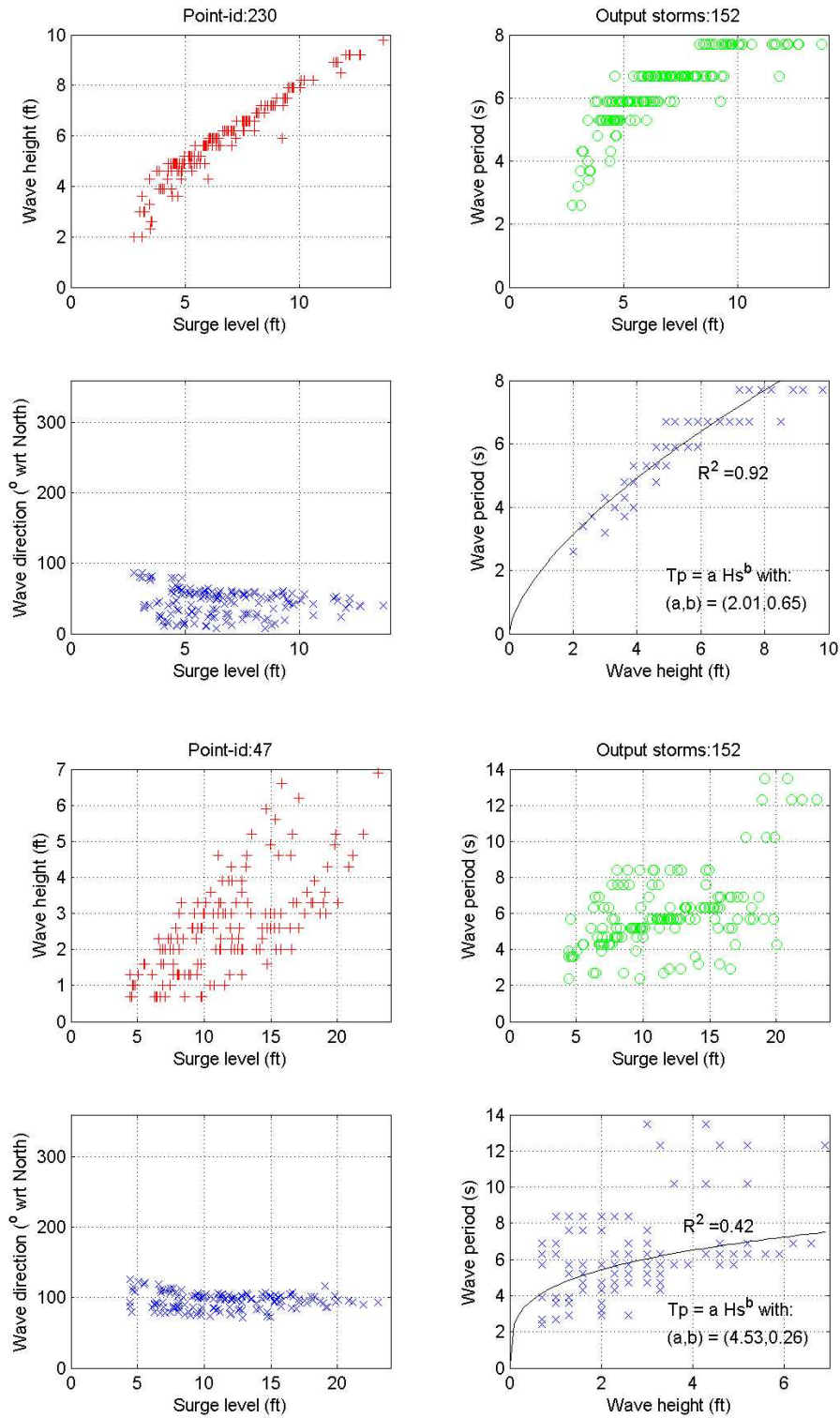


Figure 3.2 - Numerical results at Lake Pontchartrain (upper panel) and MRGO (lower panel) from ADCIRC

and STWAVE (Base condition 2007). The marks (o, x, +) represent 152 storm results.

801

802 Surge level frequency curves can be estimated from output from the 152 storms. Along the West
803 Bank, there were instances where there was no output from the 152 storms because these points
804 are dry for a specific storm. In this case, estimates were made of the surge elevation for the
805 missing output so that the frequency analysis continued to be based on 152 values. For the nodes
806 which formed the ADCIRC grids, the topographic elevation was modified for all cases where the
807 surge value for all storms did not produce a surge at that node. After this multiplication, an
808 additional check was made and if the surge was less than 0.0, the surge was set to 2.5 feet.

809

810 An important remark is the frequency range of the 152 storms that were originally selected for the
811 JPM-OS method. The original set of 152 storms was selected in such a way that it covers the
812 probabilities in the range of 1/50 – 1/5,000 per year with main emphasis on the range 1/50 – 1/500
813 year. In the framework of LACPR, the frequency analysis with the JPM-OS method ranges from
814 1/100 per year to 1/2000 per year. The 1/2,000 year return period is near the upper end of the
815 original storm set limits and it can be expected that the results for the upper end are more
816 uncertain than the results for the 1/100 – 1/1,000 year range. Nevertheless, we believe that the
817 results can be used after careful checks within the LACPR evaluation because the main purpose is
818 a relative comparison between the various alternatives during these events rather than an exact
819 determination of the hydraulic boundary conditions for these extreme events.

820

821

822 **3.2 Fit procedure for surge levels**

823 The LACPR analysis evaluates alternative storm surge protection systems using many levee
824 alignments. For each of these alternatives, ADCIRC grid geometry was created to model the
825 system and provide results from which levee heights can be determined. However, simulation of
826 the entire 152 suite of storms for each of these alternative geometries is impossible due to the
827 enormous computational time necessary, in conjunction with highly critical and short project
828 deadlines. Thus, for each alternative, a subset of storms was selected from the suite of 152 storms
829 for simulation on the appropriate alternative geometry (see Table 2-5). For instance, only 48
830 storms were computed for the 2010 LACPR East A grid.

831

832 In order to use the JPM-OS software to create statistical files to compare against the original 2007
833 conditions 152 storm suite, a surge value was needed for the storms not simulated for that
834 particular geometry. Commonly there is a relationship between the original results from the 2007
835 conditions and the results for the other conditions or alternatives (2010, 2010 LACPR East A, 2010
836 LACPR East B, etc.). If no variances exist in a specific area, one may expect similar results for the
837 2007 condition and another condition. If changes to the nearby coastal hydrodynamic features
838 have occurred however (e.g. adding a barrier), one may expect an altered response in the
839 distinctive condition surge levels. To find a relationship between the surge level effect of a specific
840 condition (i.e., 2010 LACPR East A) and the original surge level (2007), we examined the results
841 for a few cases (Figure 3.3 and Figure 3.4) in the New Orleans area. Note that the 2010 case
842 includes the barrier at the entrance of GIWW in the New Orleans East area.

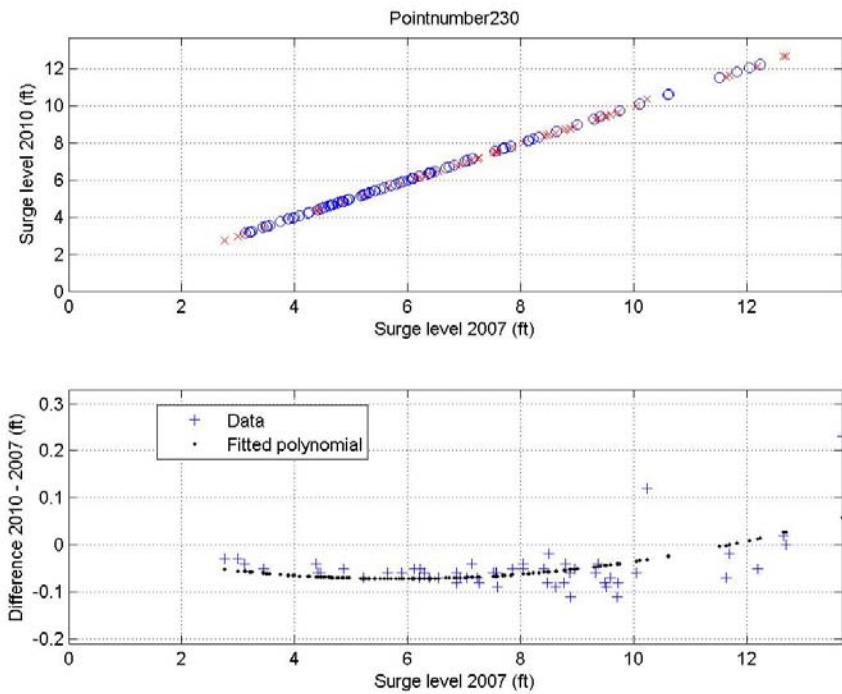
843

844 Based on inspection of various plots, we have chosen to use the following relationship between
845 the effect on the maximum surge level and the original maximum surge level of 2007:

846
847
$$\Delta\zeta_{2010-2007} = a_1\zeta_{2007} + a_2\zeta_{2007}^2$$
 Equation (1)

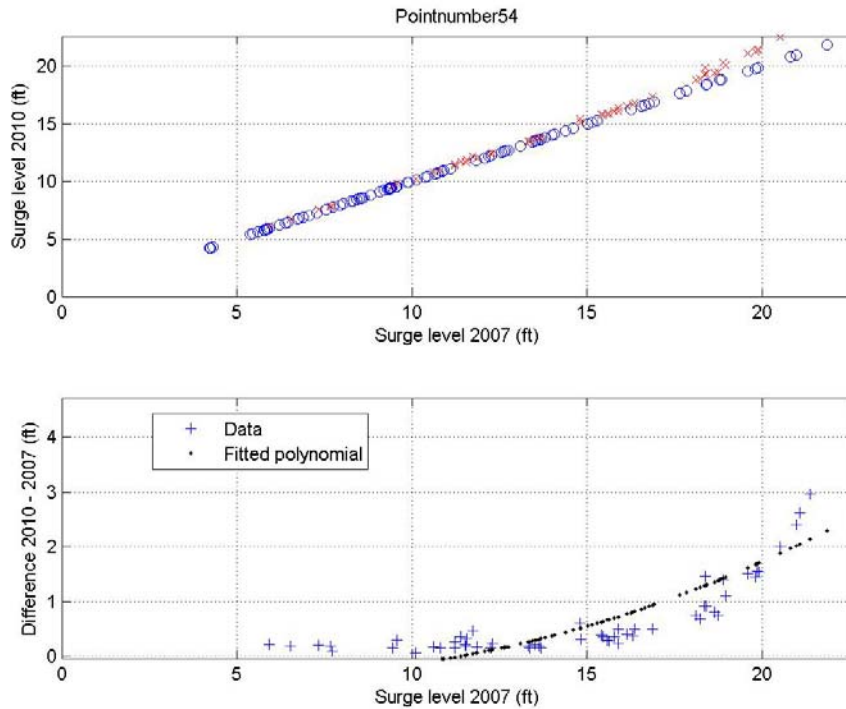
848
849 where:
850 $\Delta\zeta$: difference in maximum surge level [ft]
851 ζ_{2007} : maximum surge level 2007 [ft]
852 a_1, a_2 : coefficients [-, 1/ft]
853

854 The coefficients a_1, a_2 are fitted using the data of the storms available using a MATLAB routine.
855



856
857 **Figure 3.3 - Correlation between maximum surge levels at Lake Pontchartrain for Base condition 2010 and Base**
858 **condition 2007.**

859

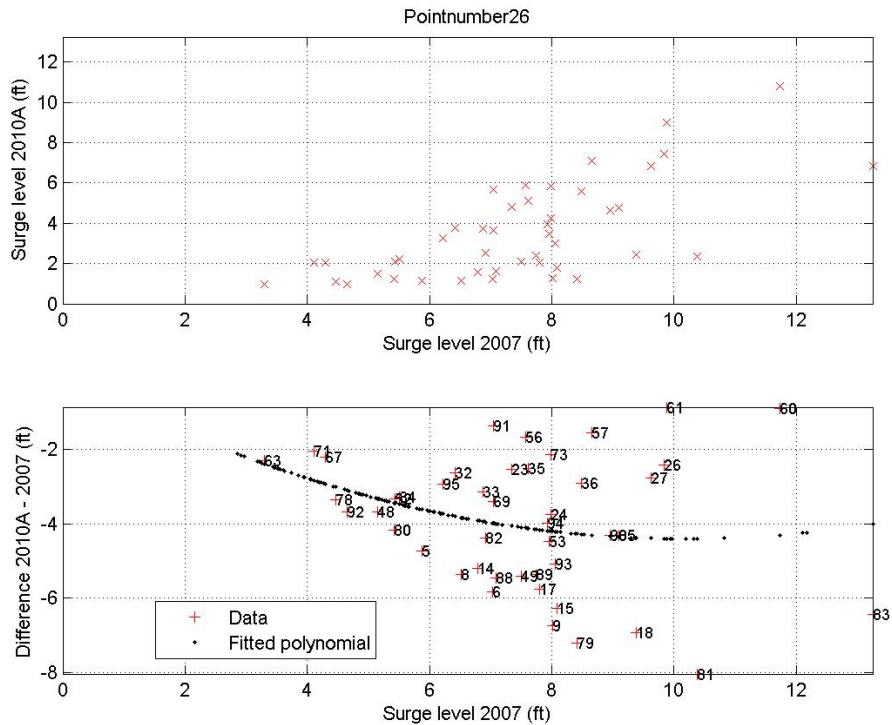


860
861 **Figure 3.4 - Correlation between maximum surge levels at Lake Pontchartrain for Base condition 2010 and Base**
862 **condition 2007.**

863
864 The final step for the surge levels is to compute the 152 storm results for the new situation (2010,
865 2010 LACPR East A, 2010 LACPR East B, etc.). For this purpose, the fitted line according to Eq.
866 (1) has been used for all storms (including the storms that were originally run for the new
867 situation). The 152 results for the new situation are used as input for the probabilistic JPM-OS
868 method to obtain the frequency curves.

869
870 For specific cases, the correlation of the fit is relatively low. One example is shown in Figure 3.5.
871 This plot shows the effect on the surge levels for 2010 LACPR East A condition (i.e. full closure of
872 Lake Pontchartrain). As can be observed, the correlation between the surge level of the base case
873 (2007 conditions) and the effect of the surge level between 2010 LACPR East A and 2007
874 conditions, according to Eq. (1) is not very good. Despite this low correlation, we have produced
875 152 storm results based on this fit and computed the frequency curve using the JPM-OS method.
876 Note, that points of no-data (-99999) are discarded and not used in the created polynomial curve
877 fit between the datasets.

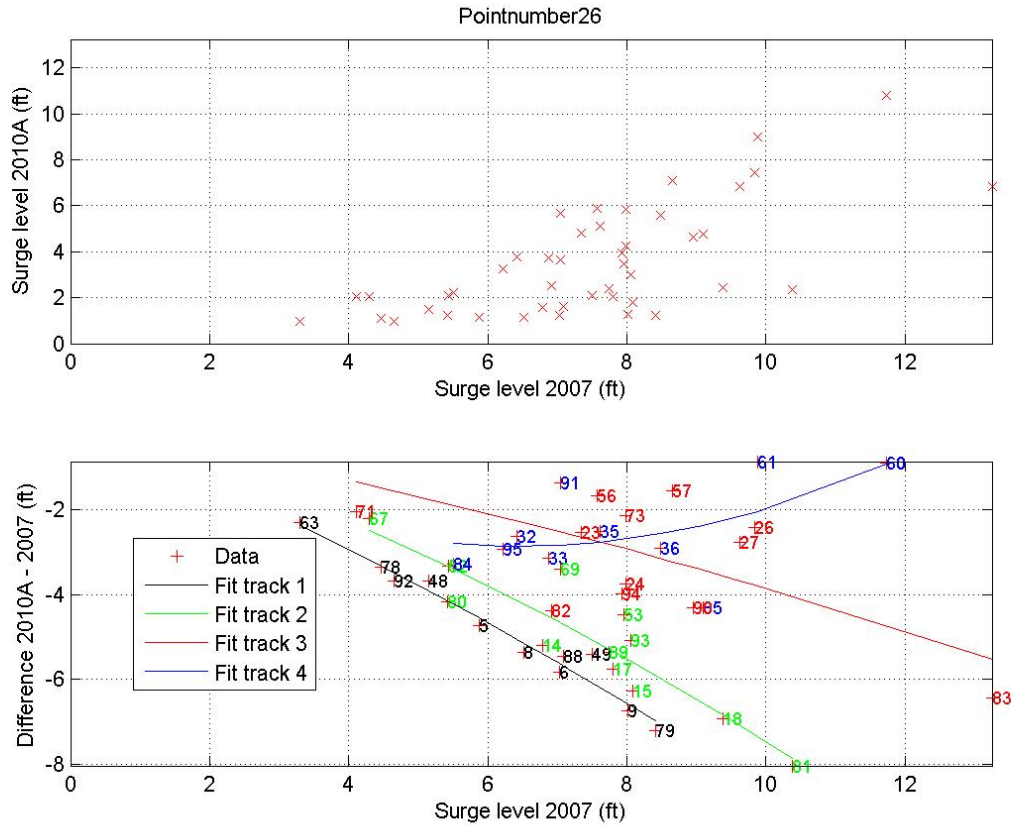
878
879



880
 881 **Figure 3.5 - Effect of maximum surge level at Lake Pontchartrain (grid 2010 East A) with fit for all storms**

882
 883 Due to the low correlation we have investigated whether the various storm tracks could explain this
 884 low correlation. In the Figure 3.6 the colored dots indicate the various hurricane tracks: black =
 885 track 1, green = track 2, red = track 3, blue = track 4. It can be observed that the relationship
 886 between the surge level of 2007 conditions and the effect of the surge level for the data points of
 887 track 1 (black points) is very good. The relationships for the other tracks are not as strong.
 888 Nonetheless they are considerably better than the fit based on all storms. Because of this, we
 889 have produced fits for each storm track separately using Eq. (1) and computed surge levels for the
 890 152 storms applied to the 2010 LACPR East A scenario using the track information of each storm.
 891 These results have been used to compute the frequency curves for the surge levels.

892
 893



894
 895 **Figure 3.6 - Effect of maximum surge level at Lake Pontchartrain (grid 2010 East A) with fit for different storm**
 896 **tracks**

897
 898 A comparison was made between the 1% surge levels based on both methods, viz. the fit with
 899 multiple curves based on storm tracks and the results from a single curve with without regard to
 900 storm track. Although the data fits appear to be much better for each track separately, it appears
 901 that the final 1% surge levels differ less than 0.5ft. Nevertheless, the fitting procedure based on the
 902 multiple tracks has been applied throughout the entire LACPR evaluation.
 903

904
 905 **3.3 Fit procedure for wave characteristics**

906 Similarly to the surge levels, the wave characteristics of the alternative conditions (2010, 2010
 907 LACPR East A, 2010 LACPR East B, etc.) are also likely to be related to wave characteristics of
 908 the base case (2007 conditions). However, the relationship between the waves from 2007 and the
 909 other conditions (2010, 2010 LACPR East A, etc.) appears to be much less strong than for the
 910 maximum surge levels. This has to do with the sensitivity of the wave characteristics to small water
 911 level changes. Another issue is that the roughness formulation in STWAVE has been changed for
 912 the 2010 conditions (and other LACPR alternative conditions). The STWAVE model was executed
 913 with no bottom friction formulation for the 2007 conditions. Especially near the levee, the

914 roughness influence is relatively high because of the limited water depth. Therefore, a good fit
915 between the original 2007 condition wave results and the new 2010 condition wave results cannot
916 be expected.

917

918 To circumvent this problem, we have chosen to make a fit between the surge level and the wave
919 characteristics for each alternative. Based on plots we have adopted the following relationships
920 (see also Figure 3.7 and Figure 3.8):

921

$$\begin{aligned} H_s &= a_1 \zeta^{b_1} \\ T_p &= a_2 \zeta^{b_2} \end{aligned} \quad \text{Equation (2)}$$

923

924 where:

925 H_s : significant wave height [ft]

926 T_p : peak period [s]

927 ζ : Maximum surge level [ft]

928 a_1, b_1, b_2, a_2 : coefficients

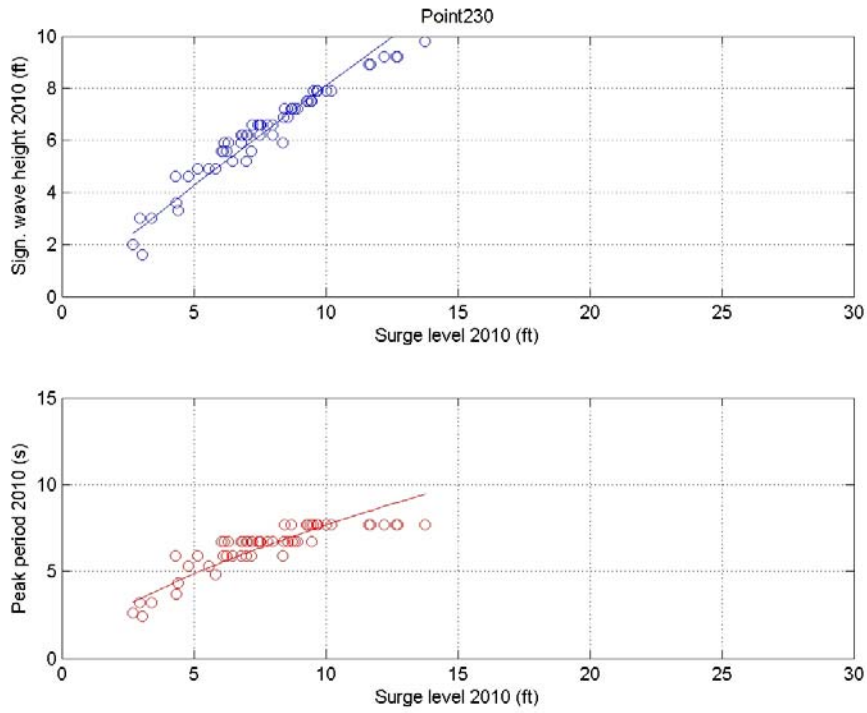
929

930 The coefficients a_1, a_2, b_1 and b_2 were fitted using the data of the storms available using a
931 MATLAB routine.

932

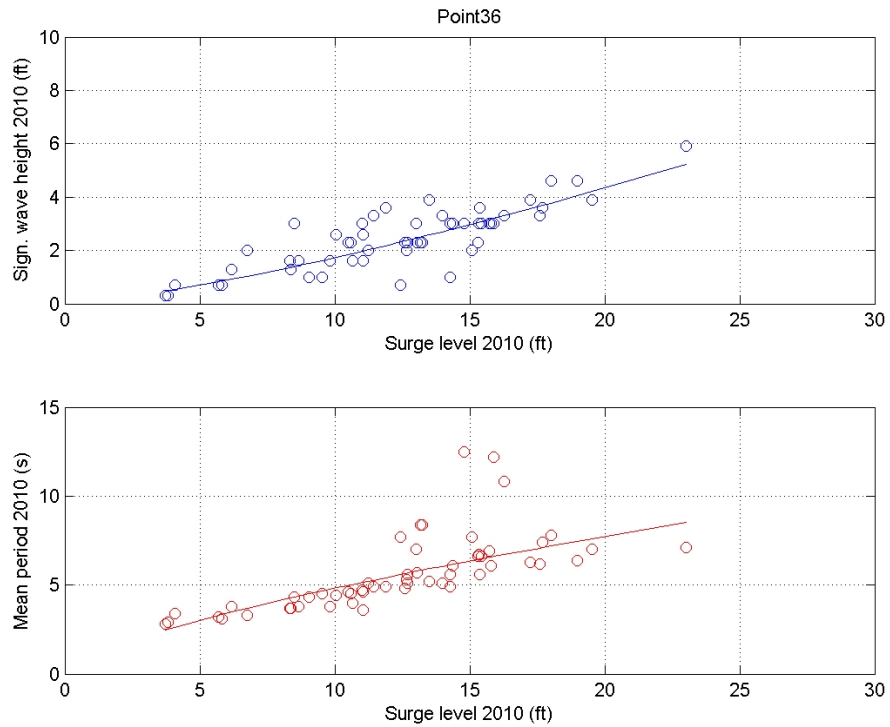
933 The final step for the wave characteristics was to compute the 152 storm results for the new
934 situation (2010, 2010 East A, East B, etc.). For this purpose, the fitted line according to Eq. (2) has
935 been used for all storms (including the storms that were originally run for the new situation) using
936 the fitted surge levels for that specific grid. Note, similarly to maximum surge levels, point locations
937 with no-data were discarded and not used to create the fit.

938



939
940

Figure 3.7 - Wave characteristics at Lake Pontchartrain for 56 storms



941

942 **Figure 3.8 - Wave characteristics at MRGO for 56 storms**

943

944 Summarizing, frequency statistics are computed for surge, wave heights, and wave periods, for all
945 LACPR alternative conditions. For each LACPR alternative condition, using the curve fitting
946 methodology described in this and the previous section, point files were created for surge, for
947 wave heights, and for wave periods. Each file contains 152 values derived as above. These files
948 are then input to the probabilistic JPM-OS software to obtain the frequency curves for the surge,
949 wave heights, and wave periods. In this manner, 50yr, 100yr,, 1950yr, 2000 yr values are
950 obtained for surges, as well as wave heights, and wave periods. In addition the standard deviation
951 of the surge level as a function of frequency is also obtained.

952

953

954 **3.4 Validity of fit procedure**

955 As listed in Table 2.2, a subset of 40 storms was selected for simulation for the East B alternative.
956 In order to validate the surge fitting model previously described, the remaining 112 storms of the
957 full suite of 152 storms were simulated for the East B levee configuration. Statistics were
958 computed for all of the point sets using the JPM-OS code to produce the full range of returns from
959 the 50 thru 2000 yr return values. The L274 point group was selected for initial evaluation. A table
960 of differences was computed for the 100 yr surge values between the fitted model results and the
961 full suite of 152 storm results. Figure 3.9 shows the 100 yr return values resulting from the analysis
962 of East B using the full 152 storm suite versus the 40 storm suite.

963

964 As can be seen in Figure 3.9 the results are almost identical and follow a straight line which
965 indicates they are the same. It appeared that approximately 30% (91 points) of the 100yr surges
966 for the 152 storm set were between 0.1 to 1.3 feet less than the fitted model values. Approximately
967 24% (67 points) were exactly the same 100 yr surge elevations. The remaining 56% were
968 between 0.1 to 1.4 feet above the fitted model values. There were 2 outliers of 7.8 and 4.2 feet.
969 These were located away from the coast, towards the upper Pearl River Basin. The larger
970 differences for these 2 points are most likely due to data processing errors. For the 100yr surge
971 levels, a standard deviation of 0.63 feet was computed for the absolute difference between the
972 results based on the full storm suite and the 40 storm suite. Also, if the 2 outlier points are
973 disregarded, the standard deviation is 0.34 feet. Thus, the fitted model procedure results agree
974 relatively well with the full 152 storm suite results.

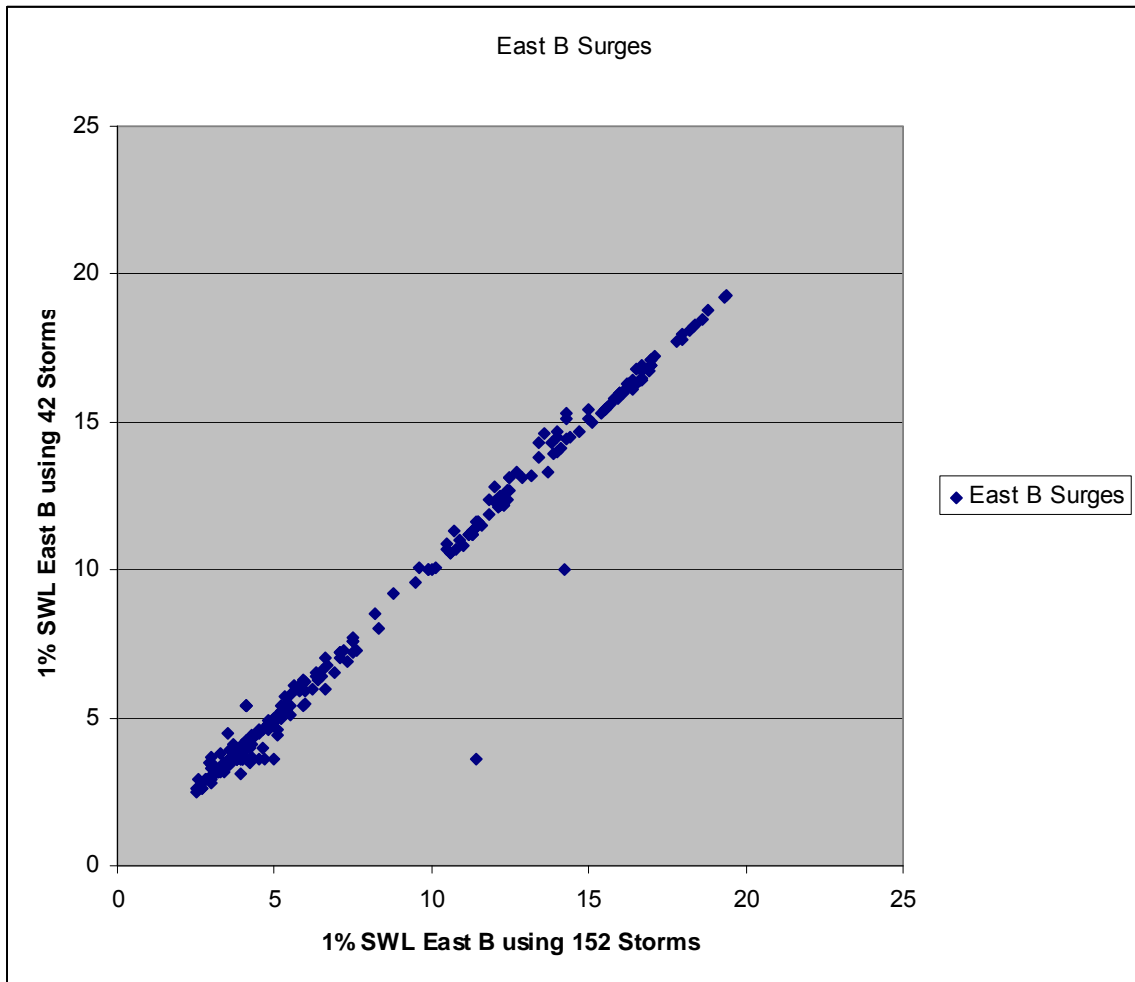
975

976

977

978

979



980
981
982
983
984
985
986

Figure 3.9 Comparison between the 1% still water levels based on the full storm set of 152 storms and based on the 42 storms using the fit procedure.

987 **4 DETERMINATION OF LEVEE HEIGHTS**

988 This chapter gives an overview of the design approach for the levee heights. The frequency results
989 of the various hydraulic variables are the inputs for this analysis (Figure 4.1). The design
990 procedure adopted herein has been developed in the framework of the current 100-year levee and
991 floodwall design effort for the Hurricane Protection System at the New Orleans District. In the
992 framework of LACPR several simplifications have been applied to make this procedure applicable
993 for this study.

994
995 The outline of this chapter is as follows. First, the step-wise approach for the levee design is
996 presented and the simplifications in the LACPR technical evaluation are described (Section 4.1).
997 Next, the general assumptions of the levee design approach are discussed in more detail (Section
998 4.2). Finally, the procedure to account for uncertainties in the levee design procedure is briefly
999 explained (Section 4.3). The final levee heights are input into the determination of the overtopping
1000 volumes (Chapter 5) and for producing construction cost estimates. The cost estimates of the
1001 levee designs are described in a separate report.
1002

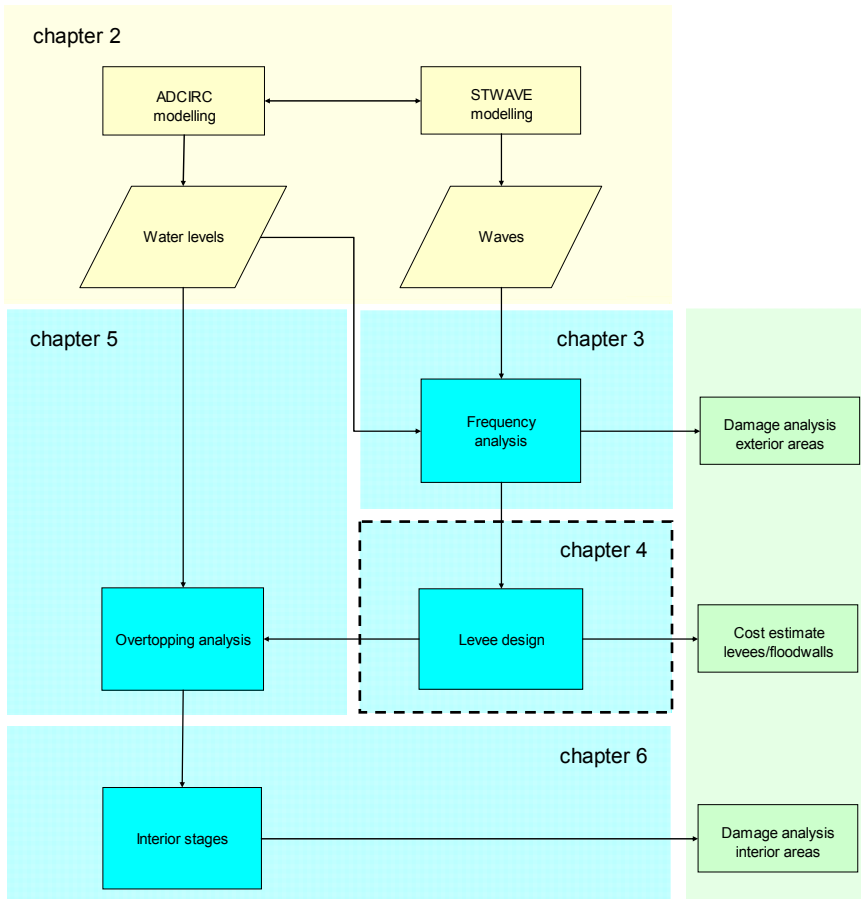


Figure 4.1 - Flow diagram of hydraulic analysis in LACPR framework

1003

1004 **4.1 Step-wise design approach**

1005 The design procedure below gives a step-wise approach for determining the levee height, within
1006 the framework of LACPR, from a hydraulic perspective. The step-wise approach is intended to be
1007 used for each section that is more or less uniform in terms of hydraulic boundary conditions (water
1008 levels, and wave characteristics) and geometry (levee, floodwall, structure). The procedure has
1009 been developed within the framework of the current 100-year levee and floodwall design effort for
1010 the Hurricane Protection System at the New Orleans District.

1011

1012 A levee design was made for three different levels of protection (100-year, 400-year and 1000-
1013 year). Several simplifications have been applied in the step-wise approach to make the procedure
1014 applicable and suitable for this study. The step-wise design approach for a given return period has
1015 been adopted as follows for LACPR:

1016

1017

Table 4.1 - Stepwise approach

Step	Description
0 – Definition of reaches	For each sub basin (or polder) the surge levels and wave characteristics are examined. Based on the variation in the hydraulic boundary conditions and the orientation, the flood protection system was divided into one or more reaches. For each reach, one or more suitable output locations were selected from the LACPR point set.
1 – Water elevation	For each levee reach the surge levels from the frequency analysis were reviewed. Based on the quality of the data a suitable output point was selected. The report with the results (Volume 2) discusses in detail the selected output points for all reaches.
2 – Wave characteristics	The wave characteristics were extracted from the same output location as the surge levels. The wave height at the toe of the structure is assumed to be reduced as a result of depth-limited breaking according to $H_{smax} = 0.4 h$. The wave period has not been changed.
3 – Overtopping rates	The overtopping rate is computed using the Van der Meer formulations (see textbox). For this purpose, a simplified levee design is assumed (Figure 4.2). The steep sloping sections near the crest and near the toe are assumed to be 1:4. In between, a wave berm is present to reduce the amount of overtopping. For all cases, the wave berm factor (γ_b) is set at 0.7 in the Van der Meer equations and the slope equals 1:4. The other influence factors regarding wave incidence, roughness and vertical wall are all set to 1.0. Hence, we assume a perpendicular wave attack against a grass-sloped levee without a wall on top.
4 – Monte Carlo simulations	The final step is a Monte Carlo simulation to compute the overtopping rate from step 3 a large number of times (5,000). Every time, the hydraulic variables and the coefficients of the overtopping equation are changed to account for the uncertainties in these parameters. The approach is explained in detail in the Section 4.3. Based on the 5,000 results, the probability distribution of the overtopping rate is determined. A check is carried out to see if the overtopping rate does not exceed the overtopping criterion of 0.1 cfs per ft with 90% confidence. If yes, the design process is finished and the levee height is set. If not, the levee height is lowered and the calculation repeated until this criterion is reached (see also Appendix B).

1018

For the purpose of LACPR, the Van der Meer equations have been adopted to compute overtopping rates for levee sections. The overtopping formulations from Van der Meer are (see TAW document):

$$\frac{q}{\sqrt{gH_{m0}^3}} = \frac{0.067}{\sqrt{\tan \alpha}} \gamma_b \xi_0 \exp\left(-4.75 \frac{R_c}{H_{m0}} \frac{1}{\xi_0 \gamma_b \gamma_f \gamma_\beta \gamma_v}\right)$$

with maximum:
$$\frac{q}{\sqrt{gH_{m0}^3}} = 0.2 \exp\left(-2.6 \frac{R_c}{H_{m0}} \frac{1}{\gamma_f \gamma_\beta}\right)$$
 (1)

With:

q : overtopping rate [cfs/ft]

g : gravitational acceleration [ft/s²]

H_{m0} : wave height at toe of the structure [ft]

ξ₀: surf similarity parameter [-]

α : slope [-]

R_c : freeboard [ft]

γ : coefficient for presence of berm (b), friction (f), wave incidence (β), vertical wall (v)

The coefficients -4.75 and -2.6 in Eq. 1 are the mean values. The standard deviations of these coefficients are equal to 0.5 and 0.35, respectively and these errors are normally distributed (see TAW document).

Eq. 1 is valid for ξ₀ < 5 and slopes steeper than 1:8. For values of ξ₀ > 7 the following equation is proposed for the overtopping rate:

$$\frac{q}{\sqrt{gH_{m0}^3}} = 10^{-0.92} \exp\left(-\frac{R_c}{\gamma_f \gamma_\beta H_{m0} (0.33 + 0.022 \xi_0)}\right)$$
 (2)

The overtopping rates for the range 5 < ξ₀ < 7 are obtained by linear interpolation of eq. 1 and 2 using the logarithmic value of the overtopping rates. For slopes between 1:8 and 1:15, the solution should be found by iteration. If the slope is less than 1:15, it should be considered as a berm or a foreshore depending on the length of the section compared to the deep water wave length. The coefficient -0.92 is the mean value. The standard deviation of this coefficient is equal to 0.24 and the error is normally distributed (see TAW document).

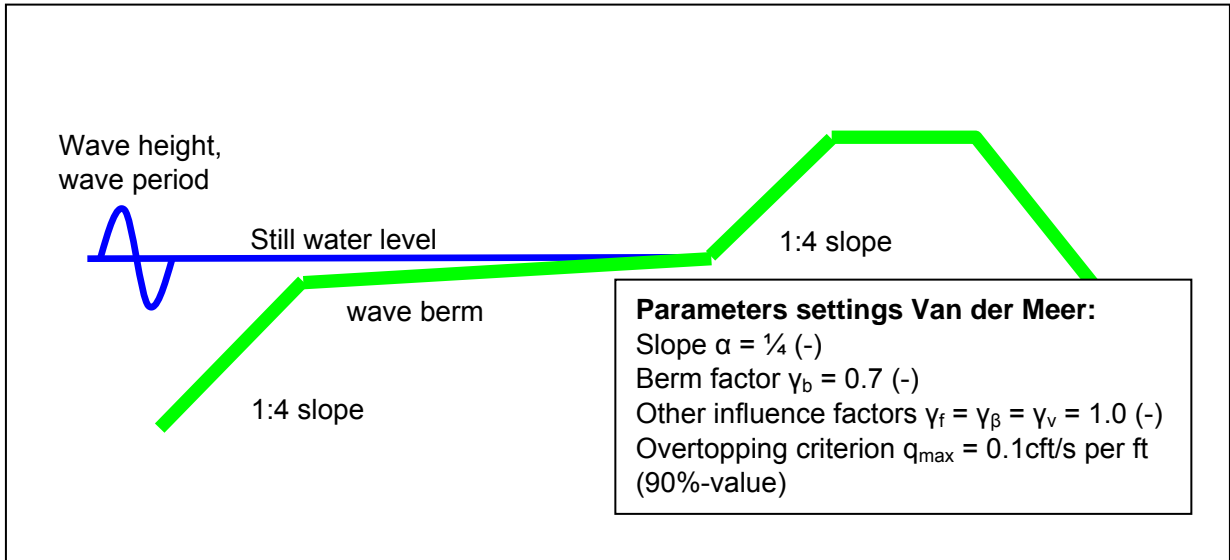


Figure 4.2 - Simplified levee cross section in LACPR evaluation

1019
 1020
 1021

4.2 Design assumptions

1022 This section briefly discusses the most important choices and assumptions in the design
 1023 approach. These items are:

1024
 1025
 1026
 1027
 1028
 1029

- Full dependency between surge levels and waves
- Simultaneous occurrence of maxima
- Breaker parameter
- Overtopping criteria

1030 *Full dependency between surge levels and waves* The step-wise design approach below is
 1031 (partly) probabilistic in the sense that it makes use of the derived water levels and wave
 1032 characteristics based on the JPM-OS method (see also Chapter 3). The procedure also includes
 1033 an uncertainty analysis that accounts for uncertainties in the hydraulic parameters and the
 1034 overtopping coefficients. However, the approach is not fully probabilistic because the correlation
 1035 between water elevation and wave characteristics is not taken into account. This assumption is an
 1036 important restriction to this approach. It is likely that the presented approach is conservative
 1037 because the correlation between the surge elevation and the wave characteristics is not taken into
 1038 account. Depending on the situation, the impact of this assumption on the final levee height can be
 1039 minimal to significant (> 1ft).

1040
 1041
 1042
 1043
 1044
 1045

Simultaneous occurrence of maxima Another assumption in the design approach is that
 the maximum water elevation and the maximum wave height occur simultaneously. Analysis of the
 ADCIRC and STWAVE results shows that the time lag between the peak of the surge elevation
 and the wave characteristics at both sites is small (< 1 hour). It should be noted that there are
 cases in which the time lag between surge and waves is larger (say 1 – 2 hours). Although this

1046 assumption may be conservative for some locations, assuming a coincidence of maximum surge
1047 and maximum waves is reasonable for most of the levee and floodwall sections in our design
1048 approach.

1049
1050 *Breaker parameter* In the design approach we compute the overtopping rates based on
1051 empirical formulations. One of the inputs to these formulations is the wave height at the toe of the
1052 structure. This value is not known, but is estimated based on the wave results from STWAVE.
1053 Because the foreshore is generally very shallow (same order as the wave height), wave breaking
1054 will play an important role in the final 600ft before the toe of the structure (floodwall/levee height).
1055 Hence, it is not likely that the wave height at 600ft in front of the structure will be equal to the wave
1056 height at the toe of the structure, but will be lower.

1057
1058 To account for breaking in front of the levee/floodwall we have reduced the wave height from
1059 STWAVE. An estimate of the wave height at the toe of the structure has been made by making
1060 use of a breaker parameter. The breaker parameter is the ratio between the significant wave
1061 height and the local water depth. In the literature, the breaker parameter is often a constant or it is
1062 expressed as a function of bottom slope or incident wave. A typical range for this parameter is
1063 between 0.5 – 0.78 for engineering purposes. These values are generally obtained for situations
1064 with a mild sloping bed.

1065
1066 However, laboratory experiments and Boussinesq runs suggest that a breaker parameter of 0.4 is
1067 a realistic choice for a relatively long shallow foreshore, as is the case around New Orleans. This
1068 value has therefore been used in the entire design approach to translate the significant wave
1069 heights based on STWAVE to the significant wave height at the toe of the structure. The wave
1070 periods from STWAVE have been used without modification.

1071
1072 *Overtopping criterion* Hughes (2007) carried out a literature survey to underpin the
1073 overtopping criterion value that has been used in the ongoing one-percent design for the Hurricane
1074 Protection System (see USACE, 2007). The survey showed that although various numbers have
1075 been proposed, the experimental validation of these numbers is very limited. Typical values are:
1076 (see also TAW, 2002):

- 1077
1078
 - 0.001 cfs/linear ft (cfs/ft) for sandy soil with a poor grass cover;
 - 1079 • 0.01 cfs/ft for clayey soil with a reasonably good grass cover;
 - 1080 • 0.1 cfs/ft for a clay covering and a grass cover according to the requirements for the outer
1081 slope or for an armored inner slope.

1082
1083 In spring 2007, USACE decided to make use of a maximum overtopping criterion of 0.1 cft/s per ft.
1084 This implies that the inner slope of the clay levee/floodwall has a well-maintained grass cover. An
1085 assurance criterion of at least 90% was used in accordance with the latest Corps guidelines (April
1086 2007). In the framework of LACPR this criterion has been applied without changes for all design
1087 events (100-year, 400-year, 1000-year)³.

³ Note that the overtopping criteria have been slightly changed for the 1% design effort in August 2007 after consultation of ASCE review team (USACE, 2007). The overtopping rate should also be less than 0.01 cfs per ft at the 50% confidence limit. Additional analysis shows that this criterion is almost

1088 **4.3 Uncertainty analysis**

1089 The design criterion in the framework of LACPR is defined as follows: *the overtopping rate should*
1090 *be less than 0.1 cft/s per ft with 90% assurance*". To determine this overtopping rate, a Monte
1091 Carlo analysis has been carried out that accounts for uncertainties in water elevations, waves and
1092 the coefficients in the overtopping formulations. Notice that we neglect the uncertainties in the
1093 geometrical parameters. In other words: we assume that the proposed heights and slopes in this
1094 design document are minimum values achieved during construction. The text below gives a brief
1095 description of this method. For more information, the reader is referred to USACE (2007).
1096

1097 The probability density distributions of the hydraulic variables and the coefficients in the wave
1098 overtopping formulation are inputs into the Monte Carlo Simulation. Frequency results of the surge
1099 levels and the waves were used from the JPM-OS method. These values are the so-called "best
1100 estimates" (or mean values). An additional analysis has provided the standard deviation in the 1%
1101 still water elevation. Standard deviation values of 10% of the average significant wave height and
1102 20% of the peak period were used; these were based on expert judgment (Smith, pers. comm.).
1103 The standard deviations of the coefficients in the Van der Meer formulations are described in the
1104 textbox in section 4.1. All uncertainties are assumed to normally distributed.
1105

1106 The Monte Carlo Analysis applied herein is executed as follows:
1107

- 1108 a) Draw a random number between 0 and 1 to set the exceedance probability p .
- 1109 b) Compute the water level from a normal distribution using the expected value 1% surge
1110 level and standard deviation as parameters and with an exceedance probability p .
- 1111 c) Draw a random number between 0 and 1 to set the exceedance probability p .
- 1112 d) Compute the wave height and wave period from a normal distribution using the expected
1113 value 1% wave height and 1% wave period and the associated standard deviations and
1114 with an exceedance probability p .
- 1115 e) Repeat step 3 and 4 for the three overtopping coefficients in the overtopping formula,
1116 independently, using estimates of variability (standard deviation) in each coefficient.
- 1117 f) Compute the overtopping rate for these hydraulic parameters and overtopping coefficients
- 1118 g) Repeat the steps 1 through 5 a large number of times ($N = 5,000$)
- 1119 h) Compute the 50%, 90% and 95% value of the overtopping rate (i.e. q_{50} , q_{90} and q_{95})
1120

1121 The procedure is implemented in MATLAB. Several test runs show that 5,000 runs are sufficient to
1122 reach statistically stationary results for q_{50} , q_{90} and q_{95} . The computation time to perform this
1123 analysis is in the order of tens of seconds on a current state of the art personal computer. Thus,
1124 the proposed method is straightforward and can be applied in a relatively quick way.
1125

1126 Figure 4.3 shows the result of this design process. The probability of non-exceedance is
1127 shown as a function of the overtopping rate. The levee design height for this specific section is
1128 24ft. With this height, the 90% overtopping rate is 0.082 cfs per ft which meets the design
1129 criterion.

everywhere fulfilled with the original criterion. The LACPR methodology has therefore not been updated
with this extra criterion.

1130

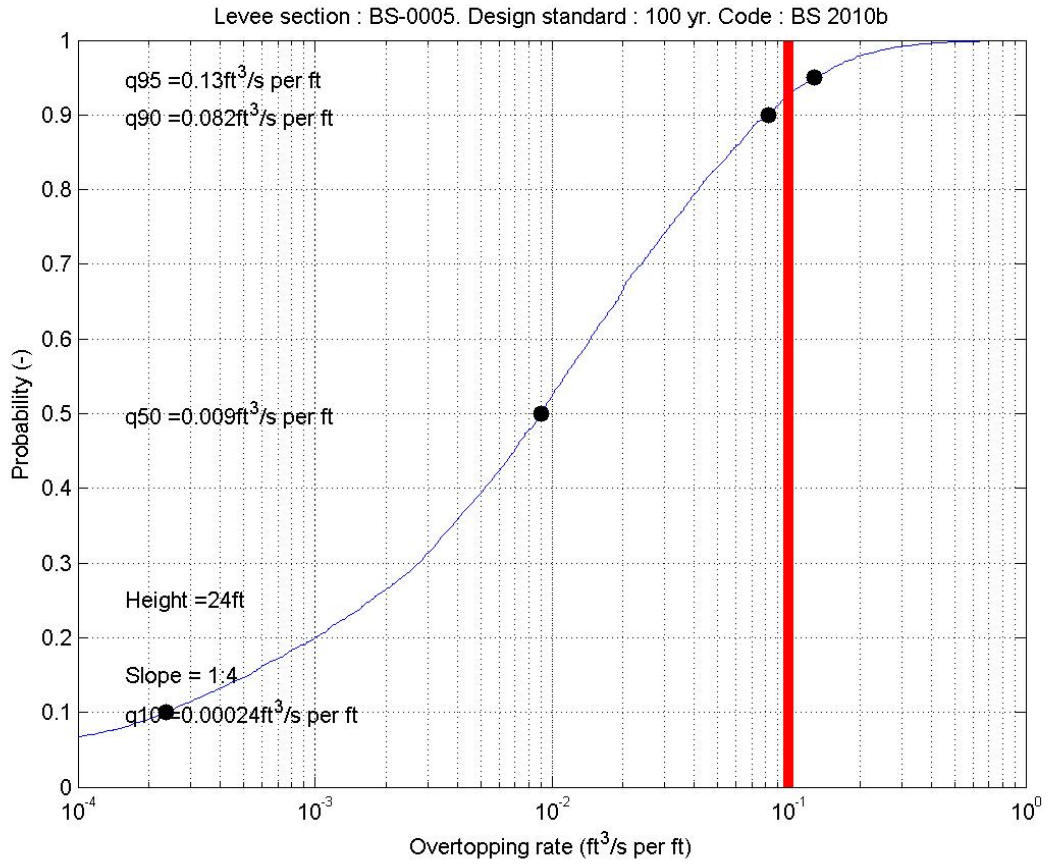


Figure 4.3 - Result for 100-year design height along MRGO levee (Base condition 2010).

1131
 1132

1133 **5 OVERTOPPING RATES**

1134 This chapter describes the determination of the overtopping rates (Figure 5.1). Within the
 1135 framework of LACPR an estimate of the overtopping rate are needed for a given return period. The
 1136 temporal variation of the hydraulic boundary conditions to compute the overtopping rate for a given
 1137 return period is not easily available from ADCIRC and STWAVE. Therefore, the temporal variation
 1138 of the surge level and the wave characteristics is parameterized (Section 5.1). These three load
 1139 factors are used as input to the overtopping formulae, in addition to the design heights of the
 1140 levees to compute the overtopping rates (Section 5.2). The overtopping rates are used as input for
 1141 the interior stage analysis (Chapter 6).
 1142

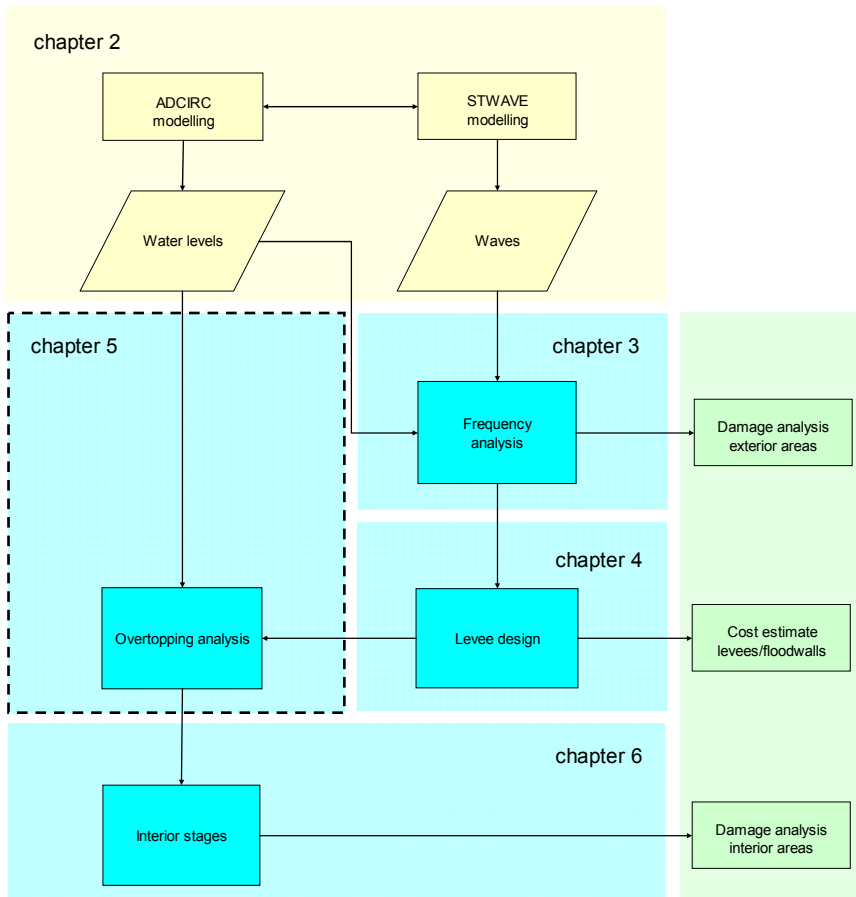


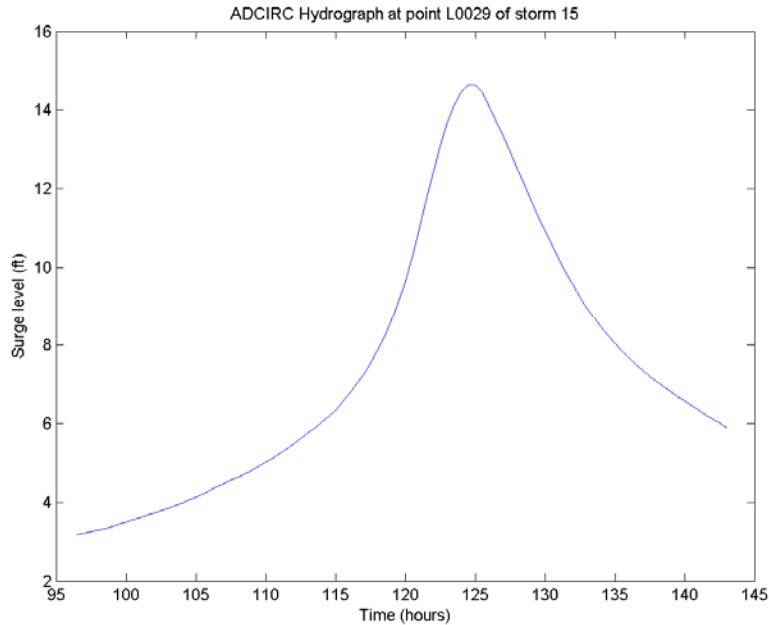
Figure 5.1 - Flow diagram of hydraulic analysis in LACPR framework

1143
 1144
 1145

5.1 Parametrical description of hydrographs

1146 The overtopping discharge, whether due to wave overtopping or free overflow, is determined from
 1147 the variation in time of the surge level and the wave characteristics. In the framework of LACPR
 1148 the overtopping rates need to be determined for a given return period. To estimate these rates, a

1149 description is needed of the temporal variation of the hydraulic boundary conditions for that
1150 specific return period. However, these variations in time are not directly available from the
1151 numerical models ADCIRC and STWAVE. Time series are available for a specific set of storms
1152 (with a maximum of 152) for the water level, wave height and wave period. A typical hydrograph at
1153 a given point is given in Figure 5.2.
1154



1155
1156 **Figure 5.2 - Example of hydrograph from ADCIRC results.**

1157
1158 Within the framework of the JPM-OS method, a conditional approach has been adopted (see
1159 Resio, 2007). This implies that all parameters can be determined as a function of the surge level
1160 (η_{max}) for a given return period (1/100 years, 1/500 years, etc). Along similar lines, the shape of a
1161 hydrograph is also likely to be correlated to the maximum surge level. One may expect that a
1162 correlation can be found between the maximum surge level and the width of a hydrograph,
1163 *normalized by the maximum surge height*. This means that the shape of the hydrograph is more
1164 peaked for large surges than for a smaller surge at the same location. Although the maximum
1165 surge level of a hydrograph at a given location is much higher, the width of the normalized
1166 hydrograph will be less than the width of a normalized hydrograph corresponding to a smaller
1167 maximum surge level.

1168
1169 Based on these considerations, a parametric hydrograph has been developed which takes into
1170 account the variation of the shape of the hydrograph for the 152 (or less) storms. For this process,
1171 we have chosen to assume a Gaussian shape for the hydrograph:

1172
1173
$$\frac{\eta(t)}{\eta_{max}} = e^{-\frac{(t-t_{\eta_{max}})^2}{2\sigma^2}}$$

1174

1175

with:

1176 η : surge level [ft]

1177 σ : width of hydrograph [hrs]

1178 $t_{\eta_{\max}}$: moment with maximum surge level [hrs]

1179

1180 Because the hydrographs clearly show an asymmetric behavior with time, a distinction has been
1181 made between the surge level curve before the peak and after the peak. For both sides, the width
1182 of the hydrograph is estimated from the zero-th and second-order moments for the upper 30% of
1183 the normalized hydrograph (Note: the subscripts l and r refer to left-hand and right-hand side of the
1184 hydrograph):

1185

1186

$$\sigma_{l,r} = \sqrt{\frac{\int_{\tau(0.7^*\eta_{\max})_{l,r}}^{\tau(\eta_{\max})} t^2 \eta(t) dt}{\int_{\tau(0.7^*\eta_{\max})_{l,r}}^{\tau(\eta_{\max})} \eta(t) dt}}$$

1187

1188

with:

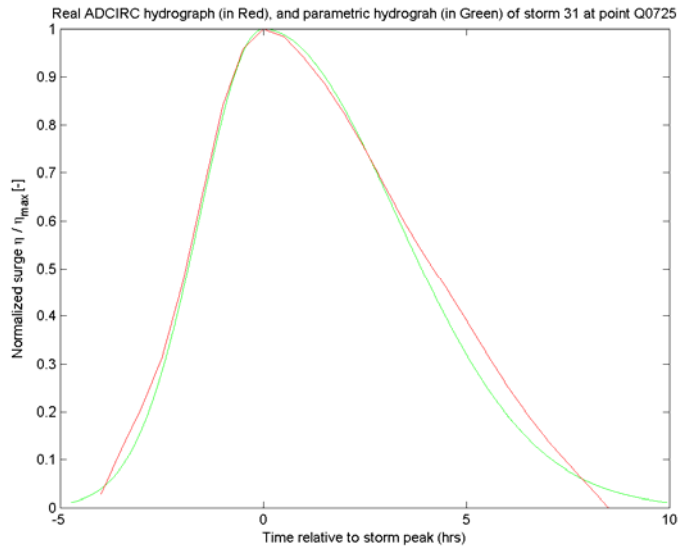
1189 σ : width of hydrograph [hrs]

1190 t : time [hrs]

1191

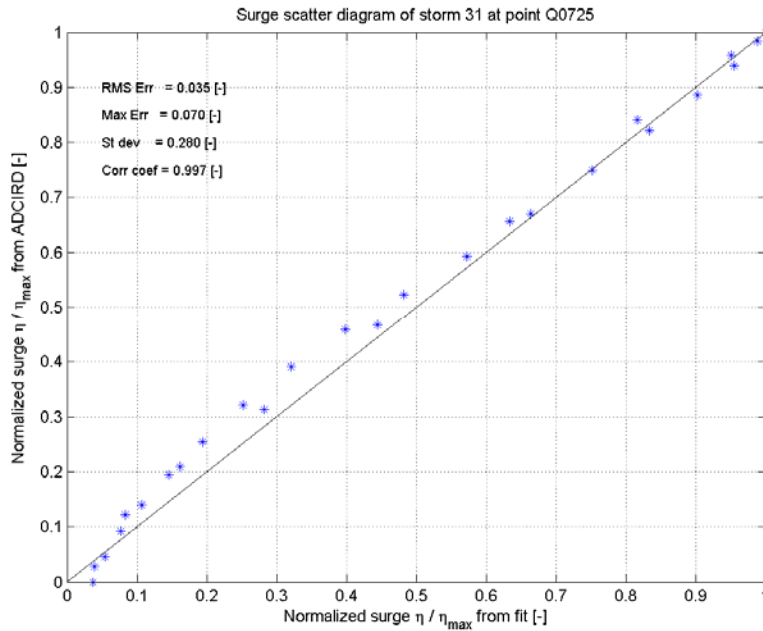
1192 Figure 5.3 presents one example of the real hydrograph from ADCIRC and the estimated Gaussian
1193 shaped hydrograph. Based on visual inspection it can be concluded that the shape of the top of
1194 the hydrograph is well represented by the fitted Gaussian formula. A more detailed view of the
1195 same comparison is shown in Figure 5.4. This figure presents a comparison between the real and
1196 the parameterized hydrograph at one location for one storm. The dots represent the output from
1197 ADCIRC in time along the hydrograph. It can be observed that the fit is good ($R^2 = 0.99$).

1198



1199
1200
1201

Figure 5.3 - Real hydrograph from ADCIRC (in red) and parameterized hydrograph (in red)

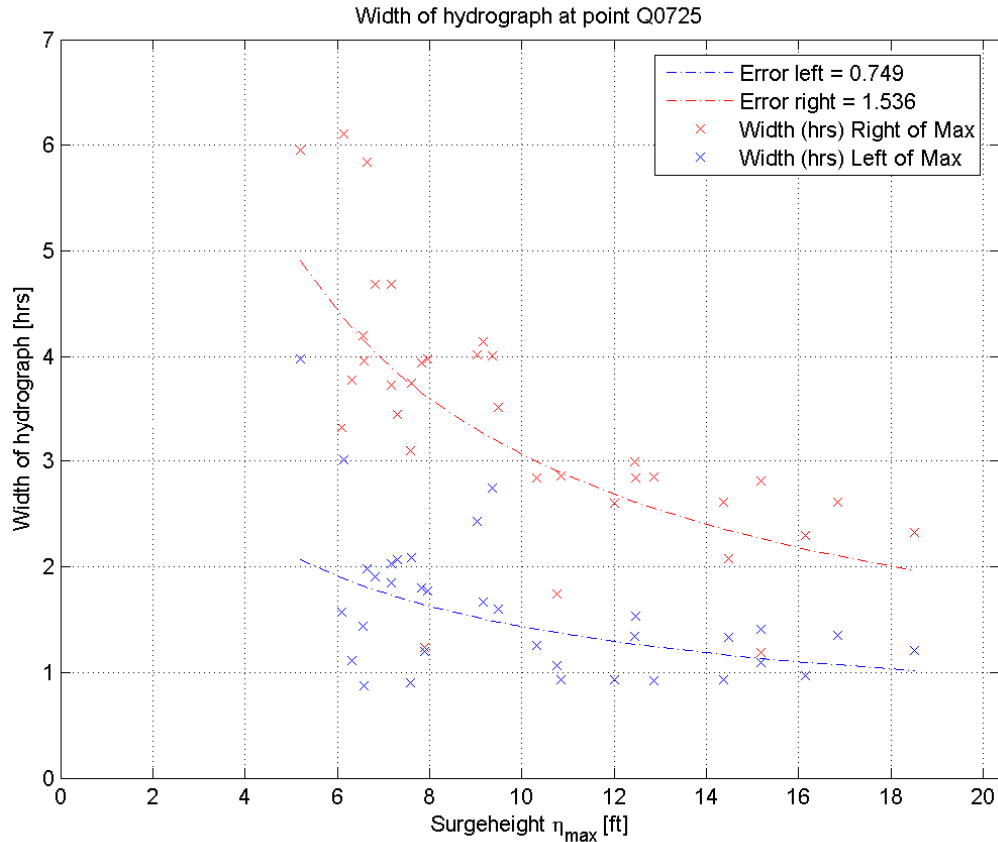


1202
1203
1204
1205
1206
1207
1208
1209

Figure 5.4 - Normalized surge from ADCIRC plotted against the normalized parameterized surge

The next step is to establish a relationship between the width of the hydrograph and the maximum surge level. A log-linear fit has been used. Figure 5.5 presents this relationship for one output point in which the crosses represent the storms. Although the scatter is quite large, there is a visible tendency for smaller widths with higher surge levels. Furthermore, it appears that the correlation seems to be better for higher surge levels. This is related to the fact that the upper 70% of the

1210 hydrograph of a severe storm scenario has a better defined peak compared with a mild to
1211 moderate storm. Because the scatter in the fits cannot be disregarded, this aspect has been taken
1212 into account in the uncertainty analysis of the overtopping discharges. This will be further
1213 discussed in Section 5.2.



1214 **Figure 5.5 - Width of the hydrograph plotted against the maximum surge level. Crosses indicate**
1215 **the different storms, the lines are the fit through the data points**
1216

1217
1218 Apart from the surge levels, the temporal variation in the wave characteristics may also play a role
1219 in the overtopping rates. A similar approach as described above could be used for the wave
1220 characteristics as well. It appears, however, from the wave data that the variation in wave height
1221 around the peak surge is not considerable. In our approach, we have therefore used the maximum
1222 wave height for the entire surge hydrograph. A sensitivity analysis has been executed and the
1223 impact on the total overtopping volume appears to be small.
1224

1225 5.2 Overtopping volumes

1227 The overtopping rates have been computed using empirical equations. In contrast with the design
1228 approach in Chapter 4, the surge level may be (far) above the crest level for some cases. For
1229 instance, a 100-year level of protection in combination with a 1000-year event can easily give

1230 surge levels higher than the crest level. Therefore, two contributions are taken into account for the
1231 overtopping rate computation: wave overtopping and free flow overtopping.

1232

1233 To compute the overtopping rates a distinction has been made between two cases:

1234

- 1235 • Surge level *below* the crest level : only wave overtopping
- 1236 • Surge level *above* the crest level : wave overtopping and free flow

1237

1238 For the situation with wave overtopping only, the empirical equations from Van der Meer have
1239 been applied (see Chapter 4). If the surge level is above the crest level, both free flow and wave
1240 overtopping are taken into account (TAW, 2003):

1241

$$1242 \quad q_{tot} = m(\eta - z_{crest})^{3/2} + 0.13\sqrt{gH_s^3} \quad (5.1)$$

1243

1244 with:

1245 q_{tot} : total overtopping rate (cft/s per ft)

$$1246 \quad m : \text{weir coefficient} \left(= \frac{2}{3} \sqrt{\frac{2}{3} g} \approx 3.1 \text{ ft}^{0.5} / \text{s} \right)$$

1247 g : gravitational acceleration (= 32.2 ft/s²)

1248 z_{crest} : crest level [ft]

1249 η : water level [ft]

1250 H_s : significant wave height [ft]

1251

1252 The first contribution in Eq. 5.1 is due to free flow, the second part is due to wave overtopping.

1253

1254 The overtopping rates have been computed using a Monte Carlo Simulation to account for the
1255 various uncertainties. The uncertainty in hydrograph width is initially considered, followed by the
1256 uncertainties in wave height, wave period and the coefficients of the overtopping formulation. The
1257 following procedure is followed:

1258

- 1259 a) Set the confidence level of the overtopping rate (in this case: 10%, 50% or 90%)
- 1260 b) Compute the width of the hydrograph associated with this probability from step a) using the
1261 expected values and the standard deviation (assuming a normal distribution).
- 1262 c) Draw a random number between 0 and 1 to set the exceedance probability p .
- 1263 d) Compute the maximum water level from a normal distribution using the expected value 1%
1264 surge level and standard deviation as parameters and with an exceedance probability p .
- 1265 e) Generate a hydrograph with this maximum water level and the given width of the
1266 hydrograph (10%, 50% or 90%)
- 1267 f) Compute the wave height and wave period from a normal distribution using the expected
1268 value 1% wave height and 1% wave period and the associated standard deviations and
1269 with an exceedance probability p .
- 1270 g) Repeat step c) and d) for the three overtopping coefficients in the overtopping formula,
1271 independently, using estimates of variability (standard deviation) in each coefficient.
- 1272 h) Compute the overtopping rate for these hydraulic parameters and overtopping coefficients

- 1273 i) Repeat the steps c) through h) a large number of times (N = 5,000)
 1274 j) Select the overtopping rate from the results at i) with the confidence level at step a)
 1275

1276 The procedure is implemented in MATLAB to automate this procedure.
 1277

1278 The above described approach results in overtopping rates with a 10%, 50% and 90% confidence.
 1279 As an example, Figure 5-6 presents the overtopping rates as a function of time for one levee
 1280 design with a 100-year level of protection. Every plot has a unique label at the top:
 1281

- 1282 • DSX: Design standard with X-year return period (in this case 100-year)
- 1283 • RPX: Hydraulic boundary condition with X-year return period (in this case
 1284 100/400/1000/2000 year)
- 1285 • BSX: Base situation at location X (in this case 0001)
- 1286 • BS : Evaluated situation (BS = Base situation, EA = East A, EB = East B, etc)
 1287

1288 So, each plot represents a different return period for the hydraulic boundary conditions, viz. 100-
 1289 year, 400-year, 1000-year and 2000-year. Furthermore, each plot gives the 10%, 50% and 90%
 1290 overtopping rates in different colors.
 1291

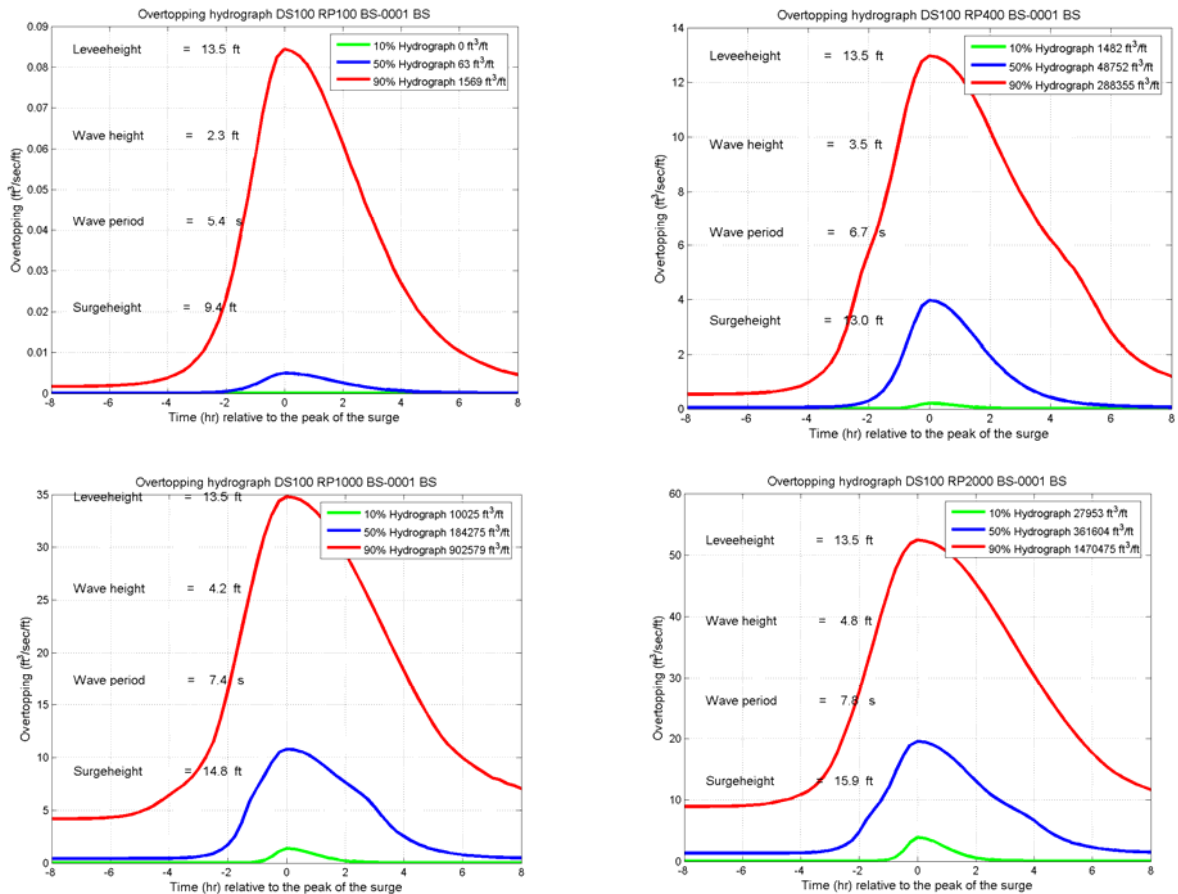


Figure 5.6 - Overtopping rates for different return periods (100-year, 400-year, 1000-year and 2000-

year) at a level with a 1% design elevation

1292

1293

A few remarks are made regarding Figure 5.6:

1294

- The maximum overtopping rate for the 100-year hydraulic situation equals about 0.1 cft/s per ft because this was the design criterion of the levee section. For the higher return periods the overtopping rates increase with several orders of magnitude.

1295

1296

1297

- The 1000-year and 2000-year return period give free flow over the levee because the maximum surge level is higher than the levee crest.

1298

1299

- The form of the overtopping curve is not symmetrical but resembles the relatively steep front of the surge.

1300

1301

1302

In total, approximately 6,000 overtopping hydrographs have been produced with the automated script for the LA-East alternatives within the framework of LACPR. This number consists of 7 (Louisiana East alternatives) x 35 (economic sub basins) x 2 (two levee sections per sub basin on average) x 4 (hydraulic return periods) x 3 (design protection levels). These overtopping volumes have been used as an input into the interior drainage modeling which is discussed in Chapter 6.

1303

1304

1305

1306

1307 **6 INTERIOR DRAINAGE**

1308 This chapter discusses the process of converting overtopping into interior drainage areas into
 1309 stage frequency relationships (Figure 6.1). First the internal drainage areas are defined (section
 1310 6.1). Next, the basic methodology for considering the interior drainage process is explained
 1311 (section 6.2). Sections 6.3 to 6.5 describe the dominant processes that occur during a hurricane
 1312 event which affect internal flooding: rainfall, overtopping and pumping. The interior stage
 1313 frequency curves developed are used as input into the economic analysis.
 1314

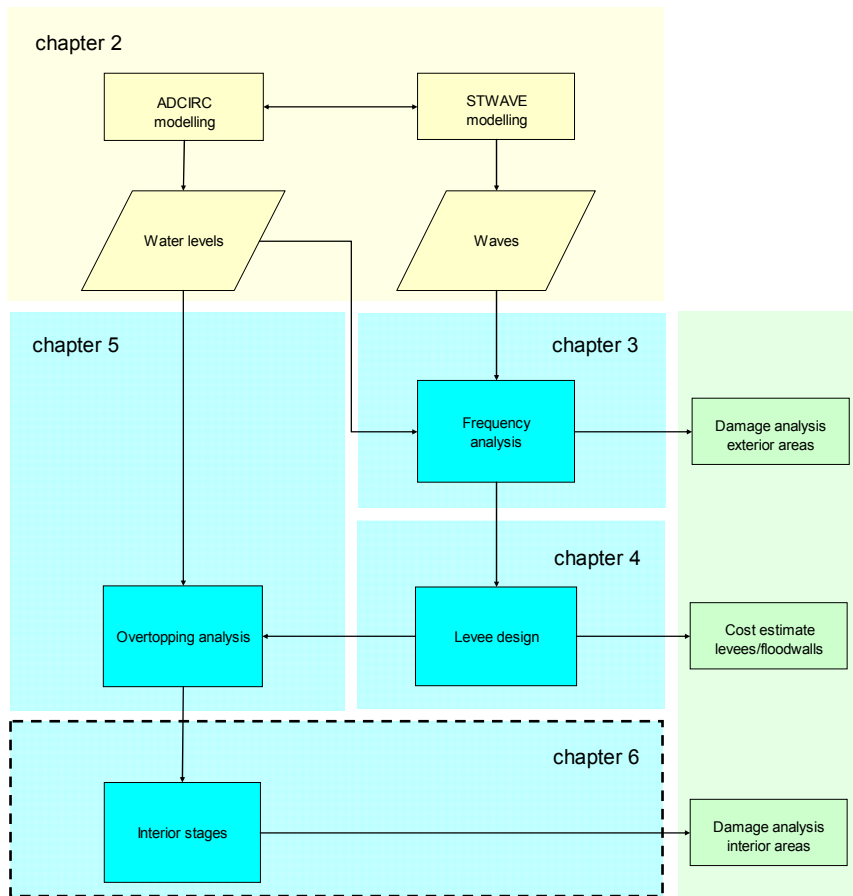


Figure 6.1 - Flow diagram of hydraulic analysis in LACPR framework

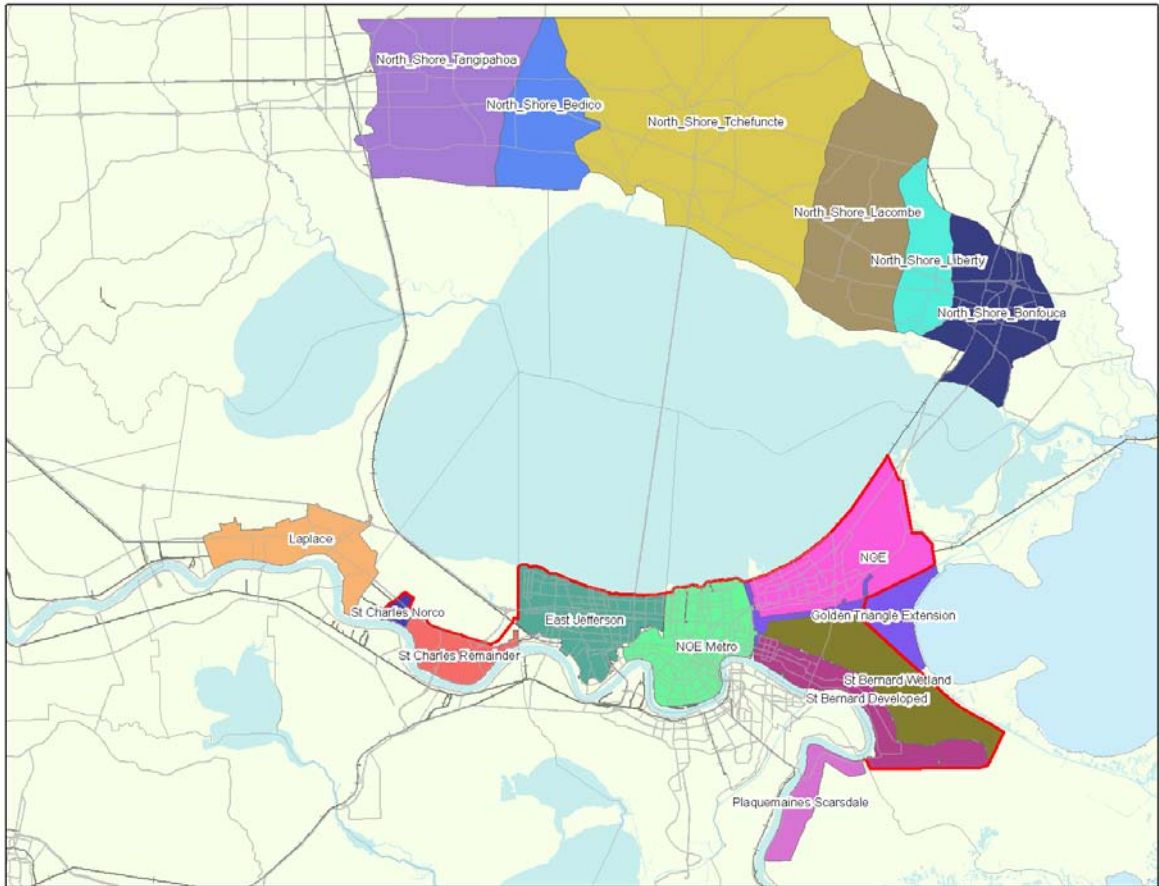
1315
 1316
 1317

6.1 Storage areas

1318 The LACPR planning area is visualized in Figure 1.1. For the purposes of LACPR, the eastern
 1319 side of the planning area has been divided into two planning units. Planning Unit 1 is situated on
 1320 the east bank of the Mississippi and includes Lake Pontchartrain whilst Planning Unit 2 covers the
 1321 west bank of the Mississippi and the Barrataria Basin as far as Bayou Lafouche, as indicated in
 1322 Figure 6.2 and Figure 6.3.

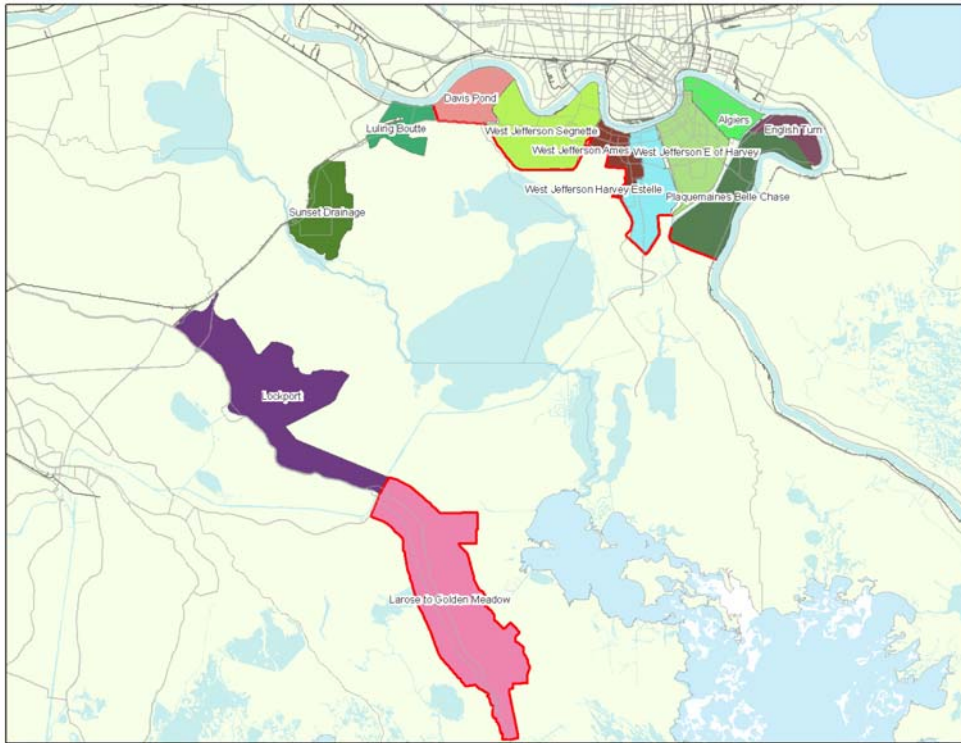
1323
1324
1325
1326
1327
1328
1329
1330
1331
1332
1333
1334

Within each planning area the area within the authorized levee systems or for which levees are being planned have been sub-divided into smaller areas, called internal planning subunits. Most of the existing internal planning subunits are located in the vicinity of the city of New Orleans. New internal planning subunits have been developed for areas such as the north shore of Lake Pontchartrain where there currently is no levee but in one of the alternatives a levee is planned. Within the metropolitan areas of New Orleans the internal planning subunits have been defined either by parish boundaries or other defined features (such as raised roads or existing internal levees). For evaluation purposes the planning subunits in Planning Unit 3a, 3b and 4 are grouped into interior drainage areas. These areas are outlined in red.



1335
1336
1337

Figure 6.2 - Subunits Planning Unit 1



1338
1339

Figure 6.3 - Subunits Planning Unit 2

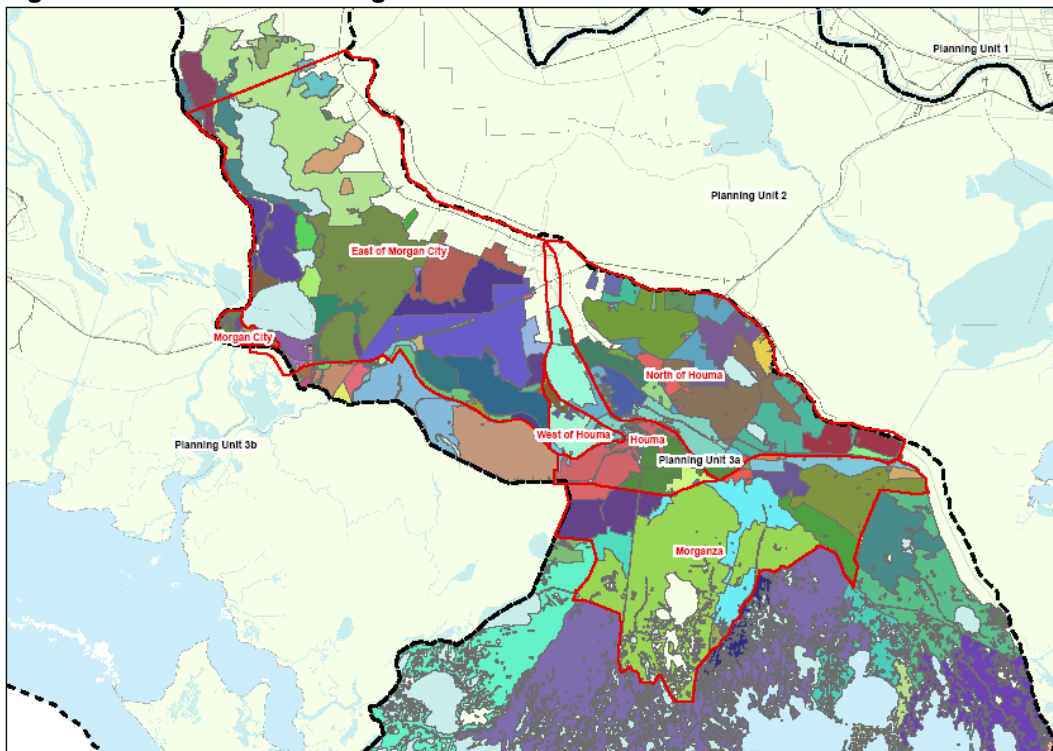


Figure 6.4 - Planning Subunits and Drainage Areas for Planning Unit 3a

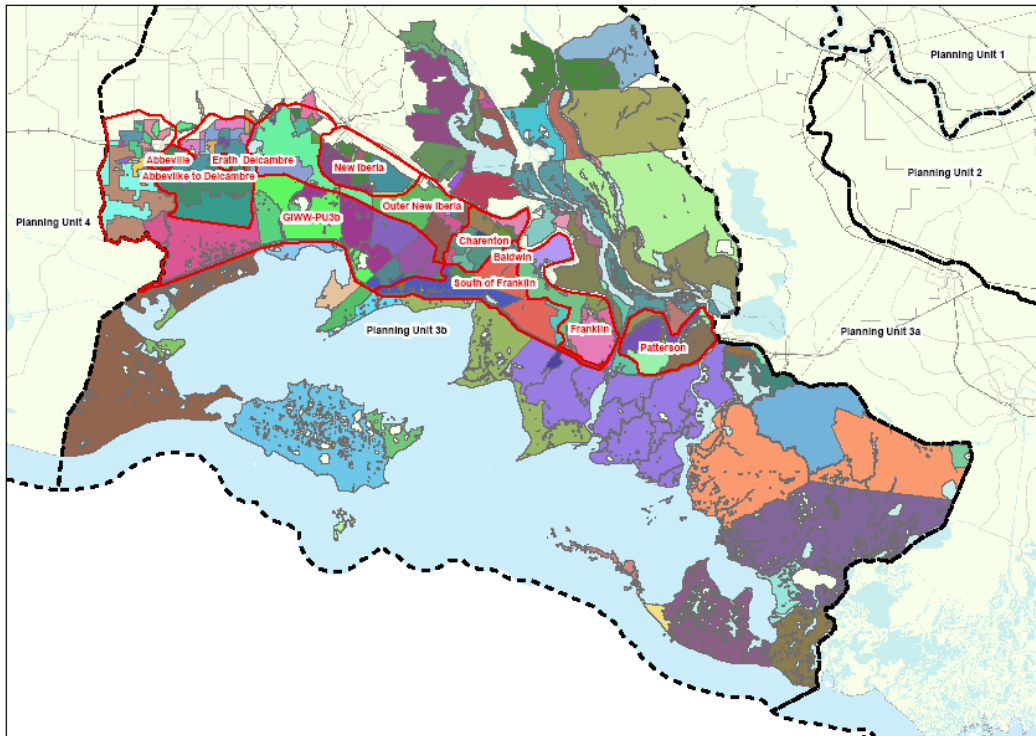


Figure 6.5 - Planning Subunits and Drainage Areas for Planning Unit 3b

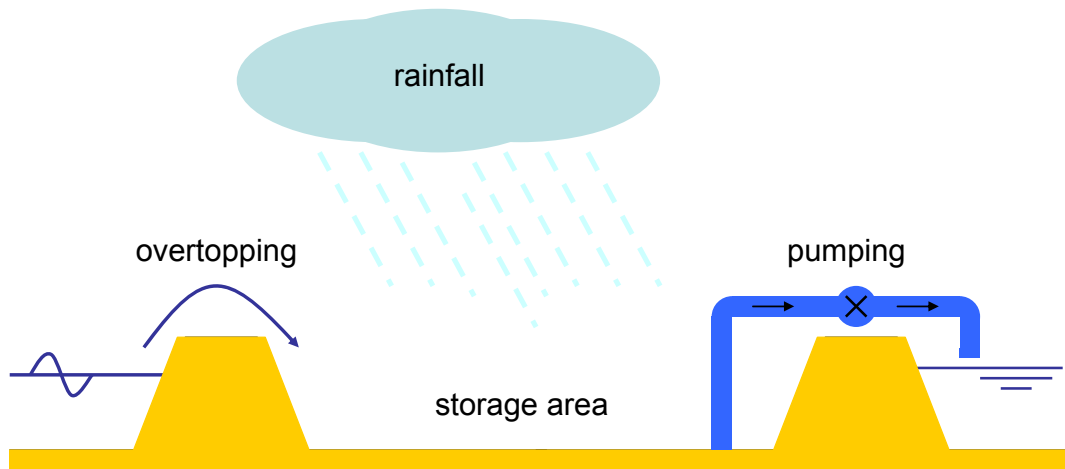
1340



Figure 6.6 - Planning Subunits and Drainage Areas for Planning Unit 4

1341 **6.2 Methodology**

1342 Each internal planning subunit has been schematized as a box model for which a stage-storage
1343 curve has been established. This information has been extracted from existing rainfall-runoff
1344 models or from LIDAR data for these areas. During a hurricane event the water balance is
1345 dominated by rainfall, wave or surge water overtopping and pumping (see Figure 6.7). The interior
1346 stage frequency has been based on the sum of the overtopping volume together with rainfall in the
1347 sub basin. The effect of pumping in reducing flood volume has been taken into account if
1348 applicable. Where economic sub-basins join, a flow of water has been allowed to occur between
1349 areas above defined thresholds.
1350
1351

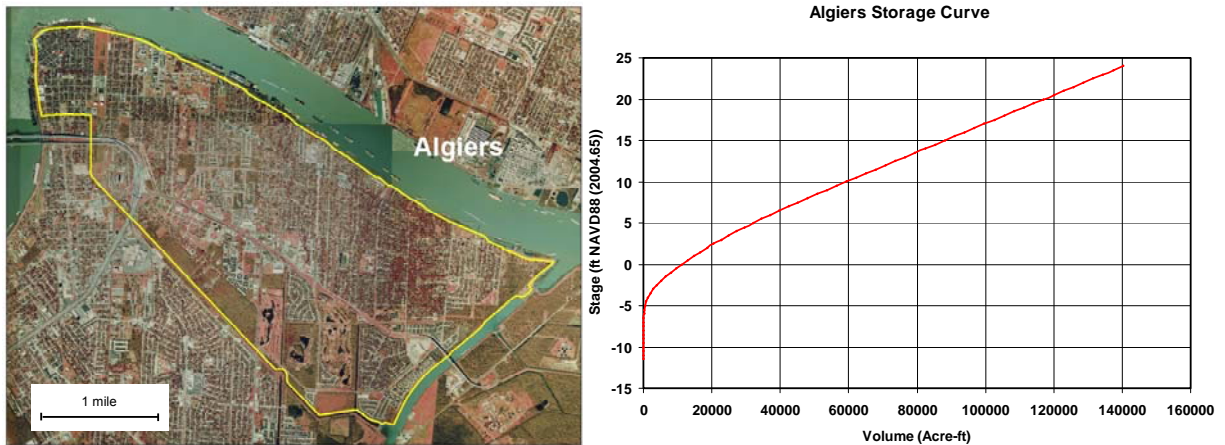


1352 **Figure 6.7 - Principle water system**
1353
1354

1355 The rainfall used in the evaluation was the 10 year rainfall and the development of the rainfall
1356 hydrograph is described further in Section 6.3.
1357

1358 For each of the overtopping edges of an internal planning subunit, overtopping hydrographs were
1359 established based on the levee design height or the current authorized levee heights, whichever
1360 was the higher. These hydrographs are described in more detail in Section 6.4.
1361

1362 An example of an internal planning subunit development is given below. This shows the extent of
1363 an area, the stage storage relationship (in acre-ft) extracted or developed, and the overtopping
1364 lengths of the levees adjacent to the internal planning subunit.
1365



1366
1367 **Figure 6.8 - Internal planning subunit and stage storage relationship**
1368
1369
1370

6.3 Rainfall

1371 The LACPR project concentrates on the development of flood protection systems (wetlands,
1372 levees) that protect against a range of hurricane surge events. Rainfall, however, also contributes
1373 to the interior flooding. Although this phenomenon is not the primary focus of this study, rainfall
1374 has been taken into account. Historical data gives some insight in the order of magnitude of the
1375 rainfall during hurricanes in Louisiana. Based on these records, the heaviest rains during Betsy
1376 were reported 2 to 6 inches of rain in from 40 miles west to 80 miles east of the center path (Pfof,
1377 1993). Camille showed average precipitation of 5 inches within the area 20 miles west and 80
1378 miles east of the hurricane path. Large-scale total rainfall during Katrina was around 8-10 inches in
1379 the eastern region of Louisiana.
1380

1381 In the framework of LACPR, it has been decided to use a constant rainfall event across all storm
1382 surge events (100-year, 400-year, etc.), confidence bands (10%, 50% and 90%) and for all
1383 planning units. Interior drainage is in essence fixed so that interior responses to overtopping over
1384 the flood protection system can directly be compared from one plan to another. Based on earlier
1385 work, it appears that the heaviest rainfall have been from storms of less than hurricane intensity
1386 (Shoner and Molansky, 1956). In other words, it is not likely that an extreme hurricane event (100-
1387 year event, 400-year event, etc.) coincides with a rare rainfall event. Therefore, a relatively mild
1388 rainfall event has been selected for this evaluation (10-year) which has rainfall intensity
1389 comparable to the historical rainfall during Camille and Betsy.
1390

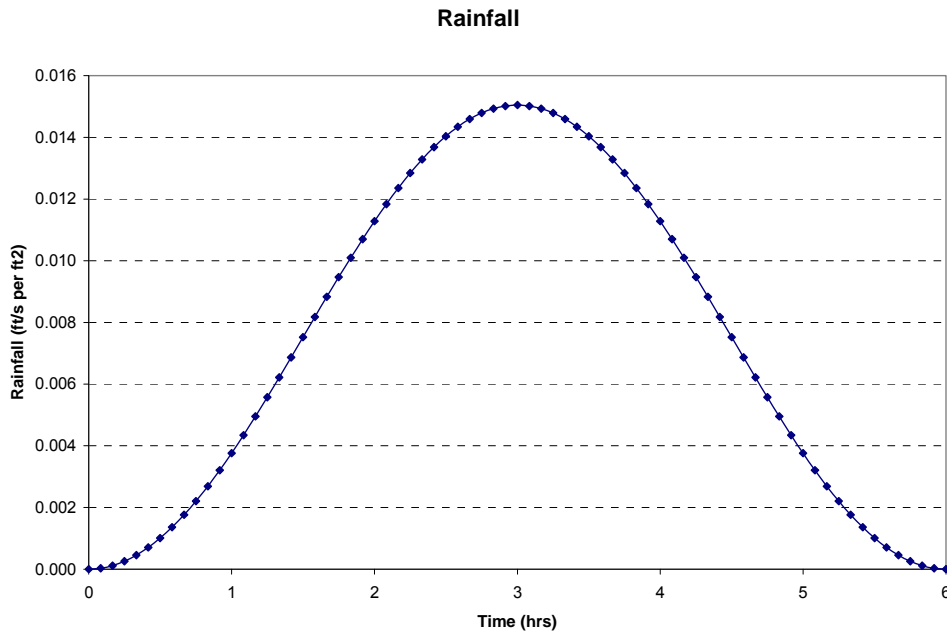
1391 The rainfall event values were obtained for a range of storm durations from TP-40 documentation.
1392 These data were used because the hydrologic work done for the South East Louisiana Urban
1393 Flood Control Project (SELA) applied these data. The basic assumption in the populated areas of
1394 New Orleans is that pumping can cope with 1" of rainfall in the first hour, and 0.5" in subsequent
1395 hours. Using this assumption, the various 10-year rainfall events (3-hour, 6-hour, 12-hour, 24-
1396 hour) were evaluated and the 6 hour duration storm was shown to give the highest rainfall rate
1397 over pumping. Since the stage storage routings do not account for lag times, a short duration

1398 rainfall event (6 hour) also has the advantage that the storage would more closely replicate
1399 flooding as predicted with the unsteady flow HEC-RAS analysis.

1400

1401 The total rainfall is 6.5" for a 10-year rainfall event of 6 hours according to TP40 documentation.
1402 The rainfall hydrograph was calculated as a sinusoidal distribution over a six hourly period, and
1403 values were obtained in steps of 5 minutes. Note that in reality, the temporal development of
1404 rainfall events can be quite different from a sinusoidal shape. Figure 6.9 shows the standardized
1405 rainfall hydrograph resulting from this 10 year return period rainfall event. The rates are given in
1406 cft/s per square foot and a sinusoidal curve has been assumed. No routing of rainfall has been
1407 considered within the volume balance model. All rainfall collecting within a 5 minute time step is
1408 assumed to be available for pumping at the same time.

1409



1410

1411 **Figure 6.9 - Standardized rainfall hydrograph**

1412

1413

1414

6.4 Overtopping

1415

1416 The levee overtopping rates (10%, 50% and 90% confidence) were computed using the methods
1417 described in Chapter 5 for a number of different design standards (100, 400 and 1000 years) and
1418 the range of return periods 100, 400, 1000 and 2000 years. Examples for the 100-year design
1419 standard and 100 and 400 year storm events for the New Orleans East internal planning subunit
1420 are given in Figure 6.10. These show both the rainfall hydrograph and the levee overtopping
1421 hydrographs for three different defense lengths. In the same way as with the rainfall no allowance
1422 has been made for flood routing between the levees and the pumps.

1423

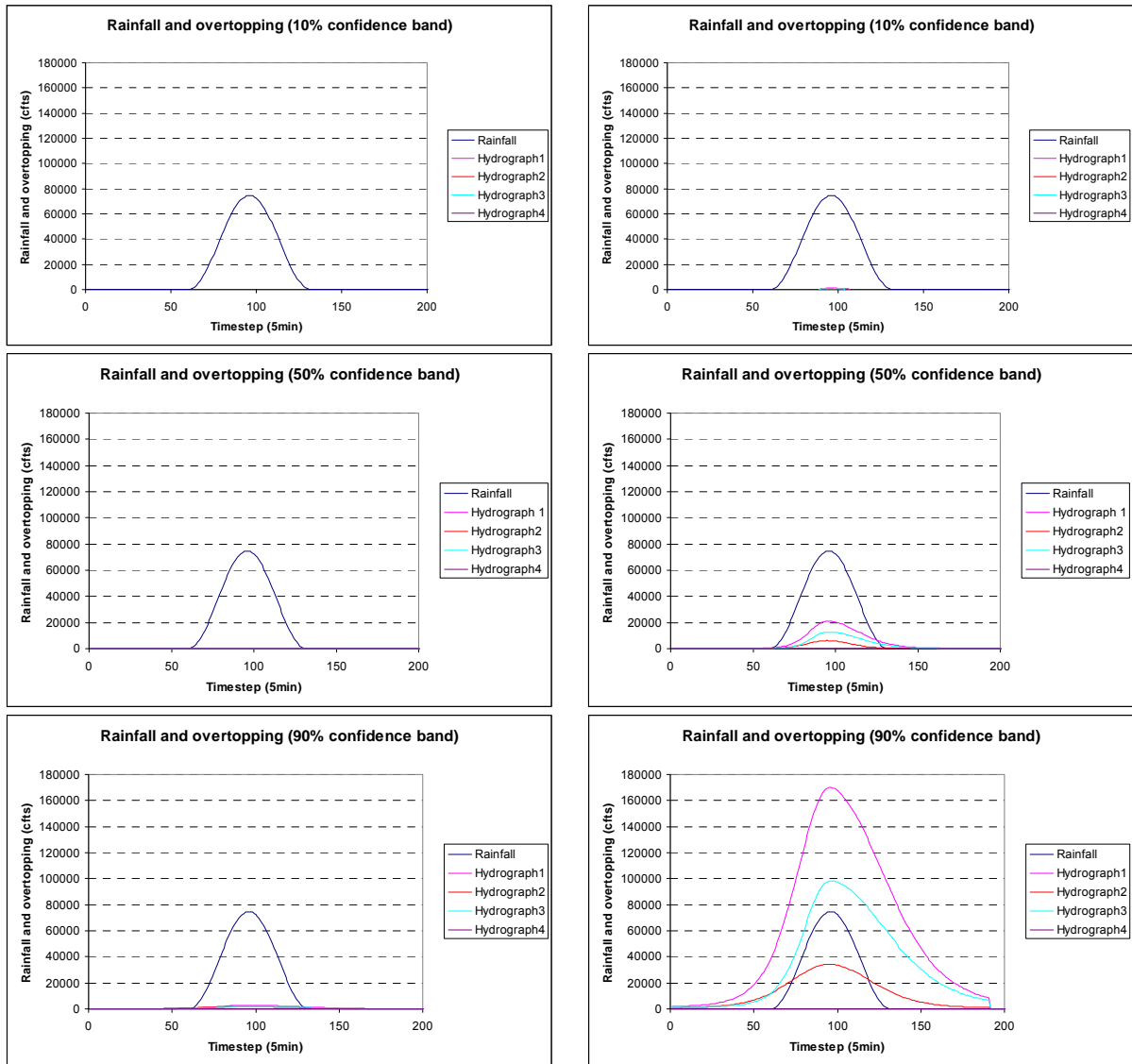


Figure 6.10 - Rainfall Hydrograph of NEO (design standard 100 year en return period 100 year (left) and return period 400 year (right)

1424

1425 **6.5 Pumping**

1426

1427 Pumping for each drainage area has been considered as a fixed rate of outflow. The pumping
 1428 rates were obtained from the Corps for those locations where pumps were thought to exist. The
 1429 values ranged from around 20,000 cft/s in East Jefferson to around 800 cft/s in St Charles Norco.
 1430 Once the volume of pumping is exceeded by the inflow into the area in any 5 minute time step
 1431 then flooding occurs.

1432

1433 New pump capacities were not estimated because of time limitations and the complexity of
 1434 analyzing a very complex interior drainage system. For instance, the New Orleans area is

1435 composed of numerous interior pumping stations that are fed by a complex system of canals and
1436 subsurface drainage systems. The primary stations along the outfall canals are operated in
1437 conjunction with the other stations. In order to increase the capacities of the outfall canal pumping
1438 stations and make sure that the added capacity is usable, one would have to redesign the
1439 complete interior delivery system to insure that flow could reach the outfall canal pump station.

1440
1441
1442

6.6 Flood Volumes and Stage Frequencies

1443 The rate of flooding in each time step is considered by comparing the rate to the pumping rate and
1444 then if the difference is positive, recording the difference. These positive rates are then summated
1445 and multiplied by 300 to convert /s rates to totals over 5 minutes and then divided by 435000 to
1446 convert from cft to acre-ft. This gives a total volume of flooding for this condition. This is repeated
1447 for each confidence band and each design standard.

1448

1449 The flood stage in each internal planning subunit is established by interpolating the total flood
1450 volume into the stage storage relationship (as shown in section 6.2). The stage for each return
1451 period and design event is then compared with the levee height and the event surge height and
1452 the higher stages are capped at the higher of the levee height or surge elevation.

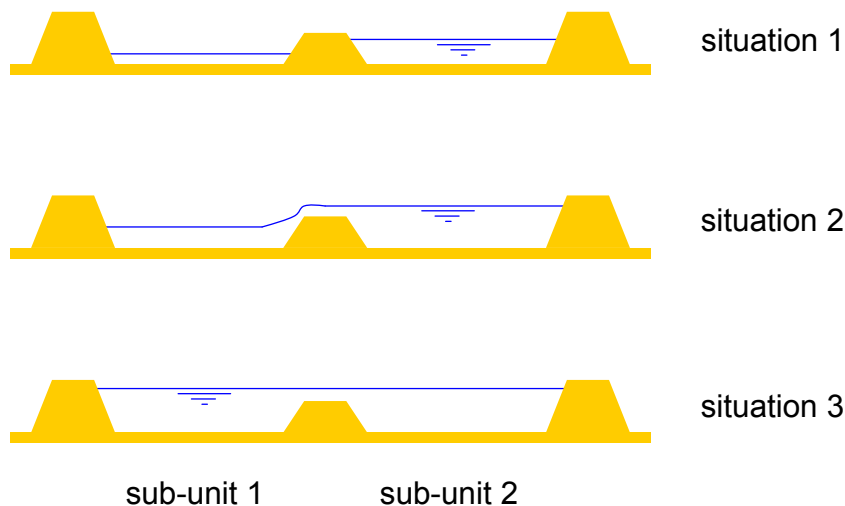
1453

1454 For those interior planning subunits which are internally connected the total flood volumes are
1455 used within separate calculations to consider the volumes flowing between adjacent storage areas
1456 and then to see whether the combined system fills above the levels of the divides or to the top
1457 level of the levees (see Figure 6.11).

1458

1459

1460



1461

1462

1463

Figure 6.11 - Water volumes flowing between adjacent sub-units

1464 **7 REFERENCES**

1465

- 1466 1. Plan Formulation Atlas, April 16 2007, <http://lacpr.usace.army.mil/default.aspx?p=atlas>
- 1467 2. Resio et al., 2007. White paper on estimating Hurricane Inundation Probabilities, USACE, ERDC-
- 1468 CHL.
- 1469 3. TAW, 2003. Technische Adviescommissie voor de Waterkeringen, Leidraad kunstwerken (In
- 1470 Dutch), May 2003.
- 1471 4. TAW, 2002: Wave runup and overtopping at Dikes, Technical Report, Delft, 2002. See also:
- 1472 www.tawinfo.nl.
- 1473 5. USACE, 2007. Elevations for design of hurricane protection levees and structures, Lake
- 1474 Pontchartrain, Louisiana and vicinity hurricane protection project, west bank and vicinity. Draft
- 1475 report, Final report, Prepared by New Orleans District, 15 October 2007.
- 1476 6. TAW, 2002. Technical Report Wave Run-up and Wave Overtopping at Dikes, Delft, The
- 1477 Netherlands.
- 1478 7. IPET, 2007. Performance Evaluation of the New Orleans and Southeast Louisiana Hurricane
- 1479 Protection System, L.E. Link (editor).
- 1480 8. FEMA, 2007. Flood insurance Study: Southeastern Parishes Louisiana, DRAFT, Intermediate
- 1481 Submission 1: Scoping and Data Review. September 19, 2007. FEMA Region 6 and USACE MVN
- 1482 District.
- 1483 9. R.L. Pfost, 1993. Technical Attachment Rainfall patterns and Hurricane Andrew. A Hydro-
- 1484 meteorological Survey, Lower Mississippi River Forecast Center, Slidell, Louisiana
- 1485 10. R.W. Shoner and S. Molansky, 1956. Rainfall associated with Hurricanes. National Hurricane
- 1486 Research Project. Report No. 3. Prepared under P.L.71, 84th Congress, 1st Session.
- 1487 11. Hughes, S.A., 2007: Evaluation of Permissible Wave Overtopping Criteria For Earthen Levees
- 1488 Without Erosion Protection, ERDC-CHL, Vicksburg.
- 1489 12. U.S. Army Corps of Engineers, 2001: Coastal Engineering Manual. Engineer Manual 1110-2-1100,
- 1490 U.S. Army Corps of Engineers, Washington, D.C. (in 6 volumes).

1491

1492

1493

1494

1495

1496

1497

=O=O=O=

1498

1499

1500

1501

1502 **ANNEXES**

1503

1504

1505

1506
1507
1508
1509
1510
1511
1512
1513
1514
1515
1516
1517
1518
1519
1520

Annex A
Sea level rise

1521 Author: Kevin Knuuti, ERDC-CHL

1522

1523 Variations and trends in the relationship between local mean sea level (LMSL) and land elevations
1524 are important considerations in the planning and design of structures in areas that are currently
1525 tidally influenced or that could become tidally influenced in the future. In areas where the LMSL is
1526 rising relative to land elevation, the relative sea-level rise (RSLR) is often divided into a global
1527 increase in water mass (eustatic rise), a rise in local water level due to density changes in the
1528 water (steric rise), and a drop in local land elevation (subsidence). Throughout the 20th century,
1529 the global average SLR due to eustatic and steric effects has been approximately 1.8 mm/year
1530 (Meehl, 2007). Examination of tide gauges on geologically stable platforms in the northern Gulf of
1531 Mexico indicates a regional average SLR of approximately 1.8-2.0 mm/year during that same time
1532 period. Throughout coastal Louisiana, rates of subsidence exceed the rate of SLR by varying
1533 amounts. The resulting rates of RSLR throughout coastal Louisiana are significantly higher than
1534 the global average and regional average SLR rates.

1535

1536 Though the causes of climate change and future projections of climate change are somewhat
1537 controversial, it is well accepted that RSL has been rising across coastal Louisiana and will
1538 continue to do so in the future. Because of the difficulty associated with quantifying the rates of
1539 SLR that will occur in different areas of Louisiana, a sensitivity analysis is performed to determine
1540 how different project designs would respond to a range of SLR rates. For this sensitivity analysis,
1541 an extrapolation of the historic rates of RSLR is used as the low level for future sea-level rise and
1542 accelerated rates of rise based on National Research Council (NRC, 1987) and Intergovernmental
1543 Panel on Climate Change(IPCC) (Meehl, 2007) projections are used for higher rates of rise.
1544 Historic rates of RSLR vary across Louisiana and also vary depending on the methods used to
1545 estimate those rates. The two most commonly cited methods of estimating historic RSLR rates in
1546 Louisiana are radiometric dating of organic deposits (mostly peat) and analysis of long-term tide-
1547 gauge data. Because the RSLR rates determined from tide gauge data are based on more recent
1548 (20th century) data and because these rates are generally greater than the rates determined from
1549 radiometric dating, tide gauge RSLR rates are used for the low rate of RSLR in the sensitivity
1550 analysis.

1551

1552 Both the National Ocean Service and the U.S. Army Corps of Engineers have maintained long-
1553 term water-level gauges that can be used to calculate historic RSLR rates across coastal
1554 Louisiana. Because of the distance between these gauges, and the engineering difficulty
1555 associated with using numerous historic RSLR rates for analysis, coastal Louisiana was divided
1556 into different geomorphic regions for RSLR analysis. Within each geomorphic region, subsidence
1557 rates were thought to be relatively uniform due to relatively homogeneous geologic conditions.
1558 The geomorphic regions considered were based on the historic shifting of the Mississippi River's
1559 main stem and the associated delta lobes the river created, as shown in figure A.1 and as
1560 described by Penland (1990). Based on similarities in historic RSLR rates, alternative screening
1561 further grouped the regions into three primary geomorphic regions: the Chenier Plain (region 1 in
1562 figure A.1), the Delta Plain (regions 2-6 in figure A.1), and the Pontchartrain Basin (region 7 in
1563 figure A.1).

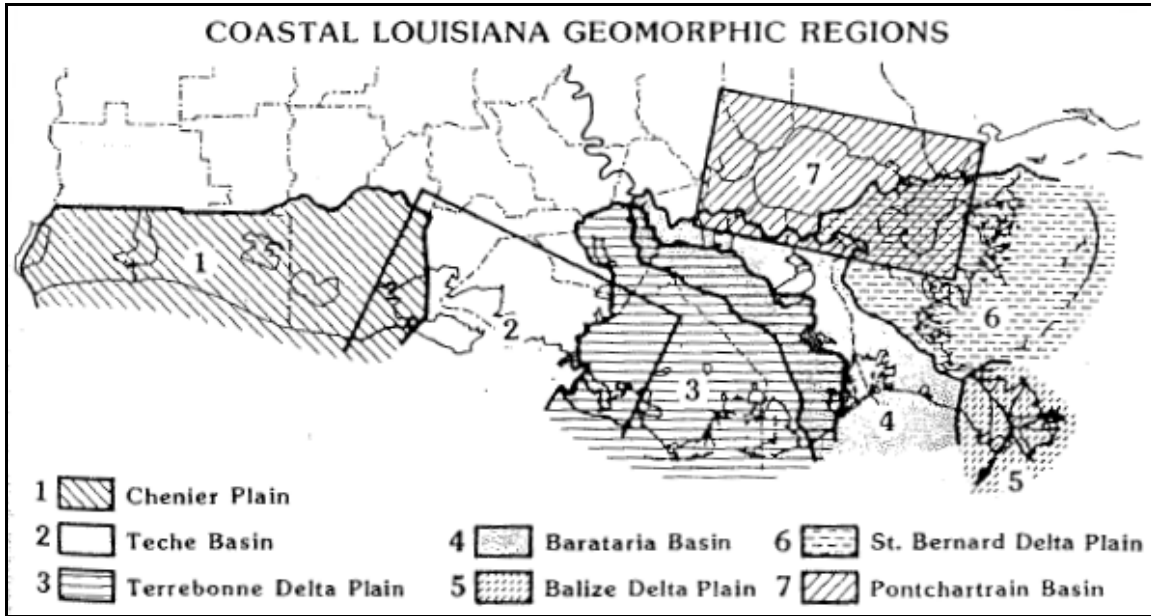


Figure A.1, from Penland, 1990

1564
1565

1566

1567 Future rates of RSLR were determined by considering both the 1987 NRC global mean SLR
 1568 projections and the 2007 IPCC global mean SLR projections, along with estimates for local and
 1569 regional subsidence rates across coastal Louisiana. While the 2007 IPCC projections are
 1570 considered the most current and rigorous effort to estimate future global mean SLR rates there
 1571 has been some criticism that these projections do not adequately consider the potential for
 1572 extreme scenarios such as massive ice loss and melting from Antarctica. The 2007 IPCC mean
 1573 central value estimate for global mean SLR by 2100 is 0.343 meters and the upper limit value is
 1574 0.59 meters. Due to the uncertainties associated with the IPCC estimate methods, a conservative
 1575 value of 0.5 meters of rise by 2100 is used for rigorous sensitivity analysis, with the acceleration
 1576 rate being the same as that described in the 1987 NRC report and modified by Knuuti (2002):

$$E(t_2) - E(t_1) = 0.0012(t_2 - t_1) + b(t_2^2 - t_1^2) \quad \text{eqn A.1}$$

1577

(see Knuuti, 2002, for description of variables and derivation of equation).

1578

1579

1580 To account for possible extreme scenarios of global mean SLR and the associated RSLR
 1581 across Louisiana, the sensitivity analysis also considered the “Curve III” value from the 1987
 1582 NRC report, which estimates a global mean SLR of 1.5 meters by 2100.

1583

1584 Estimates of local and regional subsidence rates were calculated by subtracting the regional
 1585 historic SLR rate (2.0 mm/year) from the local and regional RSLR rates described earlier.
 1586 These subsidence rates were combined with the future projections described in the previous
 1587 two paragraphs to determine local and regional projections for future rates of RSLR. Table A.1
 1588 summarizes the RSLR values developed for the sensitivity analysis scenarios.

1589
1590

Table A.1: Relative Sea-Level Rise Values, 50-year project life

	Relative Sea-Level Rise Values between 2010 and 2060 (meters)		
Basis for value	Chenier Plain	Delta Plain	Pontchartrain Basin
Historic rate	0.2	0.4	0.2
Future scenario 1	0.4	0.6	0.4
Future scenario 2	0.8	1.0	0.8

1591
1592
1593
1594
1595
1596
1597
1598
1599
1600
1601
1602
1603
1604
1605
1606

References:

- National Research Council (NRC), 1987. *Responding to Changes in Sea Level: Engineering Implications*.
- Corps of Engineers policy, as described in ER 1105-2-100 (dated 22 April 2000),
- Knuuti, K. (2002). "Planning for Sea-Level Rise: U.S. Army Corps of Engineers Policy" in *Solutions to Coastal Disasters '02*. ASCE, Alexandria, VA.
- Meehl, G. (Intergovernmental Panel on Climate Change), 2007. *The Scientific Basis*.

1607
1608
1609
1610
1611
1612
1613
1614
1615
1616
1617
1618
1619
1620
1621
1622

Annex B
The maximum possible intensity and its use for coastal hazard estimation

The Maximum Possible Intensity and Its Use for Coastal Hazard Estimation

Don Resio

The Maximum Possible Intensity (MPI) of a hurricane has been recognized as a parameter that critically affects the probabilities of extreme tropical cyclone intensities at least since the late 1970's (see for example: World Meteorological Organization, 1976 and Mooley, 1980). Even before that time, theoreticians had recognized the existence of thermodynamic and dynamic constraints on the energy available for tropical cyclone intensification, even when it is unencumbered by the proximity of land (see for example: Riehl, 1954; Miller, 1958; and Malkus and Riehl, 1960). More recently, Emanuel (1986, 1991) and Holland (1997) formulated theoretical models for estimating maximum tropical cyclone intensity. In an evaluation of the performance of these two MPI models, Tonkin *et al.* (2000) examined storms within 1) the Australian/southwest Pacific region, 2) the northwest Pacific region, and 3) the North Atlantic region. Since our primary interest is focused on the Gulf of Mexico, we will limit our discussion here to results for that region.

Figure 1 shows the geographic area encompassed within the “North Atlantic region” as defined by Tonkin *et al.* Figure 2 presents the results from Tonkin *et al.*'s application of the Emanuel Model (black dots joined by a solid line), Holland's model (dashed line), and observed intensities (open triangles joined by a solid line). This application used a climatological mean Sea Surface Temperature (SST) defined over the period 1950-1979. According to Tonkin *et al.*, Evans (1993) results suggest that there is little gain in predictive skill when actual monthly SST values are used in place of the climatological mean.

As can be seen in Figure 2 and as widely recognized from theoretical considerations, a strong relationship exists between climatological SST values and the lowest central pressures. We see that, in the range of SST values from 26° to 28° (C), the minimum central pressures of the Holland Model, the Emanuel model and the observed intensities are all in approximate agreement. Above 28° (C) the observations continue to show decreasing central pressures with increasing values of SST; whereas, the Emanuel and Holland models do not.

Figure 3, taken from Schade (2000), shows another approximation for the MPI. In this paper, Schade suggests that the effect of the SST field on tropical cyclone intensity is twofold. First, the large-scale ambient SST field “sets the stage for the tropical cyclone.” Second, the intensity of a tropical cyclone is highly sensitive to the reduction of the SST in the interior region of the storm due to the response of the ocean to surface winds. Thus, whereas the concept of the MPI is well founded, some of its details are still under development.

Figure 4 shows the average August-September SST for the Gulf of Mexico for the period 1940-2006. As can be seen here, the highest average values during this part of the

1668 year (the peak of hurricane season) have varied from as low as 28.17° C in 1984 to as high
1669 as 29.49° C in 1962. The dotted vertical line in Figure 3 shows this historical maximum
1670 plotted on top of Schade's results. The heavy solid line along the top of that Figure denotes
1671 the MPI value without consideration of any negative feedback of the type discussed by
1672 Schade; thus, it is expected to represent a maximum possible threshold for the MPI. From
1673 Figures 2, 3, and 4, we can deduce that a value of 880mb represents a very sensible
1674 (perhaps slightly conservative) value for the MPI in the Gulf of Mexico.

1675

1676 Once the value of the MPI is established, we can construct a set of storms that
1677 represents the envelope of worst conditions for different size storms. Since the present state
1678 of the art does not indicate a strong dependence between storm size and the value of the
1679 MPI for a given ambient SST field, we will assume here that the MPI is a fixed value,
1680 independent of storm size. If we select the storm track which produces the maximum surge
1681 values for specified size and intensity, we can make the somewhat conservative assumption
1682 that integrates all storms into that class of storm track. In this context, the probability of a
1683 storm can be estimated simply from the joint probability of size and intensity along the MPI
1684 line, i.e.

1685

$$1686 \quad P(storm) = P(C_p = 880mb) \times P(R_p | C_p = 880mb)$$

1687

1688

1689 If we select values of R_p ranging from small to large, we can estimate the maximum possible
1690 surges for any coastal site. This is an important improvement over concepts which attempt
1691 to relate storm surge maxima to the Saffir-Simpson scale, which considers only storm
1692 intensity.

1693

1694 Figure 5 shows the preliminary results of some runs with a radius to maximum winds
1695 of 25 nautical miles along three tracks. For the New Orleans area, the cumulative
1696 distribution function (CDF) for hurricane intensity (peripheral pressure minus central
1697 pressure) is given by

$$p(c_p \leq 880\text{mb and } R_p \geq 25\text{nm}) = \Lambda_1 \cdot \Lambda_2$$

$$\Lambda_1 = F[a_0, a_1] = \exp \left\{ -\exp \left[-\frac{\Delta P - a_0}{a_1} \right] \right\} \text{ (Gumbel Distribution)}$$

$$\Lambda_2 = p(R_p | c_p) = \frac{1}{\sigma(\Delta P)\sqrt{2\pi}} e^{-\frac{(\bar{R}_p(\Delta P) - R_p)^2}{2\sigma^2(\Delta P)}} \text{ (Conditional Normal Distribution)}$$

where

c_p is the central pressure

R_p is the scale function for the radius to maximum wind speed

$F(\square)$ is the CDF for the argument \square

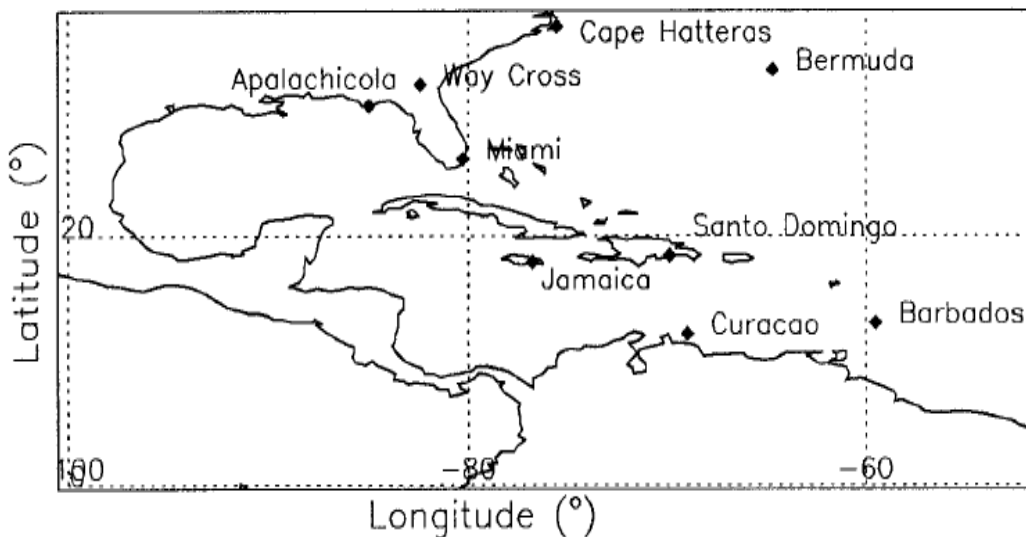
ΔP is the pressure differential = $(p_0 - c_p)$ where p_0 is the peripheral pressure

\bar{R}_p is the conditional mean value of R_p - given ΔP

σ is the conditional standard deviation of R_p - given ΔP

1698
 1699
 1700
 1701
 1702
 1703
 1704
 1705
 1706

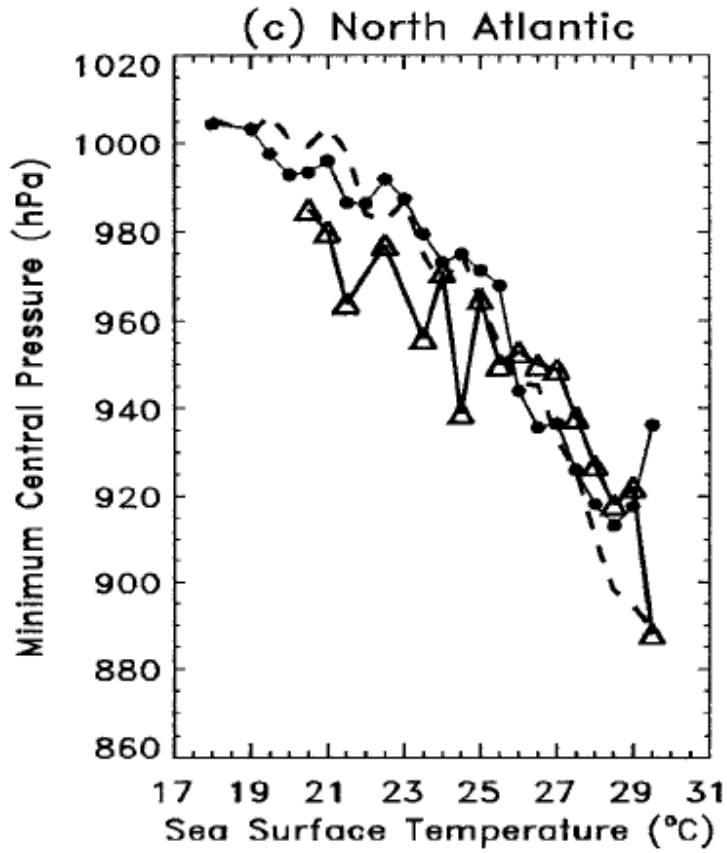
Using values for the Gumbel coefficients which are identical to those described in Resio *et al.* (2007) and using values for the conditional mean and conditional standard deviations capped to be no smaller than the value at 900 mb, the estimated return period for a storm with a central pressure of 880 is 2905 years. The combination of this central pressure with a size of 25 nm or larger is expected only once every 74,848 years.



1707
 1708
 1709

Figure 1. Geographic area considered under heading of “North Atlantic” by Tonkin *et al.* (2000).

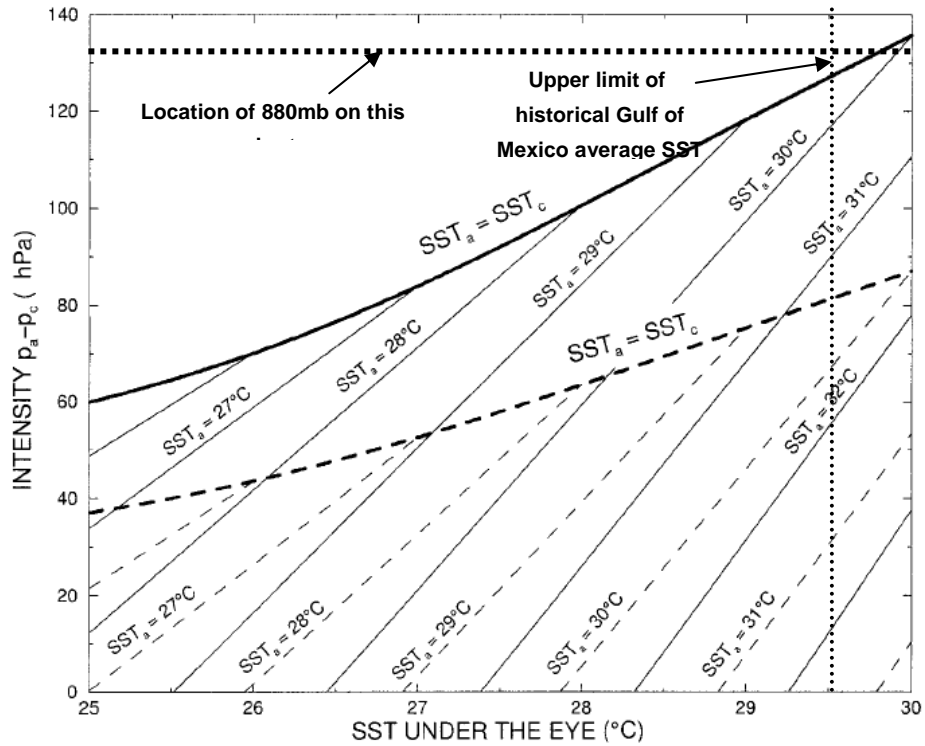
1710
1711
1712



1713
1714
1715
1716
1717

Figure 2. Relationship between observed minimum central pressures (maximum intensities) and sea surface temperature in the North Atlantic basin (from: Tonkin et al., 2000)

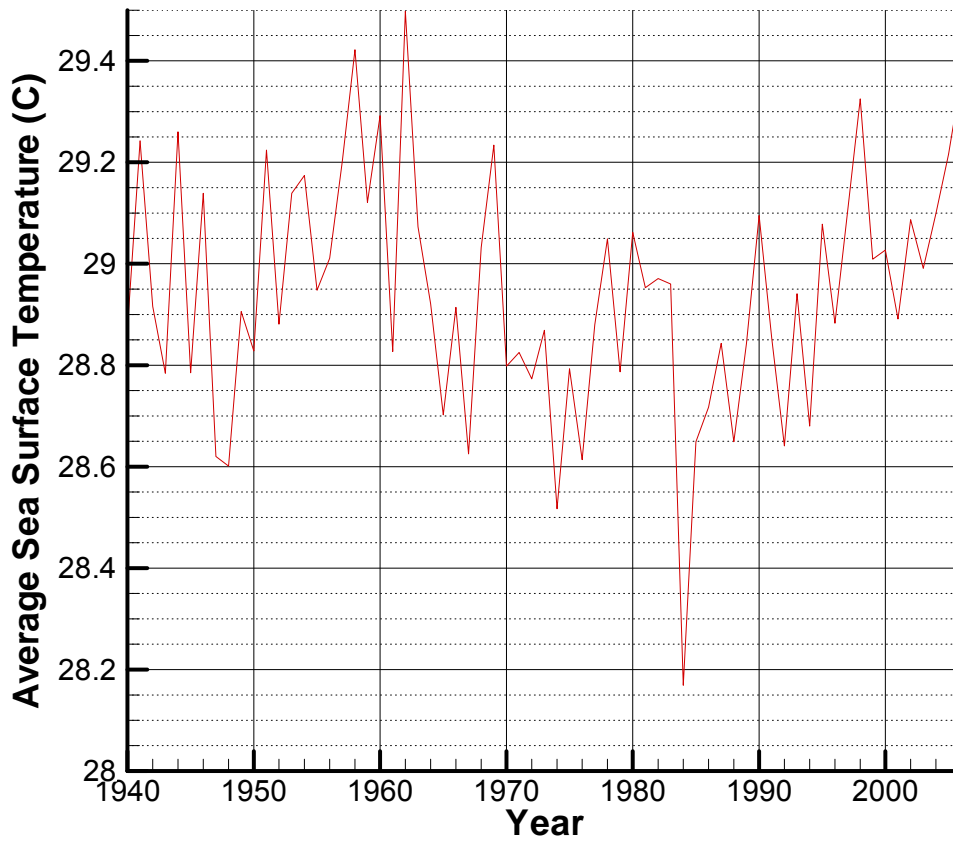
1718
1719
1720
1721
1722
1723



1724
1725
1726
1727
1728
1729
1730
1731
1732
1733
1734

Figure 3. Estimated cyclone intensity as a function of the SST under the eye of the storm (from: Schade, 2000). The solid and the dashed lines correspond to ambient relative humidities of 75% and 85%, respectively. The heavy lines mark the maximum possible intensity that is realized neglecting (negative) SST feedback. The thin lines connect points with the same ambient SST.

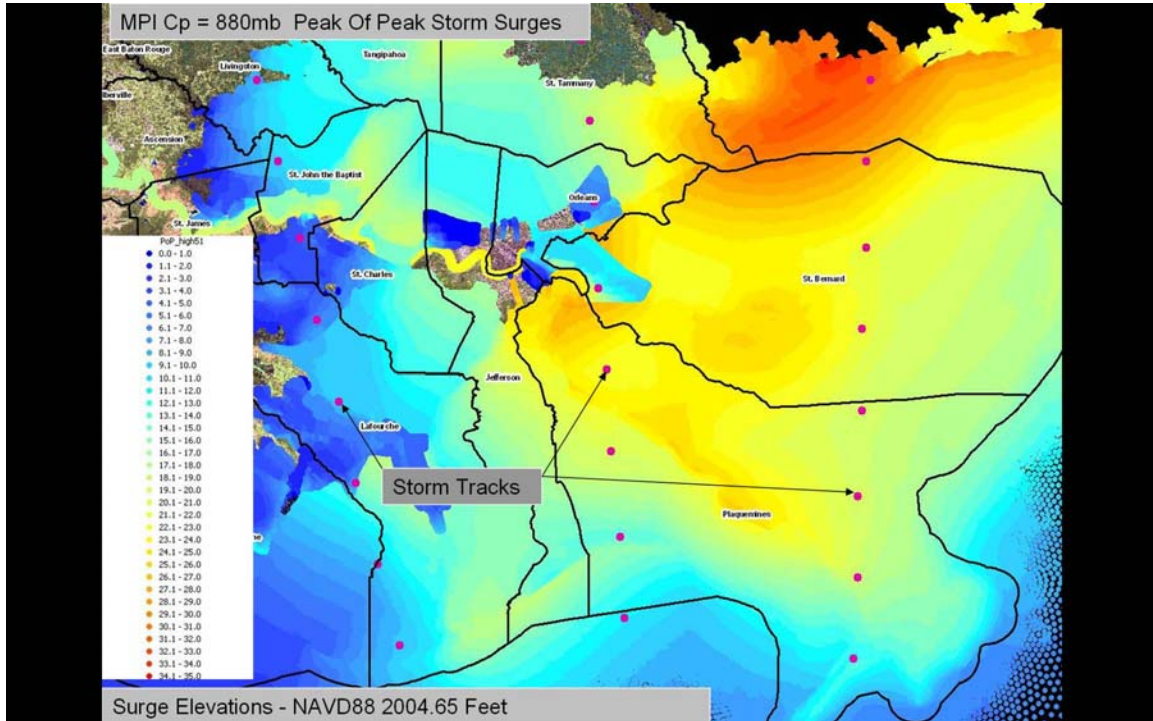
1735
1736
1737
1738
1739
1740



1741
1742
1743
1744

Figure 4. Variation of average annual (unsmoothed) Gulf of Mexico SST's from 1940 through 2006.

1745
1746
1747
1748
1749



1750
1751
1752
1753
1754
1755
1756
1757
1758
1759

Figure 5. Preliminary results showing contours of the maximum elevation of maximum surges for three tracks (paths shown by sequences of red dots) for a storm with central pressure equal to 880 mb and a radius to maximum wind speed of 25 nautical miles. In these storms, the Holland B term and the pressure and size variations during approach to the coast were treated in the same fashion as the rest of the storms described in the White Paper by Resio et al. (2007).

1760